Master Thesis

Cooling system control of a fuel cell-powered inland container vessel

Louwerens Vos

Delft University of Technology

TU Delft

Thesis for the degree of MSc in Marine Technology in the specialization of Marine Engineering

Cooling system control of a fuel cell-powered inland container vessel

by

Louwerens Vos

Performed at

Future Proof Shipping

This thesis MT.23/24.027.M is classified as confidential in accordance with the general conditions for projects performed by the TUDelft

to be defended publicly on Wednesday May 15, 2024 at 14:00 PM.

Company supervisors
Responsible supervisor: Dr. ir. M. Godjevac

Thesis exam committee
Chair/Responsible Professor: Dr. ir. L. van Biert
Staff Member: Dr. ir. P. de Vos
Company Member: Dr. ir. M. Godjevac

Author Details
Studynumber: 438236

Cover: The H2 Barge 1 owned by Future Proof Shipping [12]

Abstract

With fuel cells making their way into the maritime sector, cooling systems are becoming a more important aspect of ship design with regard to power saving. Because fuel cells generate heat at a lower temperature, they require a cooling system that is comparatively larger than that of conventional power trains. Ship cooling system research mainly focuses on the implementation of variable-speed pumps, with little research focusing on the control of cooling systems. For this reason, this research aims to examine the performance of different rule-based and optimisation-based control systems applied to the cooling system of a fuel cell-powered ship.

In this research, a cooling system based on the FPS Waal is modelled in Simulink using Simscape. The cooling system consists of two coolant pumps, two river water pumps, a three-way valve, and two heat exchangers that cool six fuel cell units.

Four rule-based control methods and three optimisation-based control methods were tested. Two rule-based control methods, standard rule and temperature difference, have a rule-set based on just temperature measurements. The other two, load-based flow and load-based pump, have an additional basic algorithm where the control system knows the current cooling system configuration. Two optimisation-based control methods, steady-state optimised and lookup, are based on steady-state operation, and current-state optimised is based on the current system state. The optimisation models used are Mixed Integer Quadratic Constrained Programs (MIQCP). The control methods are tested in three types of simulations. A constant heat load is used to compare temperature control, pump on/off cycles, and power consumption; a step load is used to compare temperature control, and scenario simulations are used to compare temperature control and power consumption.

Optimisation-based control methods perform better, with regard to temperature control, pump on/off cycles and cooling system power consumption, in constant load despite suffering from nonlinearities. With step load, the rule-based control methods have better temperature control because they have spare cooling capacity. In the scenario simulations, the optimisation-based control methods have significantly lower cooling system power consumption than rule-based control methods. Load-based flow has an average power consumption over the scenario simulations, which is 39.2% higher than the average power consumption of steady-state optimised. load-based pump, temperature difference, and standard rule perform significantly worse with 96.4%, 179.5%, and 197.0%, respectively. Current-state optimised only has a 0.85% higher average power consumption and lookup a 5.85% higher average power consumption.

While the overall performance of the optimisation-based control methods was superior, simplifications in the optimisation models resulted in steady-state errors in temperature control. Further research is required to implement optimisation-based control methods for cooling systems to reduce the errors from simplifications and take into account cooling system component degradation.

Contents

List of Figures

List of Tables

Nomenclature

Abbreviations

Abbreviation	Definition
PEM	Proton-Exchange Membrane
NTU	Number of Transfer Units
MIQCP	Mixed Integer Quadratic Constrained Program

Symbols

Symbol	Definition	Unit
A	Pipe area	[m^2]
A_{int}	Internal surface area of a pipe	[m^2]
A_{leak}	Valve leakage area	[m^2]
A_{max}	Maximum valve area	[m^2]
$A_{orifice}$	Orifice area	[m^2]
C_C	Thermal capacity of the cold flow	[J/(s·K)]
C_d	Discharge coefficient	[-]
C_H	Thermal capacity of the hot flow	[J/(s·K)]
c_p	Specific heat capacity	[J/(kg·K)]
D_h	Hydraulic diameter	[m]
f	Darcy friction factor	[-]
h	Heat transfer coefficient	[W/(m^2K)]
ΔH	Pump head	[mH2O]
ΔH_{ref}	Reference pump head	[mH2O]
k	Thermal conductivity	[W/(m·K)]
L	Pipe length	[m]
L_{add}	Aggregate equivalent length of local resistances	[m]
$\dot{m}$	mass flow	[kg/s]
$\dot{m}_A$	Mass flow through port A	[kg/s]
$\dot{m}_B$	Mass flow through port B	[kg/s]
NTU	Number of transfer units	[-]
Nu	Nusselt number	[-]
Δp	Pressure difference	[mH2O]
Δp_{crit}	Critical pressure difference	[mH2O]
P	Pump power	[kW]
P_{ref}	Reference pump power	[kW]
PR_{loss}	Pressure loss factor	[-]
Q	Heat transfer	[kW]
Q_{cond}	Heat transfer due to conduction	[kW]
Q_{conv}	Heat transfer due to convection	[kW]
R_C	Capacity ratio	[-]
Re	Reynolds number	[-]
S	Valve control member position	[m]
ΔS	Valve control member position travel distance	[m]
ΔS_{max}	Maximum valve control member position travel distance	[m]

Symbol	Definition	Unit
$S_{orifice\_max}$	Valve control member position with maximum orifice area	[m]
T_C	Temperature of the cold stream inside the heat exchanger	[°C]
T_H	Temperature of the hot stream inside the heat exchanger	[°C]
T_I	Temperature of fluid inside the pipe	[°C]
T_{in}	Temperature of the fluid at the inlet	[°C]
T_{pipe}	Temperature of the pipe wall	[°C]
$\dot{V}_{ref}$	Reference pump volumetric flow rate	[m^3/h]
U	Heat exchanger heat transfer coefficient	[W/(m^2K)]
ε	Heat exchanger effectiveness	[-]
ε	Effective roughness height	[m]
ρ	Density	[kg/m^3]
ξ	Specific dissipation	[kW/K]
ω	Pump shaft speed	[rpm]
ω_{ref}	Reference pump shaft speed	[rpm]

1

Introduction

When in 1992 countries agreed to the United Nations Framework Convention on Climate Change [33] the industry focus shifted from maximising profit to taking harmful emissions into account. Over time, the restrictions on emissions increased with examples such as the establishment of the SECA zones [19] and the Paris agreement [25]. While these restrictions have reduced the SO_x emissions, the CO_2 emissions have remained largely unaffected.

To decrease the CO_2 emissions, there are three approaches [28]. The first option is to use synthetic fuels rather than their fossil fuel variant. This results in net zero CO_2 if the fuels are synthesised using CO_2 from carbon capture and green energy. The second option is to eliminate fuel use and instead have a rechargeable battery that provides all the energy needed. This results in no emissions, assuming that the energy used to charge is green energy. The last option is to use fuels that have no harmful emissions. Two examples are hydrogen (H_2) and ammonia (NH_3). These fuels have zero CO_2 emissions when produced with green energy.

The shipping industry prefers a fuel that combines a high volumetric density and a high gravimetric density. A lithium-ion battery has both a low volumetric density and a gravimetric density and is, for that reason, undesirable as sole energy storage [6]. Carbon-based fuels have a decent gravimetric density and a high volumetric density [18]. These qualities and the fact that the design doesn't need changing from the current design are the driving forces behind synthetic fuels. Hydrogen has a very high gravimetric density, offset by a very low volumetric density. However, it is still considered one of the fuels that could power the future. Research is done into designing turbines capable of running on 100% hydrogen [17]. There is also research into running internal combustion engines on hydrogen, but this is less successful as both the efficiency and the power output are lower compared to burning carbon-based fuels [15]. An alternative to the internal combustion engine is a fuel cell, where the energy of the hydrogen gets directly converted into electrical energy. This achieves an efficiency of up to 60% and is, for this reason, the preferred option over internal combustion engines with their efficiency of 35% - 45% [3].

Fuel cells have already been in use in the maritime sector, with one of the first examples of projects with Proton-Exchange Membrane (PEM) Fuel cell powered ships dating back to 2006 when the project ZemShip started [8]. Recently, more projects have been conducted regarding hydrogen fuel cell ships. The Energy Observer 2 is a newly proposed 5000-ton deadweight multi-purpose ship powered by PEM fuel cell units of 2.5 MW using liquid hydrogen as a fuel storage mechanism [7]. Rivercell is a project to design and run the inland pushing boat ELEKTRA powered by a PEM fuel cell unit of 200 kW and a 1276 kWh battery using 500 bar hydrogen as a fuel storage mechanism [21]. The project HyShip is designing and constructing the ship Topeka, a ro-ro demonstration vessel powered by a 3 MW PEM fuel cell using liquid hydrogen as a fuel storage mechanism [1]. Future Proof Shipping is retrofitting the inland container vessel FPS Maas to install an 825 kW fuel cell system with a 504 kWh Lithium-ion battery using 300 bar hydrogen as a fuel storage mechanism [9].

1.1. Problem definition

A significant focus of society these days is reducing emissions. One of the possible solutions to emission reduction in the maritime industry is replacing fossil fuel-burning engines with fuel cell units that run on hydrogen or other non-polluting fuels. While having slightly higher efficiency than internal combustion engines, PEM fuel cells generate a lot of heat at a comparatively low temperature. This results in the PEM fuel cell system requiring a more extensive cooling system, which comes with additional parasitic losses due to increased pumping power. For this reason, an increase in the cooling system's efficiency sees more results for a PEM fuel cell cooling system. It could help it become financially competitive with internal combustion systems. The two ways of increasing the efficiency of the cooling system are by increasing the efficiencies of the individual components or the way this research focuses on, which is to improve the efficiency of the control of the system.

Both the degradation [2] as well as the performance [32] of a fuel cell depend on the fuel cell operating temperature. For this reason, accurate control of PEM fuel cell systems is necessary to minimise operating costs. While there is literature regarding fuel cell cooling systems on board ships [5][14], these papers focus more on proving that there is a possibility of improving the control of the cooling system rather than testing their new control system in multiple operational scenarios and environmental conditions. Considering operational scenarios and environmental conditions is not foreign to ship cooling system literature as it is a common method applied to evaluate the benefit of having a variable-speed pump [31][20][24].

Optimisation-based control has shown the capability of more accurate temperature tracking and more efficient cooling system running. While Optimisation-based control is well known in the maritime research literature for energy management systems [16][34], there is little research into applying Optimisation-based control for the control of a ship's cooling system. There is abundant research into applying Optimisation-based control to cooling systems from other sectors [29].

1.1.1. Research gap

What is currently lacking concerning research into ship cooling systems is the comparison between control systems in multiple operational scenarios and environmental conditions, especially involving optimisation-based control. Optimisation-based control is comparatively underrepresented in the ship cooling system literature, but it has shown promising results with regard to temperature control and power consumption reduction in other sectors. This is especially relevant for fuel cell cooling systems as the fuel cells are sensitive to overheating due to degradation.

1.1.2. Proposed research

To fill this gap, the proposed research is a case study in which both optimisation-based control and rule-based control can be directly compared. A case study will provide a realistic basis for a cooling system configuration, operational profile, and environmental conditions. It will also provide insight into the possible savings one can expect as a ship owner.

1.1.3. Research questions

The main research question that this research aims to answer is as follows:

How does the performance of rule-based control methods compare with optimisation-based control methods when applied to the cooling system of an inland ship with multiple pumps, heat exchangers, and fuel cell units?

To help answer this main research question, the following sub-questions have been defined:

What are the important performance indicators for a PEM fuel cell cooling system on a ship?

Which rule-based control methods are considered?

Which optimisation-based control methods are considered?

Which scenarios are simulated?

1.2. Scope

To ensure that the research does not lose focus on answering the main research question, the scope has been defined as follows:

The fuel cell cooling system layout considered in this research will be based on the proposed cooling system of the FPS Waal, and the area of operation considered is the Rhine. For this reason, results found during this project may not be applicable to different cooling system configurations operating in different environmental conditions.

The main aim of this research is to create an idea of the performance of different control methods. It does not aim to maximise the performance of the individual methods, as that would take too much time. For that reason, when comparing the performance of the methods, one method may be better tuned than the other, slightly skewing the result.

This is the same reason why fuel cells are considered a heat source with a single thermal mass. While a more accurate model of a fuel cell would improve the accuracy of this research, there is a lack of readily available information required to model the fuel cells, and the increase in accuracy would be unlikely to change the outcome of this research.

1.3. Thesis structure

After this introduction, the thesis will provide the background on the Simulink model in chapter 2. Here, the choice for Simscape and how components of the cooling system are modelled will be explained. This is followed by Chapter 3, which will detail how optimisation models were made based on the Simulink model. After that, in chapter 4, control methods for the Simulink model based on a rule set or the optimisation models are explained, and the simulations run to test these methods are detailed. In chapter 5, the results of the simulations are presented and discussed. In chapter 6, the findings of chapter 5 are discussed, the limitations of this research are presented, and recommendations for future research are given. Finally, chapter 7 provides an answer to the main research question.

2

Simulink model

A model is often used in research as a substitute for the physical system, as constructing a system for research purposes takes a lot of resources. This chapter provides an explanation of the makeup of the model used in this research and expands on why certain choices were made in the model. Section 2.1 details the reasoning for choosing Simscape as a basis to make the model and showcases the underlying equations of the most important Simscape blocks used. Section 2.2 provides an overview of the modelled cooling system. The chapter closes with sections 2.3, 2.4 and 2.5, which go into detail about how the fuel cell units, the pumps, and the heat exchangers are modelled.

2.1. Simscape

The choice was made to make the model of the cooling system in the MATLAB Simulink environment using Simscape. Simscape was chosen for three main reasons. The first reason is that a model made using Simscape blocks provides a clearer overview while working than a fully custom Simulink model. The second reason is that the embedded equations in the Simscape blocks prevent errors in a large model. Since this research aims not to create an exact copy of a cooling system but rather a similar system, being limited by the Simscape equations is not a drawback. The third and most important reason is the logging of data available within Simscape and subsequently viewing the logged data with the Simscape Result Explorer. Selecting which components to log data for, viewing the logged data, and accessing this data within the MATLAB workspace are extremely conveniently implemented.

2.1.1. Pipe

The Simscape pipe element handles three sets of equations corresponding to the mass transport from entry port ”A” to exit port ”B”. The pipe element calculates the pressure losses, heat transfer with the pipe wall and it ensures mass balance. The mass balance is simplified to equation 2.1 since the fluid is considered incompressible and the pipe is rigid.

$$\dot{m}_A = \dot{m}_B \tag{2.1}$$

Equation 2.2 displays the calculation used for the pressure loss in the pipe. f is the Darcy friction factor, which is approximated through the Haaland equation 2.3 [13]. The Darcy friction factor depends on the surface roughness ε, the hydraulic diameter D_h, and the Reynold number Re. A_{int} is the internal surface area of the pipe. L is the total length of the pipe with L_{add} being the aggregate equivalent length of local resistances. L_{add} is a theoretical added length to take into account additional resistances in the pipe without changing the physical dimension of the pipe for other calculations.

$$\Delta p = \frac{f}{2\rho A_{int}^2}\frac{L + L_{add}}{2}\dot{m}|\dot{m}| \tag{2.2}$$

$$f^{-0.5} = -1.8\, log_{10}\left[\left(\frac{\varepsilon/D_h}{3.7}\right)^{1.11} + \frac{6.9}{Re}\right] \tag{2.3}$$

There are two components to the heat transfer calculations that together sum to the total heat transfer in a pipe element. The first component is the heat transfer through conduction and is displayed in equation 2.4, where k is the thermal conductivity of the fluid, T_{pipe} is the temperature of the pipe wall and T_I is the temperature of the fluid inside the pipe. The second component is the heat transfer through convection, as displayed in equation 2.5. T_{in} is the temperature of the fluid entering the pipe segment and h is the heat transfer coefficient calculated using equation 2.6. The Gnielinski correlation [11] is used to determine the Nusselt number, Nu.

$$Q_{cond} = \frac{kA_{int}}{D_h}(T_{pipe} - T_I) \tag{2.4}$$

$$Q_{conv} = c_p\dot{m}(T_{pipe} - T_{in})\left[1 - exp\left(-\frac{hA_{int}}{c_p\dot{m}}\right)\right] \tag{2.5}$$

$$h = \frac{Nuk}{D_h} \tag{2.6}$$

2.1.2. Valves

The three types of valves that have been used in the model are the butterfly valve, the three-way valve, and the check valve. The butterfly valve and the three-way valve both use equation 2.7 to calculate their pressure drop and mass flow.

$$\dot{m} = \frac{C_d A_{orifice}\sqrt{2\rho}}{\sqrt{PR_{loss}\left(1 - \left(\frac{A_{orifice}}{A}\right)^2\right)}}\frac{\Delta p}{\left[\Delta p^2 + \Delta p_{crit}^2\right]^{1/4}} \tag{2.7}$$

$A_{orifice}$, the orifice open area, is calculated using equations 2.8 - 2.10, where butterfly valves and one of the directions in the three-way valve use equation 2.9 to calculate their ΔS while the other direction of the three-way valve uses equation 2.10. S is the control member position of the valve leading to $S_{orifice\_max}$ being the control member position where $A_{orifice}$ is maximum and ΔS_{max} being the largest possible difference in S. C_d is the discharge coefficient parameter. PR_{loss} is the parameter for the pressure loss and pressure recovery over the valve due to the change in area. A is the pipe area. Δp is the change in pressure over the valve. Δp_{crit} is the pressure differential associated with the critical Reynolds number, being the Reynolds number, which is the transition point between laminar and turbulent flow.

$$A_{orifice} = \frac{(A_{max} - A_{leak})}{\Delta S_{max}}\Delta S + A_{leak} \tag{2.8}$$

$$\Delta S = S_{orifice\_max} - \Delta S_{max} + S \tag{2.9}$$

$$\Delta S = S_{orifice\_max} + \Delta S_{max} - S \tag{2.10}$$

2.1.3. Heat exchanger

Within Simscape, there are two modelling options for the heat exchangers. The simple model was chosen for this research as the alternative, E-NTU, requires input parameters regarding the internal dimensions of the heat exchangers and wall thermal dynamics that could not be validated. The simple

model revolves around equation 2.11, which states that the heat transferred is equal to the temperature difference of the two liquids at the inlet multiplied by ξ. ξ is the specific dissipation, a tabulated function of the mass flow rates into the exchanger. The specific dissipation, ξ, corresponds to the amount of heat transferred for one degree in temperature difference between the two flows. The value of ξ changes based on the mass flow rates of both thermal liquids entering the heat exchanger.

$$Q = \xi(T_{in,1} - T_{in,2}) \tag{2.11}$$

2.1.4. Pump

The chosen way to model the pumps within Simscape is using 1-D tabulated data parameterisation with head and brake power as a function of capacity at reference shaft speed, as the data for this approach is available. For cases where the shaft speed differs from the reference shaft speed, Simscape applies the affinity laws displayed in equations 2.12, 2.13, and 2.14. ω is the shaft speed. H is the pump head. P is the brake power used by the pump.

$$\dot{V}_{ref} = \frac{\dot{m}}{\rho}\frac{\omega_{ref}}{\omega} \tag{2.12}$$

$$\frac{\Delta H_{ref}}{\Delta H} = \frac{\omega_{ref}^2}{\omega^2} \tag{2.13}$$

$$\frac{P_{ref}}{P} = \frac{\rho_{ref}}{\rho}\frac{\omega_{ref}^3}{\omega^3} \tag{2.14}$$

2.1.5. Thermal liquid properties

Simscape uses tabulated data for the thermal liquid properties at different temperatures and pressures. The properties most relevant to this research are the density, specific heat capacity, and the kinematic viscosity of the liquids. The change in density is relatively small in the temperature and pressure brackets that this research operates in. Figure 2.1 shows the variance in specific heat capacity. The kinematic viscosity of 50% ethylene glycol displayed in figure 2.2 has an even more significant variance in the relevant temperature bracket, as it varies between 1 mm^2/s and 7 mm^2/s.

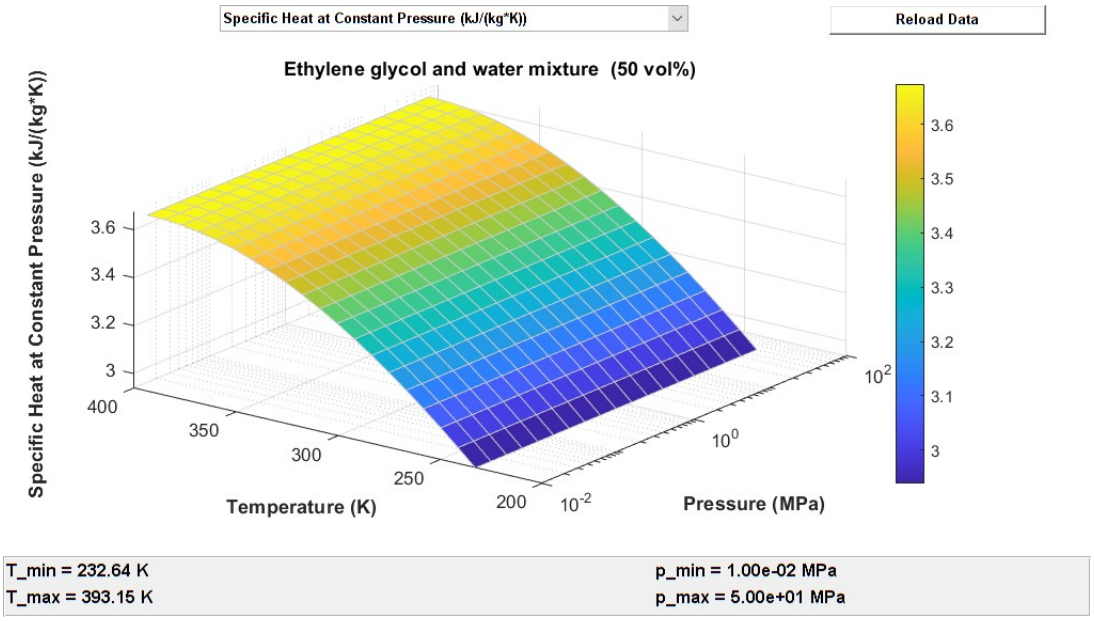

Figure 2.1: Specific heat capacity of 50% ethylene glycol at different temperatures and pressure

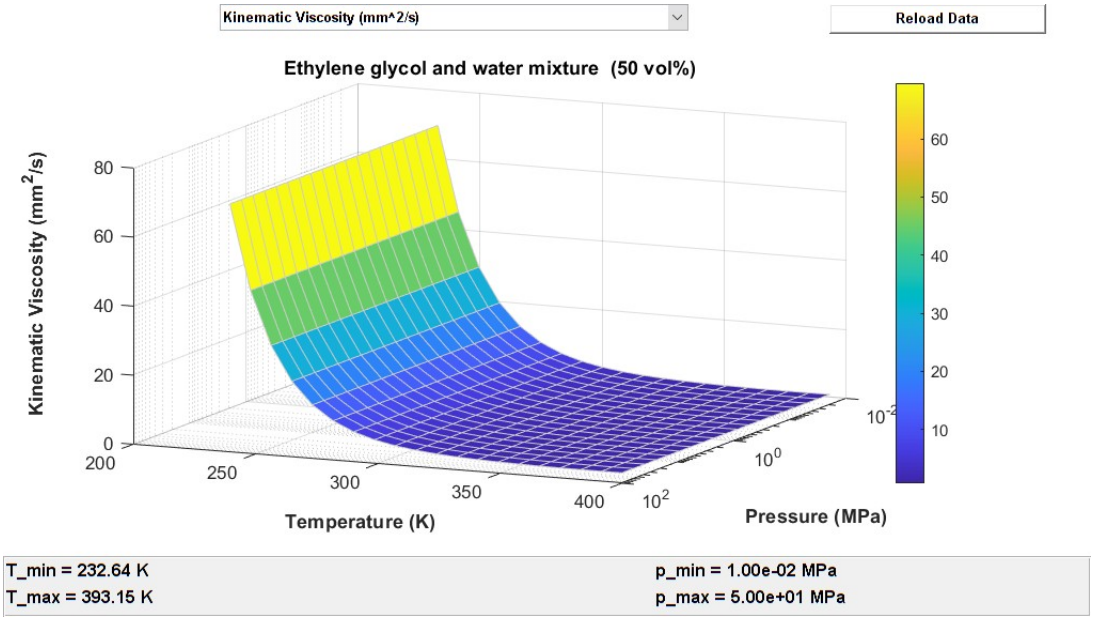

Figure 2.2: Kinematic viscosity of 50% ethylene glycol at different temperatures and pressure

2.2. System model

The cooling system used in this research is a cooling system that uses two coolant circulation pumps and two heat exchangers with river water supplied by two pumps, which provides cooling to six fuel cell units. This cooling system is based on a proposed cooling system for an inland container vessel with an installed electrical fuel cell power of 1200 kW. Figure 2.3 shows a schematic overview of the cooling system. The coolant circulation pumps, the heat exchangers, and the fuel cell units are installed in a parallel configuration. Both coolant circulation pumps have a check valve on the pressure side to prevent flow back in cases where one pump overpowers the other.

The coolant flow is provided by pumps PU05 and PU06. Pump PU05 is a variable-speed pump. Together, they provide the nominal coolant flow of 24.4 kg/s. The maximum heat load of a fuel cell unit is 350 kW. Six fuel cell units result in a total heat load of 2100 kW. To cope with this, two heat exchangers have been installed. Heat exchanger 1 is capable of transferring up to 1420 kW of heat with an outside river water temperature of 25 °C. Heat exchanger 2 is capable of transferring up to 710 kW of heat in those same conditions. The heat exchangers are provided with river water by pumps PU01 and PU02, which provide a flow of 18.61 kg/s and 9.44 kg/s, respectively.

The only validation data available for the entire system is the nominal operation. The pressure drop over the heat exchangers is known. The pressure drop over the pipes and valves was left as is within Simscape. To ensure that the system had the proper flow in nominal conditions, a ”tuning” resistance needed to be added. The cooling system side of the fuel cell units was chosen as increasing the pressure drop in this section of the system would have a similar effect on the system pressure drop regardless of the number of active fuel cell units due to them being installed in parallel. This increase in pressure drop was achieved by increasing L_{add} for these pipe elements. This results in no changes within the heat flow calculations.

To aid with the resistance calculations used for the optimisation models, the model was divided into 11 main sections, with sections 5 and 7 having sub-sections. All sections are parts of the cooling system between two junctions. Table 2.1 provides an overview of these sections. The four pipe dimensions used within the cooling system can be seen in table 2.2. The dimensions for the three different valves used in the model are shown in table 2.3. Cd and Re_{crit} are unchanged from the Simscape preset, as these valves lacked validation data. The maximum orifice area, A_{max}, is portrayed based on the pipe diameter A as valves for different pipe dimensions were used throughout the model. A_{max} for the butterfly valve is an estimate based on a schematic drawing of the valve. A_{max} for the three-way valve and for the check valve are not based on validated data or a drawing and could be misaligned

with reality. The pipes in the model have been assigned a thermal mass to account for their resistance against temperature change. The thermal mass for components where it was impossible to assign their thermal mass to their Simscape element was added to the thermal mass of surrounding pipes. These components include the heat exchangers and the pumps.

Table 2.4 provides an overview for each section of the length of the pipes, the sizing of the pipes, the thermal mass of the section, and the number of bends. Valves in a section have the same sizing as the pipes of that section. The bend radius for all bends equals 1.5 times the pipe diameter.

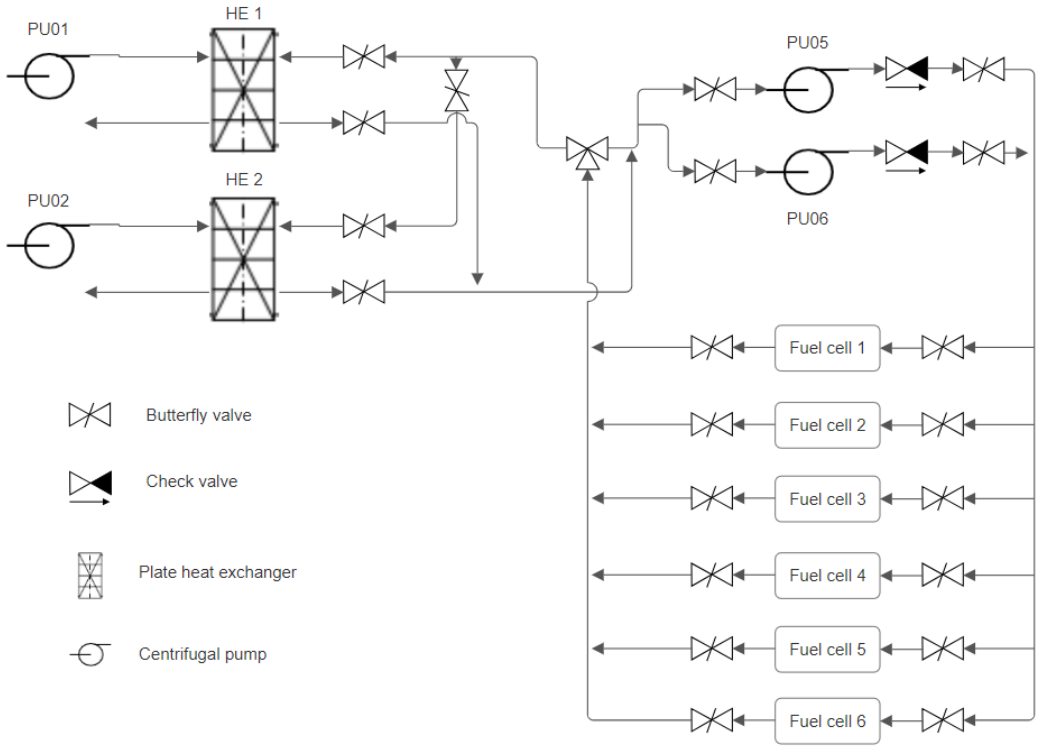

Figure 2.3: PI&D overview of the cooling system

Table 2.1: Cooling system zones

Section 1	Pipes and valves connecting to and from pump PU05
Section 2	Pipes and valves connecting to and from pump PU05
Section 3	Pipes from the connection of zone 1 and zone 2 until the separation to fuel cell unit 1
Section 4	Pipes from the connection of the bypass and the heat exchanger path until the separation into zone 1 and zone 2
Section 5_1	Pipes from the junction to fuel cell unit 1 until the junction to fuel cell unit 2
Section 5_2	Pipes from the junction to fuel cell unit 2 until the junction to fuel cell unit 3
Section 5_3	Pipes from the junction to fuel cell unit 3 until the junction to fuel cell unit 4
Section 5_4	Pipes from the junction to fuel cell unit 4 until the junction to fuel cell unit 5
Section 5_5	Pipes from the junction to fuel cell unit 5 until fuel cell unit 6
Section 6	Pipes and valves connecting to and from a fuel cell unit
Section 7_1	Pipes from the junction from fuel cell unit 1 until the three-way valve
Section 7_2	Pipes from the junction from fuel cell unit 1 until the junction from fuel cell unit 2
Section 7_3	Pipes from the junction from fuel cell unit 2 until the junction from fuel cell unit 3
Section 7_4	Pipes from the junction from fuel cell unit 3 until the junction from fuel cell unit 4
Section 7_5	Pipes from the junction from fuel cell unit 4 until the junction from fuel cell unit 5
Section 7_6	Pipes from the junction from fuel cell unit 5 until fuel cell unit 6
Section 8	Pipes from the three-way valve until the connection of the bypass and the heat exchanger path
Section 9	Pipes from the three-way valve until the split to the heat exchangers
Section 10	Pipes and valves to and from heat exchanger 1 including heat exchanger 1
Section 11	Pipes and valves to and from heat exchanger 2 including heat exchanger 2

Table 2.2: Pipe dimensions

DN50	Diameter	54.79	[mm]
	Area	2354.83	[mm^2]
DN80	Diameter	82.80	[mm]
	Area	5387.09	[mm^2]
DN100	Diameter	108.20	[mm]
	Area	9225.79	[mm^2]
DN125	Diameter	134.49	[mm]
	Area	14193.52	[mm^2]

Table 2.3: Valve dimensions

Butterfly valve	Cd	0.64	[-]
	A_{max}	$0.85A$	[mm^2]
	Re_{crit}	150	[-]
Three-way valve	Cd	0.7	[-]
	A_{max}	$0.95A$	[mm^2]
	Re_{crit}	12	$[-]$
Check valve	Cd	0.64	[-]
	A_{max}	$0.85A$	[mm^2]
	Re_{crit}	12	[-]

Table 2.4: Cooling system pipe length, size, thermal mass and bends, per section

	DN50 [mm]	DN80 [mm]	DN100 [mm]	DN125 [mm]	Mass [kg]	Bends
Section 1	-	-	1200	-	106	-
Section 2	-	1200	-	-	76	-
Section 3	-	-	-	7600	143	3
Section 4	-	-	-	1200	24	-
Section 5.1	-	-	-	1286	25	-
Section 5.2	-	-	1082	71	27	-
Section 5.3	-	-	1287	-	19	-
Section 5.4	-	1103	75	-	23	-
Section 5.5	1200	77	-	-	17.5	-
Section 6	1160	-	-	-	22.4	2
Section 7.1	-	-	-	3500	73	1
Section 7.2	-	-	-	1286	25	-
Section 7.3	-	-	1082	71	27	-
Section 7.4	-	-	1287	-	19	-
Section 7.5	-	1103	75	-	23	-
Section 7.6	1200	77	-	-	17.5	-
Section 8	-	-	-	1800	20	-
Section 9	-	-	-	1200	20	2
Section 10	-	-	-	1800	330	-
Section 11	-	-	-	1800	310	-

2.3. Fuel cell model

The fuel cell unit is modelled using three pipe segments and a thermal mass as the main components based on the PEM fuel cell system example by Mathworks [26]. Two pipe segments simulate the heat exchanger within the fuel cell unit, allowing heat transfer between the cooling system and the fuel cell unit. The third pipe segment simulates the cooling channels within the fuel cell unit through which the heat generated by the fuel cell unit is transported away. The thermal mass is connected to the third pipe segment and simulates the thermal mass of the fuel cell unit.

The thermal mass block requires the mass of the object and the specific heat capacity. The mass of the fuel cell unit was estimated using the specification sheet provided by Ballard [10]. They estimate the total weight of a fuel cell unit to be around 1000 kg. This weight includes systems like the air and H2 supply, parts of which do not experience exposure to the heat generated within the fuel cell unit. For this reason, the weight of the mass that would experience significant heating was estimated to be 700 kg per fuel cell unit.

The specific heat capacity used for the thermal mass of the fuel cell unit is 870 J/(kgK). This value is a decent average of the components of a PEM fuel cell unit as laid out by Spiegel [30]. Boulmrharj et al. [4] provide a specific heat capacity of 881 J/(kgK) for the frame of a PEM fuel cell unit, which is in line with the chosen specific heat capacity.

The fuel cell unit for this research is capable of regulating its own temperature. To achieve this, the fuel cell unit has a cooling loop that is separate from the main cooling system. It is assumed this loop also uses 50% ethylene glycol as a coolant and maintains a constant mass flow of 4.07 kg/s through the fuel cell unit, which is the nominal coolant flow of the cooling system through a single fuel cell unit. To determine the amount of heat transferred between the fuel cell unit and the cooling system, a lookup table was made, displayed in figure 2.4. The addition of the fuel cell units self-regulating their temperature came late into the making of the model. For this reason, the lookup table solution was chosen over implementing a heat exchanger block, as the lookup solution did not change the main cooling system. No data was available on the internal heat exchange of the fuel cell units, so using a heat exchanger block would have also resulted in speculative data. Additionally, using Simscape heat exchangers would have required flow management of the flow inside the fuel cell unit to manage the amount of heat flow. Until the thermal mass representing the fuel cell unit has reached a temperature of 64 °C, no heat transfer occurs between the fuel cell unit and the main cooling system. Between

64 °C and 65 °C, the heat transferred increases to 102% of the heat generated by the fuel cell unit. The choice of 64 °C is relatively arbitrary for this specific research as during all simulations, the fuel cell units are already at their nominal operating temperature of 65 °C at the start of the simulation. If one were to look into controlling the fuel cell unit start-up procedure, then this is an area that requires further research. After 65 °C, the amount of heat transferred keeps rising. At 66 °C, the maximum amount of heat transferred is equal to 115% of the fuel cell heat load. From 66 °C onwards, the maximum amount of heat transfer increases with 5% of the fuel cell heat load per 1 °C of fuel cell unit temperature. The amount of heat transferred between the fuel cell unit and the cooling system is capped by $\dot{m}_{coolant\_main} c_{p,coolant\_main} (T_{coolant\_fuelcell} - T_{coolant\_main})$ to prevent heat flow from a cold source to a warm sink.

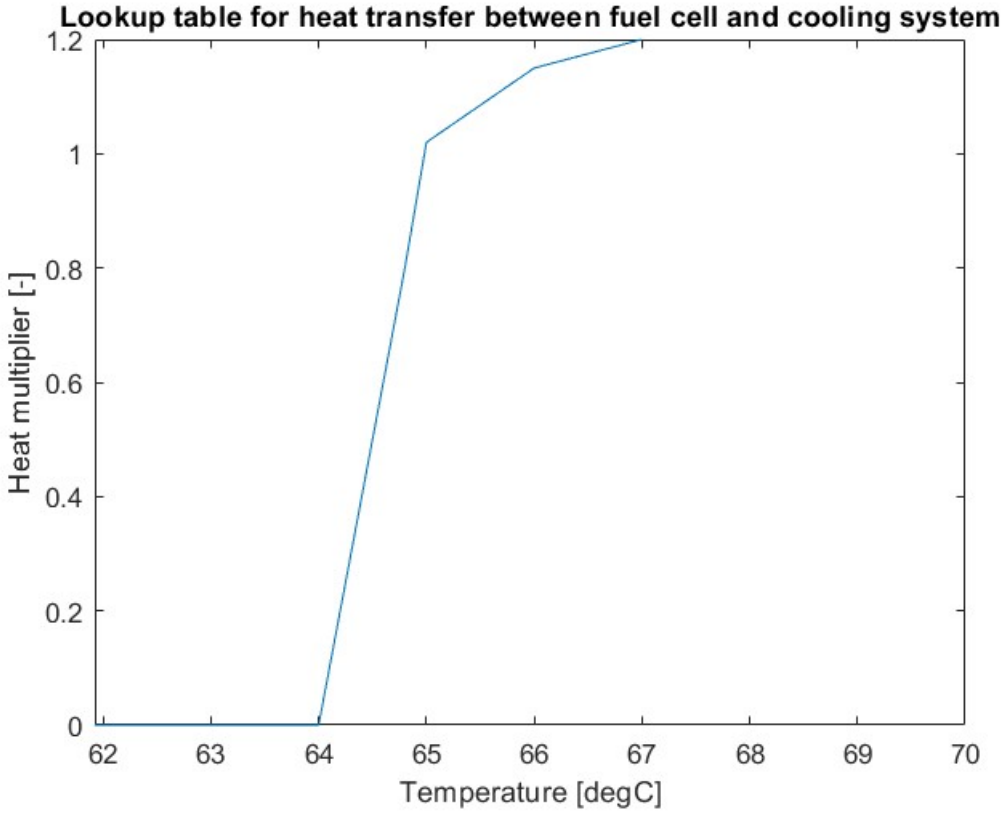

Figure 2.4: Graph of the 1-D lookup table used for heat transfer between fuel cell unit and cooling system

The dimensions of the pipe that simulate the fuel cell cooling channels are based on the method used in the Mathworks example [26]. They determine the pipe length as the square root of the active area of the fuel cell unit times the number of passes; the cross-sectional area is the coolant channel width squared times the number of coolant channel layers, and the hydraulic diameter is equal to the width of a coolant channel. The fuel cell active area was calculated by scaling the fuel cell unit used in the paper by Liso et al. [22] as this paper uses a fuel cell unit made by the same manufacturer. The assumption was made that the coolant channel and the connected thermal mass needed to maintain a temperature of 65 °C with a heat load of 350 kW and a coolant mass flow of 4.07 kg/s with a temperature of 40 °C. This was empirically achieved by increasing the number of passes, which increases the pipe element length. The length was chosen as changing this parameter has a more positive influence on changing the surface area of the pipe. Increasing the pipe diameter was also an option, but this resulted in a comparatively larger increase in pipe volume. An actual fuel cell unit has multiple cooling channels, resulting in a larger surface area to volume ratio, which is why minimising the volume increase was preferred. The three pipe elements have the same dimensions except for the fuel cell unit side of the heat exchanger. This pipe element has 10% of the length compared to the other pipe elements in a bid to minimise the coolant volume inside the fuel cell unit. This results in a faster temperature response for

the fuel cell temperature. No thermal mass is connected to this pipe element, and the wall temperature of this pipe is irrelevant to the results. This means that while it results in a very cold wall temperature, it does not impact the rest of the model and will provide the same amount of heat transfer.

An overview of the fuel cell pipe dimensions can be seen in table 2.5. The resulting pipe element ends up being a long and narrow pipe. Calculating the heat transfer in nominal conditions using equations 2.4 and 2.5 results in a Q_{cond} of 2.75 kW and a Q_{conv} of 353.38 kW, which is sufficiently close to the target of 350 kW.

Table 2.5: Fuel cell pipe dimensions

L	17.12	[m]
A	20	[cm^2]
D_h	1	[cm]
L_{add}	15.5	[m]

2.4. Pump model

The cooling system has a total of four pumps. The river water pumps PU01 and PU02 have a nominal flow of 66 m^3/h and 33 m^3/h, respectively. PU01 provides the flow of river water to the larger heat exchanger HE1 and PU02 to the smaller heat exchanger HE2. Both pumps are fixed-speed pumps with a nominal speed of 2900 rpm. The coolant flow is provided by pumps PU05 and PU06 placed in parallel. PU05 is the larger of the two pumps with a nominal design flow rate of 56 m^3/h and is a variable-speed pump. PU06 is a fixed-speed pump with a nominal design flow rate of 28 m^3/h. Graphs of the tabulated data used to model the pumps are displayed in figures 2.5, 2.6, 2.7 and 2.8 for pumps PU01, PU02, PU05, and PU06 respectively.

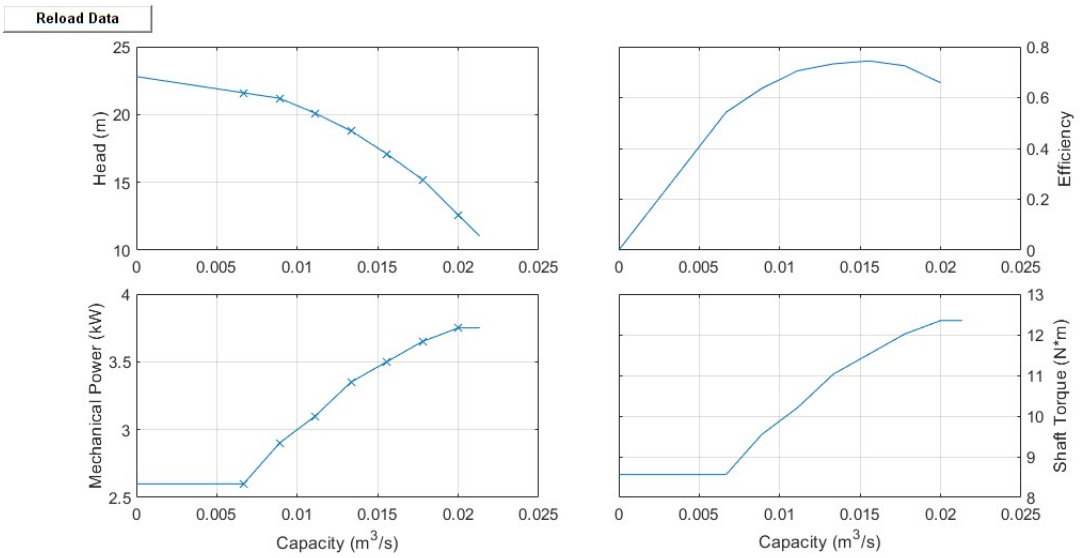

Figure 2.5: Tabulated data for pump PU01 showing the pressure increase, efficiency, mechanical power and shaft torque

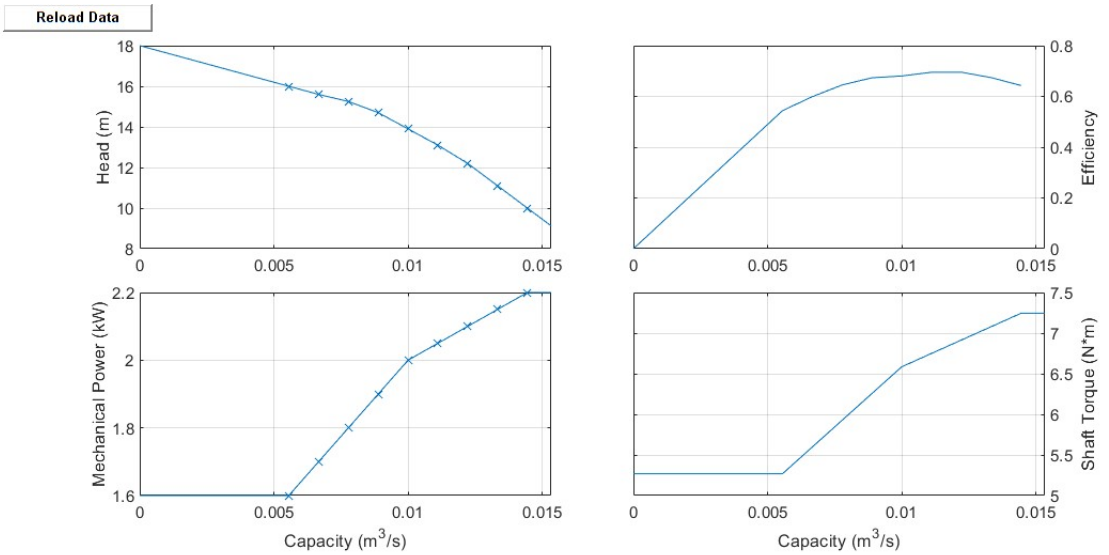

Figure 2.6: Tabulated data for pump PU02 showing the pressure increase, efficiency, mechanical power and shaft torque

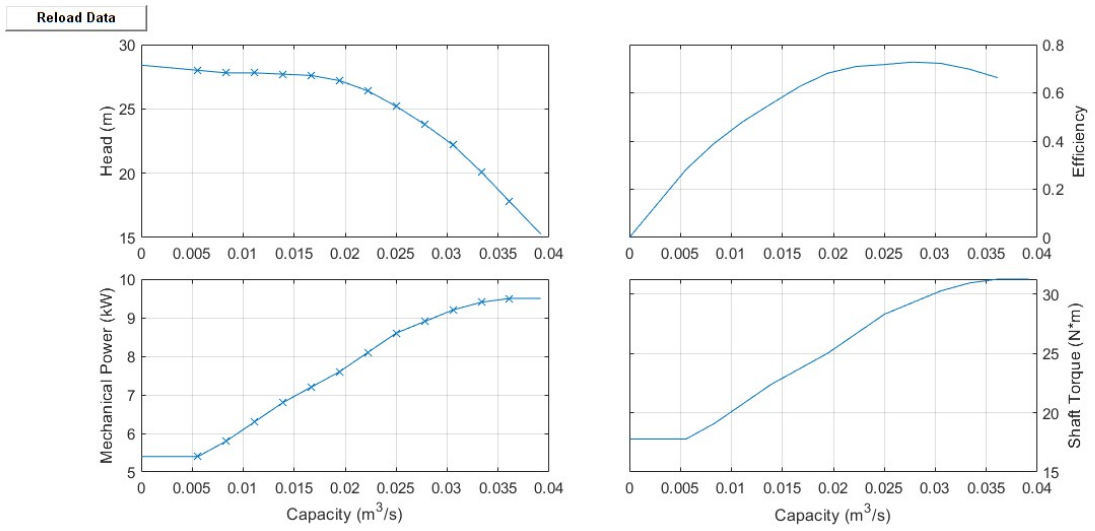

Figure 2.7: Tabulated data for pump PU05 showing the pressure increase, efficiency, mechanical power and shaft torque

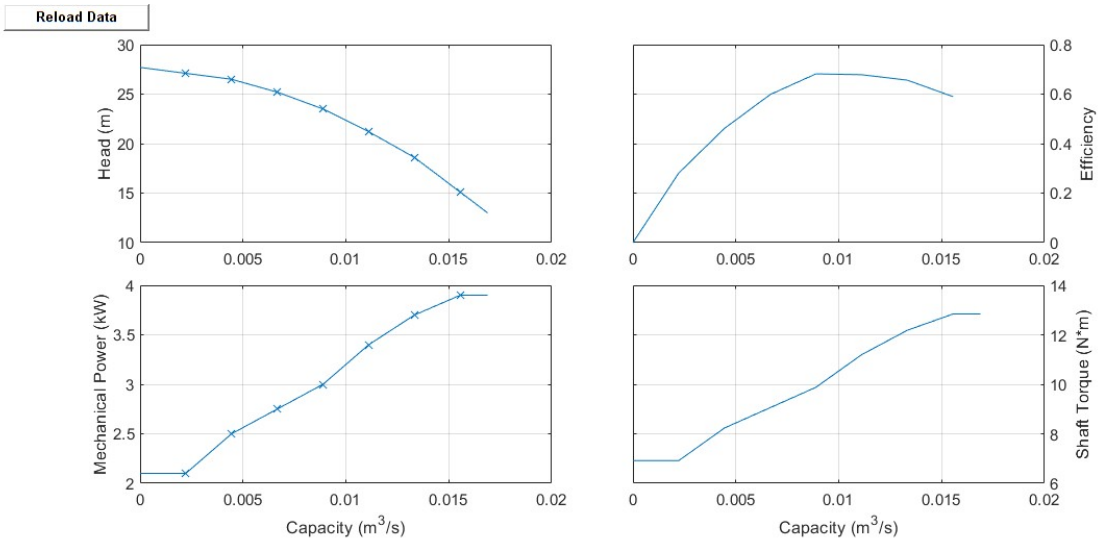

Figure 2.8: Tabulated data for pump PU06 showing the pressure increase, efficiency, mechanical power and shaft torque

2.5. Heat exchanger model

The specific dissipation ξ of both heat exchangers needs to be calculated to model the heat exchangers. ξ is a 2D array calculated by varying the flow of the warm and cold streams through the heat exchanger. Both flows vary from 0.01% to 110% of the nominal flow with steps of 10%. Effectiveness and number of transfer units as described by A.F. Mills and C.F.M. Coimbra [23] was used to calculate the value of ξ for these 144 different flow conditions. The heat transfer coefficient U needs to be calculated for both heat exchangers. The first step is to calculate the thermal capacities C_H and C_C of the hot and cold flow, respectively. These are the product of the mass flow rate and the heat capacity of the fluid as shown in equation 2.15.

$$C_H = \dot{m}_H c_{p,H} \tag{2.15}$$

Using equation 2.16, the capacity ratio R_C can be determined as it is the ratio between the highest value and the lowest value of C_H and C_C. The effectiveness of the heat exchanger ε can be calculated using equation 2.17 as it corresponds to the ratio between the actual heat transfer happening within the heat exchanger and the maximum possible heat transfer based on the lowest thermal capacity and maximum temperature difference.

$$R_C = \frac{C_{min}}{C_{max}} \tag{2.16}$$

$$\varepsilon = \frac{C_H(T_{H\_in} - T_{H\_out})}{C_{min}(T_{H\_in} - T_{C\_in})} \tag{2.17}$$

In turn, the number of transfer units, NTU, and the heat transfer coefficient, U, can be calculated using equations 2.18 and 2.19. The area A is the heat transfer area of the heat exchanger. The results for these calculations are displayed in table 2.6 for HE1 and in table 2.7 for HE2. The validated nominal condition of the heat exchangers was used for these calculations.

$$NTU = \frac{1}{1 - R_C} \ln\left(\frac{1 - \varepsilon R_C}{1 - \varepsilon}\right) \tag{2.18}$$

$$U = \frac{NTU C_{min}}{A} \tag{2.19}$$

Table 2.6: Calculation results of U for HE1

T_{H_in}	65	[°C]
T_{H_out}	40	[°C]
T_{C_in}	25	[°C]
T_{C_out}	44	[°C]
C_H	57104	[W/K]
C_C	77333	[W/K]
R_C	0.738	[-]
ε	0.625	[-]
NTU	1.38	[-]
A_{HE1}	15.56	[m^2]
U_{HE1}	5077	[W/(m^{2}K)]

Table 2.7: Calculation results of U for HE2

T_{H_in}	65	[°C]
T_{H_out}	40	[°C]
T_{C_in}	25	[°C]
T_{C_out}	44	[°C]
C_H	28552	[W/K]
C_C	38672	[W/K]
R_C	0.738	[-]
ε	0.625	[-]
NTU	1.38	[-]
A_{HE1}	7.91	[m^2]
U_{HE1}	4993	[W/(m^{2}K)]

The order of calculations made above is reversed to calculate the specific dissipation ξ for all 144 flow scenarios. U is now known and T_{H_out} and T_{C_out} are unknown. Either of these two temperatures must be calculated to calculate ξ. Equations 2.17, 2.18 and 2.19 are rearranged such that they solve for T_{H_out}, ε and NTU respectively. With T_{H_out} known, the total heat transfer per second Q can be calculated with equation 2.20. From equation 2.11 ξ can be calculated by dividing Q by the difference between T_{H_in} and T_{C_in}.

$$Q = C_H(T_{H\_in} - T_{H\_out}) \tag{2.20}$$

3

Optimisation models

Based on the model from chapter 2, two different optimisation models were made. The steady-state optimiser, explained in section 3.1, aims to provide an optimal configuration of the river water pumps, coolant circulation pumps, and the three-way valve based on the heat load of the fuel cell units and river water temperature. Compared to this, the current-state optimiser, explained in section 3.2, also takes the current state of the temperature of the fuel cell units and the coolant into account for multiple time steps. The chapter closes with section 3.3, which is about the differences between the values of variables obtained from the optimiser models and those variables measured in the Simulink model.

3.1. Steady-state optimiser

The steady-state optimiser works based on the idea that with a known heat load of the fuel cell units and river water temperature, the optimiser can determine the configuration of the river water pumps, coolant circulation pumps, and the three-way valve that results in the lowest power consumption of the cooling system. To achieve this, a Mixed Integer Quadratically Constrained Program (MIQCP) model was constructed. Section 3.1.1 provides the mathematical model for the 6 fuel cell units variant with sections 3.1.2 and 3.1.3 showing the changes made to the mathematical model to adapt it to 4 and 2 active fuel cell units respectively.

3.1.1. Steady-state optimiser mathematical model

This section explains the mathematical model for the 6 fuel cell units variant of the steady-state optimiser. The constant parameters are shown in table 3.1. Worth noting is that the heat load of the fuel cell units, $heat_{fc}$, and the river water temperature, T_C, have no set value in this table as they change depending on the simulation. During the optimisation, they are, however, constant.

The variables that are changed by the optimisation model are shown in table 3.2. The main variables are n_{PU01}, n_{PU02}, n_{PU05}, n_{PU06} and n_{valve} as they are the variables that correspond to the optimal cooling system configuration. Variables like $flow_{bp\_2}$ are included in the model so it can cope with multiplying more than two variables at once, as without introducing intermediate variables, an MIQCP model is incapable of doing that.

Table 3.1: Steady-state parameters

Parameters			
Name	Description	Value	Unit
ρ_{EG}	Density of 50% ethylene glycol	1057	[kg/m^3]
$c_{p,EG}$	Specific heat capacity of 50% ethylene glycol	3473	[J/(kg·K)]
Cd	Discharge coefficient	0.7	[-]
kPa_head	Conversion factor from kPa to head	0.102	[-]
A_{max}	Maximum area of the orifice of the three-way valve	0.0088	[m^2]
A	Total area of the three-way valve	0.0092	[m^2]
$heat_{fc}$	Heat load of a fuel cell unit	-	[W]
P_{PU01}	Power of pump PU01	3.67	[kW]
P_{PU02}	Power of pump PU02	1.96	[kW]
P_{PU05_nom}	Power of pump PU05	7	[kW]
T_C	Temperature of the river water	-	[°C]
K_1	Pressure drop coefficient for only section 1 of the cooling system	0.0071	[mH2O/(kg/s)^2]
K_2	Pressure drop coefficient for only section 2 of the cooling system	0.0266	[mH2O/(kg/s)^2]
K_{1_2}	Pressure drop coefficient for sections 1 and 2 of the cooling system	0.0031	[mH2O/(kg/s)^2]
K_3	Pressure drop coefficient for section 3 of the cooling system	6.17e-4	[mH2O/(kg/s)^2]
K_4	Pressure drop coefficient for section 4 of the cooling system	8.03e-5	[mH2O/(kg/s)^2]
K_{5_1}	Pressure drop coefficient for section 5_1 of the cooling system	8.91e-5	[mH2O/(kg/s)^2]
K_{5_2}	Pressure drop coefficient for section 5_2 of the cooling system	3.20e-4	[mH2O/(kg/s)^2]
K_{5_3}	Pressure drop coefficient for section 5_3 of the cooling system	2.81e-4	[mH2O/(kg/s)^2]
K_{5_4}	Pressure drop coefficient for section 5_4 of the cooling system	9.75e-4	[mH2O/(kg/s)^2]
K_{5_5}	Pressure drop coefficient for section 5_5 of the cooling system	0.0089	[mH2O/(kg/s)^2]
K_6	Pressure drop coefficient for section 6 of the cooling system	1.229	[mH2O/(kg/s)^2]
K_{7_1}	Pressure drop coefficient for section 7_1 of the cooling system	2.91e-4	[mH2O/(kg/s)^2]
K_{7_2}	Pressure drop coefficient for section 7_2 of the cooling system	8.91e-5	[mH2O/(kg/s)^2]
K_{7_3}	Pressure drop coefficient for section 7_3 of the cooling system	3.20e-4	[mH2O/(kg/s)^2]
K_{7_4}	Pressure drop coefficient for section 7_4 of the cooling system	2.81e-4	[mH2O/(kg/s)^2]
K_{7_5}	Pressure drop coefficient for section 7_5 of the cooling system	9.75e-4	[mH2O/(kg/s)^2]
K_{7_6}	Pressure drop coefficient for section 7_6 of the cooling system	0.0089	[mH2O/(kg/s)^2]
K_8	Pressure drop coefficient for section 8 of the cooling system	1.06e-4	[mH2O/(kg/s)^2]
K_9	Pressure drop coefficient for section 9 of the cooling system	2.08e-4	[mH2O/(kg/s)^2]
K_{10}	Pressure drop coefficient for section 10 of the cooling system	0.0135	[mH2O/(kg/s)^2]
K_{11}	Pressure drop coefficient for section 11 of the cooling system	0.0507	[mH2O/(kg/s)^2]

Table 3.2: Steady-state variables

Variables		
Name	Description	Unit
n_{PU05}	Continuous variable between 0 and 1 in relation to the current rmp of pump PU05	[−]
n_{PU05_2}	Continuous variable of n_{PU05} squared	[−]
n_{PU05_3}	Continuous variable of n_{PU05} cubed	[−]
n_{PU06}	Binary variable that is equal to 1 if pump PU06 is on	[−]
n_{PU01}	Binary variable that is equal to 1 if pump PU01 is on	[−]
n_{PU02}	Binary variable that is equal to 1 if pump PU02 is on	[−]
n_{PU05_on}	Binary variable that is equal to 1 if pump PU05 is on	[−]
n_{both_on}	Binary variable that is equal to 1 if pumps PU05 and PU06 are on	[−]
n_{only_PU05}	Binary variable that is equal to 1 if only pump PU05 is on	[−]
n_{only_PU06}	Binary variable that is equal to 1 if only pump PU06 is on	[−]
n_{both_he}	Binary variable that is equal to 1 if pumps PU01 and PU02 are on	[−]
n_{only_he1}	Binary variable that is equal to 1 if only pump PU01 is on	[−]
n_{only_he2}	Binary variable that is equal to 1 if only pump PU02 is on	[−]
P_{PU05}	Continuous variable of the power of PU05	[kW]
P_{PU06}	Continuous variable of the power of PU05	[kW]
n_{valve}	Continuous variable between -1 and 1 in relation to the state of the three-way valve	[−]
$flow_{total}$	Continuous variable of the total coolant flow	[kg/s]
$flow_{he}$	Continuous variable of the coolant flow to the heat exchangers	[kg/s]
$flow_{he1}$	Continuous variable of the coolant flow to heat exchanger 1	[kg/s]
$flow_{he2}$	Continuous variable of the coolant flow to heat exchanger 2	[kg/s]
$flow_{bp}$	Continuous variable of the coolant flow through the bypass	[kg/s]
$flow_{PU05}$	Continuous variable of the coolant flow generated by pump PU05	[kg/s]
$flow_{PU06}$	Continuous variable of the coolant flow generated by pump PU06	[kg/s]
$flow_{PU05\_nom}$	Continuous variable of the nominal coolant flow generated by pump PU05	[kg/s]
$flow_{bp\_2}$	Continuous variable of $flow_{bp}$ squared	[kg^2/s^2]
$flow_{he\_2}$	Continuous variable of $flow_{he}$ squared	[kg^2/s^2]
T_{total}	Continuous variable of the coolant temperature entering the fuel cell units	[°C]
T_{fc}	Continuous variable of the coolant temperature exiting the fuel cell units	[°C]
T_{he1}	Continuous variable of the coolant temperature exiting heat exchanger 1	[°C]
T_{he2}	Continuous variable of the coolant temperature exiting heat exchanger 2	[°C]
ϵ_{he1}	Continuous variable of the effectiveness of heat exchanger 1	[−]
ϵ_{he2}	Continuous variable of the effectiveness of heat exchanger 2	[−]
$he1_{in\_on}$	Continuous variable of the temperature difference of the flows entering heat exchanger 1	[°C]
$he2_{in\_on}$	Continuous variable of the temperature difference of the flows entering heat exchanger 2	[°C]
$head_{total}$	Continuous variable of the total system head loss	[mH2O]
$head_8$	Continuous variable of the head loss through section 8	[mH2O]
$head_{10}$	Continuous variable of the head loss through section 10	[mH2O]
$head_{11}$	Continuous variable of the head loss through section 11	[mH2O]
$head_{max}$	Continuous variable of the maximum value between $head_{10}$ and $head_{11}$	[mH2O]
$head_{he}$	Continuous variable of the head loss through the heat exchanger section	[mH2O]
$head_{PU05}$	Continuous variable of the head generated by pump PU05	[mH2O]
$head_{PU06}$	Continuous variable of the head generated by pump PU06	[mH2O]
$head_{PU05_nom}$	Continuous variable of the nominal head generated by pump PU05	[mH2O]
$head_{AP}$	Continuous variable of the head loss in the three-way valve leading to the bypass	[mH2O]
A_{AP}	Continuous variable of the orifice area of the three-way valve to the bypass	[m^2]
A_{AP2}	Continuous variable of A_{AP} squared	[m^4]
A_{AP_A2}	Continuous variable of A_{AP} divided by A squared	[−]
$head_{AT}$	Continuous variable of the head loss in the three-way valve to the heat exchangers	[mH2O]
A_{AT}	Continuous variable of the orifice area of the three-way valve to the heat exchangers	[m^2]
A_{AT2}	Continuous variable of A_{AT} squared	[m^4]
A_{AT_A2}	Continuous variable of A_{AT} divided by A squared	[−]

The mathematical formulation then follows as:

$$\min \quad P_{PU01}n_{PU01} + P_{PU02}n_{PU02} + P_{PU05}n_{PU05\_on} + P_{PU06}n_{PU06} \tag{3.1}$$

Subject to:

$$0.0000001 \geq n_{PU05} - 5 * n_{PU05\_on} \tag{3.2}$$
$$0.0000001 \leq n_{PU05} + 5 * (1 - n_{PU05\_on}) \tag{3.3}$$
$$0.0000001 \geq flow_{PU06} - 50 * n_{PU06} \tag{3.4}$$
$$0.0000001 \leq flow_{PU06} + 50 * (1 - n_{PU06}) \tag{3.5}$$
$$n_{both\_on} = n_{PU06} * n_{PU05\_on} \tag{3.6}$$
$$1.0001 \geq n_{PU01} + n_{PU02} - 5 * n_{both\_he} \tag{3.7}$$
$$1.0001 \leq n_{PU01} + n_{PU02} + 5 * (1 - n_{both\_he}) \tag{3.8}$$
$$n_{both\_he} = 0 \implies n_{only\_he1} = n_{PU01} \tag{3.9}$$
$$n_{both\_he} = 0 \implies n_{only\_he2} = n_{PU02} \tag{3.10}$$
$$n_{both\_he} = 1 \implies n_{only\_he1} = 0 \tag{3.11}$$
$$n_{both\_he} = 1 \implies n_{only\_he2} = 0 \tag{3.12}$$
$$flow_{he} = flow_{he1} + flow_{he2} \tag{3.13}$$
$$n_{both\_he} = 1 \implies flow_{he1} = 2 * flow_{he2} \tag{3.14}$$
$$n_{only\_he1} = 1 \implies flow_{he2} = 0 \tag{3.15}$$
$$n_{only\_he2} = 1 \implies flow_{he1} = 0 \tag{3.16}$$
$$A_{AP} = (A_{max}/2) * (1 + n_{valve}) + 0.00001 \tag{3.17}$$
$$A_{AP2} = A_{AP} * A_{AP} \tag{3.18}$$
$$A_{AP\_A2} = (A_{AP}/A) * (A_{AP}/A) \tag{3.19}$$
$$head_{AP} * (Cd * Cd * A_{AP2} * 2 * \rho_{EG}) = (1 - A_{AP\_A2}) * flow_{bp\_2} * kPa\_head/1000 \tag{3.20}$$
$$A_{AT} = (A_{max}/2) * (1 - n_{valve}) + 0.00001 \tag{3.21}$$
$$A_{AT2} = A_{AT} * A_{AT} \tag{3.22}$$
$$A_{AT\_A2} = (A_{AT}/A) * (A_{AT}/A) \tag{3.23}$$
$$head_{AT} * (Cd * Cd * A_{AT2} * 2 * \rho_{EG}) = (1 - A_{AT\_A2}) * flow_{he\_2} * kPa\_head/1000 \tag{3.24}$$
$$flow_{total} = flow_{bp} + flow_{he} \tag{3.25}$$
$$flow_{bp\_2} = flow_{bp} * flow_{bp} \tag{3.26}$$
$$flow_{he\_2} = flow_{he} * flow_{he} \tag{3.27}$$
$$head_8 = flow_{bp\_2} * K_8 + head_{AP} \tag{3.28}$$
$$head_{10} = flow_{he1} * flow_{he1} * K_{10} \tag{3.29}$$
$$head_{11} = flow_{he2} * flow_{he2} * K_{11} \tag{3.30}$$
$$head_{max} = max(head_{10} \quad head_{11}) \tag{3.31}$$
$$head_{he} = flow_{he\_2} * K_9 + head_{AT} + head_{max} \tag{3.32}$$
$$head_{he} = head_8 \tag{3.33}$$
$$n_{both\_on} = 0 \wedge n_{PU05} = 1 \implies head_{total} = flow_{total}^2 * (K_1) + flow_{total}^2 * (K_3 + K_4)$$
$$+ flow_{total}^2 * ((25/36) * K_{5\_1} + (4/9) * K_{5\_2} + (1/4) * K_{5\_3} + (1/9) * K_{5\_4} + (1/36) * K_{5\_5}$$
$$+ (1/36) * K_6 + K_{7\_1} + (25/36) * K_{7\_2} + (4/9) * K_{7\_3} + (1/4) * K_{7\_4} + (1/9) * K_{7\_5} + (1/36) * K_{7\_6})$$
$$+ flow_{bp\_2} * K_8 + head_{AP} \tag{3.34}$$
$$n_{both\_on} = 0 \wedge n_{PU06} = 1 \implies head_{total} = flow_{total}^2 * (K_2) + flow_{total}^2 * (K_3 + K_4)$$
$$+ flow_{total}^2 * ((25/36) * K_{5\_1} + (4/9) * K_{5\_2} + (1/4) * K_{5\_3} + (1/9) * K_{5\_4} + (1/36) * K_{5\_5}$$
$$+ (1/36) * K_6 + K_{7\_1} + (25/36) * K_{7\_2} + (4/9) * K_{7\_3} + (1/4) * K_{7\_4} + (1/9) * K_{7\_5} + (1/36) * K_{7\_6})$$
$$+ flow_{bp\_2} * K_8 + head_{AP} \tag{3.35}$$
$$n_{both\_on} = 1 \implies head_{total} = flow_{total}^2 * (K_{1\_2}) + flow_{total}^2 * (K_3 + K_4)$$
$$+ flow_{total}^2 * ((25/36) * K_{5\_1} + (4/9) * K_{5\_2} + (1/4) * K_{5\_3} + (1/9) * K_{5\_4} + (1/36) * K_{5\_5}$$
$$+ (1/36) * K_6 + K_{7\_1} + (25/36) * K_{7\_2} + (4/9) * K_{7\_3} + (1/4) * K_{7\_4} + (1/9) * K_{7\_5} + (1/36) * K_{7\_6})$$
$$+ flow_{bp\_2} * K_8 + head_{AP} \tag{3.36}$$

$$n_{PU05\_2} = n_{PU05} * n_{PU05} \tag{3.37}$$
$$n_{PU05\_3} = n_{PU05\_2} * n_{PU05} \tag{3.38}$$
$$flow_{PU05\_nom} = PWL(head_{PU05\_nom}) \tag{3.39}$$
$$flow_{PU06} = PWL(head_{PU06}) \tag{3.40}$$
$$P_{PU06} = 2 + flow_{PU06} * (1/8.81) \tag{3.41}$$
$$P_{PU05} = n_{PU05\_3} * (4.5 + flow_{PU05\_nom} * (1/6.851)) \tag{3.42}$$
$$flow_{PU05} = n_{PU05} * flow_{PU05\_nom} \tag{3.43}$$
$$head_{PU05} = n_{PU05\_2} * head_{PU05\_nom} \tag{3.44}$$
$$n_{PU05\_on} = 1 \implies head_{total} = head_{PU05} \tag{3.45}$$
$$n_{PU06} = 1 \implies head_{total} = head_{PU06} \tag{3.46}$$
$$flow_{total} = flow_{PU05} + flow_{PU06} \tag{3.47}$$
$$\varepsilon_{he1} = PWL(flow_{he1}) \tag{3.48}$$
$$\varepsilon_{he2} = PWL(flow_{he2}) \tag{3.49}$$
$$he1_{in\_on} = (T_{fc} - T_C) * n_{PU01} \tag{3.50}$$
$$he2_{in\_on} = (T_{fc} - T_C) * n_{PU02} \tag{3.51}$$
$$T_{he1} = -\varepsilon_{he1} * he1_{in\_on} + (T_{fc}) \tag{3.52}$$
$$T_{he2} = -\varepsilon_{he2} * he2_{in\_on} + (T_{fc}) \tag{3.53}$$
$$heat_{fc} \leq ((flow_{total}/6) * c_{p,EG}) * (65 - (T_{total} + 1.4)) \tag{3.54}$$
$$T_{total} * (flow_{total} * (1/6) * c_{p,EG}) = (T_{fc}) * (flow_{total} * (1/6) * c_{p,EG}) - heat_{fc} \tag{3.55}$$
$$T_{total} * flow_{total} = flow_{he1} * T_{he1} + flow_{he2} * T_{he2} + flow_{bp} * T_{fc} \tag{3.56}$$

Objective function 3.1 aims to minimise the total power used by the river water pumps PU01 and PU02 and the coolant circulation pumps PU05 and PU06. The constraints can be categorised into five sets of constraints. Constraints 3.2 - 3.16 keep track of which pumps are active and how that affects the flow through the heat exchangers. Constraints 3.17 - 3.24 determine the pressure drop over the three-way valve. Constraints 3.25 - 3.36 regard the system pressure drop and how this affects the flow. Constraints 3.37 - 3.47 are the coolant circulation pump calculations. Finally, constraints 3.48 - 3.56 are the system heat balance constraints.

Constraints 3.2 and 3.3 ensure that n_{PU05_on} equals 1 if pump PU05 is active. Constraints 3.4 and 3.5 ensure that there is basically no flow generated by pump PU06 if turned off. Constraint 3.6 sets the variable n_{both_on} to 1 if both pump PU05 and PU06 are active. Constraints 3.7 - 3.16 regulate the flow through the heat exchangers. Constraints 3.7 and 3.8 ensure that variable n_{both_he} is equal to 1 if both heat exchangers are active. Constraints 3.9 - 3.12 assign a value of either 1 or 0 to variables n_{only_he1} and n_{only_he2} based on the value of n_{both_he}. Constraint 3.13 enforces that the sum of the flow into the two heat exchangers equals the total flow into the heat exchanger section of the cooling system. Constraint 3.14 ensures that if both heat exchangers are active, the flow into heat exchanger 1 is twice that of heat exchanger 2. Constraints 3.15 and 3.16 set the flow of the inactive heat exchanger to 0.

Constraint 3.17 calculates the area of the orifice of the three-way valve leading to the bypass corresponding to equation 2.8. Constraints 3.18 and 3.19 square the variables A_{AP} and $\frac{A_{AP}}{A}$ respectively. Constraint 3.20 calculates the value of the variable for the pressure drop in meter water column $head_{AP}$ according to equation 2.7. Constraint 3.21 calculates the area of the orifice of the three-way valve leading to the bypass corresponding to equation 2.8. Constraints 3.22 and 3.23 square the variables A_{AT} and $\frac{A_{AT}}{A}$ respectively. Constraint 3.24 calculates the value of the variable for the pressure drop in meter water column $head_{AT}$ according to equation 2.7.

Constraint 3.25 ensures that the flow to the heat exchanger section of the cooling system and the flow through the bypass sum to the total system flow. Constraints 3.26 and 3.27 square the variables for the flow through the bypass $flow_{bp}$ and the flow to the heat exchangers $flow_{he}$. Constraints 3.28, 3.29, and 3.30 calculate the pressure drop in meter water column for sections 8, 10, and 11 of the cooling system.

Constraint 3.31 sets the value of variable $head_{max}$ equal to the highest value between variables $head_{10}$ and $head_{11}$. Constraint 3.32 calculates the total pressure drop through the heat exchanger section of the cooling system. Constraint 3.33 ensures that the pressure drop through the heat exchanger section of the cooling system is equal to the pressure drop through the bypass. Constraints 3.34, 3.35 and 3.36 calculate the total pressure drop in the system $head_{total}$ for only PU05 active, only PU06 active and both circulation pumps active, respectively.

Constraints 3.37 and 3.38 square and cube variable n_{PU05}. Constraint 3.39 is a piecewise linear constraint where, with the use of a piecewise linear function, a value of $flow_{PU05\_nom}$ can be derived from a value of $head_{PU05\_nom}$ and vice versa. Constraint 3.40 is a piecewise linear constraint where, with the use of a piecewise linear function, a value of $flow_{PU06}$ can be derived from a value of $head_{PU06}$ and vice versa. Constraint 3.41 calculates the power usage of pump PU06. Constraint 3.42 calculates the power usage of pump PU05. Constraints 3.43 and 3.44 adjust the flow and pressure increase through pump PU05 based on the pump speed. Constraints 3.45 and 3.46 ensure that the pressure generated by the pumps equals the total system pressure drop if the pump is active for both pump PU05 and pump PU06. Constraint 3.47 determines that the total system flow equals the sum of the flows generated by the circulation pumps.

Constraint 3.48 is a piecewise linear constraint where, with the use of a piecewise linear function, a value of ε_{he1} can be derived from a value of $flow_{he1}$. Constraint 3.49 is a piecewise linear constraint where, with the use of a piecewise linear function, a value of ε_{he2} can be derived from a value of $flow_{he2}$. Constraints 3.50 and 3.51 calculate the temperature difference at the inlet of the respective heat exchanger multiplied by the binary variable for the state of the river water pumps to ensure that the value is equal to 0 if the pumps are off. Constraints 3.52 and 3.53 calculate the temperature of the coolant leaving the heat exchangers. Constraint 3.54 ensures that coolant with enough cooling capacity flows through the fuel cell unit with an additional temperature buffer of 1.4 °C. Constraint 3.55 is the heat balance over a single fuel cell unit. Constraint 3.56 is the heat balance of the combined flows of the heat exchanger section of the cooling system and the bypass.

The variables for flow, power, head, and the three-way valve all have a lower bound of 0 to prevent reverse flow from being considered by the optimisation model. Furthermore, the total flow $flow_{total}$ has a lower bound of 12 kg/s, which ensures a flow of 2 kg/s through the fuel cell units.

3.1.2. 4 active fuel cell units variant

Adapting the model to 4 active fuel cell units requires changes to the constraints that deal with the flow through the fuel cell units. This leads to constraints 3.34 - 3.36, 3.54 and 3.55 being changed as followed:

$$\begin{aligned} &n_{both\_on} = 0 \wedge n_{PU05} = 1 \implies head_{total} = flow_{total}^2 * (K_1) + flow_{total}^2 * (K_3 + K_4) \\ &+ flow_{total}^2 * ((9/16) * K_{5\_1} + (1/4) * K_{5\_2} + (1/16) * K_{5\_3} \\ &+ (1/16) * K_6 + K_{7\_1} + (9/16) * K_{7\_2} + (1/4) * K_{7\_3} + (1/16) * K_{7\_4}) \\ &+ flow_{bp\_2} * K_8 + head_{AP} \end{aligned} \tag{3.57}$$

$$\begin{aligned} &n_{both\_on} = 0 \wedge n_{PU06} = 1 \implies head_{total} = flow_{total}^2 * (K_2) + flow_{total}^2 * (K_3 + K_4) \\ &+ flow_{total}^2 * ((9/16) * K_{5\_1} + (1/4) * K_{5\_2} + (1/16) * K_{5\_3} \\ &+ (1/16) * K_6 + K_{7\_1} + (9/16) * K_{7\_2} + (1/4) * K_{7\_3} + (1/16) * K_{7\_4}) \\ &+ flow_{bp\_2} * K_8 + head_{AP} \end{aligned} \tag{3.58}$$

$$\begin{aligned} &n_{both\_on} = 1 \implies head_{total} = flow_{total}^2 * (K_{1\_2}) + flow_{total}^2 * (K_3 + K_4) \\ &+ flow_{total}^2 * ((9/16) * K_{5\_1} + (1/4) * K_{5\_2} + (1/16) * K_{5\_3} \\ &+ (1/16) * K_6 + K_{7\_1} + (9/16) * K_{7\_2} + (1/4) * K_{7\_3} + (1/16) * K_{7\_4}) \\ &+ flow_{bp\_2} * K_8 + head_{AP} \end{aligned} \tag{3.59}$$

$$heat_{fc} \leq ((flow_{total}/4) * c_{p,EG}) * (65 - (T_{total} + 3)) \tag{3.60}$$

$$T_{total} * (flow_{total} * (1/4) * c_{p,EG}) = (T_{fc}) * (flow_{total} * (1/4) * c_{p,EG}) - heat_{fc} \tag{3.61}$$

The main change is removing parts of the cooling system that aren't active, which results in removing some terms and dividing by 4 rather than 6. An additional change is that in constraint 3.60 $(T_{total} + 1.4)$

is changed to $(T_{total} + 3)$. Having a 3-degree temperature buffer with 6 fuel cell units is not viable as there are scenarios where the heat exchangers don't have enough cooling capacity. Therefore, the buffer was set to 1.4 °C as this was the maximum allowable buffer. The lower bound for $flow_{total}$ has been lowered to 8 kg/s.

3.1.3. 2 active fuel cell units variant

Adapting the model to 2 active fuel cell units requires changes to the constraints that deal with the flow through the fuel cell units. This leads to constraints 3.34 - 3.36, 3.54 and 3.55 being changed as followed:

$$n_{both\_on} = 0 \wedge n_{PU05} = 1 \implies head_{total} = flow_{total}^2 * (K_1) + flow_{total}^2 * (K_3 + K_4)$$
$$+ flow_{total}^2 * ((1/4) * K_{5\_1} + (1/4) * K_6 + K_{7\_1} + (1/4) * K_{7\_2}) + flow_{bp\_2} * K_8 + head_{AP} \quad (3.62)$$
$$n_{both\_on} = 0 \wedge n_{PU06} = 1 \implies head_{total} = flow_{total}^2 * (K_2) + flow_{total}^2 * (K_3 + K_4)$$
$$+ flow_{total}^2 * ((1/4) * K_{5\_1} + (1/4) * K_6 + K_{7\_1} + (1/4) * K_{7\_2}) + flow_{bp\_2} * K_8 + head_{AP} \quad (3.63)$$
$$n_{both\_on} = 1 \implies head_{total} = flow_{total}^2 * (K_{1\_2}) + flow_{total}^2 * (K_3 + K_4)$$
$$+ flow_{total}^2 * ((1/4) * K_{5\_1} + (1/4) * K_6 + K_{7\_1} + (1/4) * K_{7\_2}) + flow_{bp\_2} * K_8 + head_{AP} \quad (3.64)$$
$$heat_{fc} \leq ((flow_{total}/2) * c_{p,EG}) * (65 - (T_{total} + 3)) \quad (3.65)$$
$$T_{total} * (flow_{total} * (1/2) * c_{p,EG}) = (T_{fc}) * (flow_{total} * (1/2) * c_{p,EG}) - heat_{fc} \quad (3.66)$$

The main change is removing parts of the cooling system that aren't active, which results in removing some terms and dividing by 2 rather than 6. Like with 4 fuel cell units, constraint 3.65 has a buffer of 3 °C. The lower bound for $flow_{total}$ has been lowered to 4 kg/s.

3.2. Current-state optimiser

The current-state optimiser is an expansion of the steady-state optimiser. Rather than basing the optimisation result on just external factors like the steady-state optimiser, the current-state optimiser takes into account the current state of the cooling system by way of integrating the current temperature of the fuel cell units, the coolant entering the fuel cell units and the coolant leaving the fuel cell units. Furthermore, to increase the ability of the model to control the temperature of the fuel cell units, the optimisation is run over multiple steps. This is to ensure that the optimisation model aims to maintain the fuel cell temperature at the reference temperature for extended periods of time rather than rushing to reach the reference temperature and subsequently overshooting or undershooting.

The current-state optimiser was split into two parts to improve computation speed. The first part is the heat flow optimiser, for which the mathematical model can be seen in section 3.2.1. This optimiser optimises the river water pump allocation and the coolant flow allocation through the three-way valve for multiple time steps. Section 3.2.2 shows the changes made to the heat flow optimiser to account for 2 and 4 active fuel cell units. The coolant flow allocation for the first time step is used in the coolant flow optimiser, which is explained in section 3.2.3. This optimiser provides the coolant circulation pump allocations and the three-way valve position to achieve the coolant flow from the first time step of the heat flow optimiser with the lowest power consumption of the coolant circulation pumps.

3.2.1. Current-state optimiser heat flow mathematical model

This section explains the mathematical model for the 6 fuel cell units variant of the current-state optimiser. Most parameters from table 3.1 also apply to the current-state optimiser. Table 3.3 shows the additional parameters required for the current-state optimiser. Table 3.4 shows the sets, indices, and variables used in the heat flow optimiser.

Table 3.3: Current-state parameters

Parameters			
Name	Description	Value	Unit
m_{fc}	Mass of a fuel cell unit	700	[kg]
$c_{p,fc}$	Specific heat capacity of a fuel cell unit	870	[J/(kg·K)]
$T_{fuelcell\_start,n}$	Initial temperature of fuel cell unit n	-	[°C]
T_{total_start}	Initial temperature of the coolant entering the fuel cell units	-	[°C]
T_{fc_start}	Initial temperature of the coolant exiting the fuel cell units	-	[°C]
$T_{fuelcell\_ref}$	Optimal fuel cell operating temperature	65	[°C]
Ts	Time step	60	[s]

Table 3.4: Current-state variables

Sets and indices		
I	Set containing the time steps	$i \in I$
N	Set containing the number of active fuel cell units	$n \in N$
Variables		
Name	Description	Unit
$n_{PU01,i}$	Binary variable that is equal to 1 if pump PU01 is on for time step i	[−]
$n_{PU02,i}$	Binary variable that is equal to 1 if pump PU02 is on for time step i	[−]
$n_{both\_he,i}$	Binary variable that is equal to 1 if pumps PU01 and PU02 are on for time step i	[−]
$n_{valve,i}$	Continuous variable between 0.01 and 0.99 in relation to the state of the three-way valve for time step i	[−]
$flow_{total,i}$	Continuous variable of the total coolant flow for time step i	[kg/s]
$flow_{he1,i}$	Continuous variable of the coolant flow to heat exchanger 1 for time step i	[kg/s]
$flow_{he2,i}$	Continuous variable of the coolant flow to heat exchanger 2 for time step i	[kg/s]
$flow_{bp,i}$	Continuous variable of the coolant flow through the bypass for time step i	[kg/s]
$T_{total,i}$	Continuous variable of the coolant temperature entering the fuel cell units for time step i	[°C]
$T_{fc,i}$	Continuous variable of the coolant temperature exiting the fuel cell units for time step i	[°C]
$T_{he1,i}$	Continuous variable of the coolant temperature exiting heat exchanger 1 for time step i	[°C]
$T_{he2,i}$	Continuous variable of the coolant temperature exiting heat exchanger 2 for time step i	[°C]
$T_{fuelcell,n,i}$	Continuous variable for the temperature of fuel cell unit n at time step i	[°C]
$Q_{fuelcell,n,i}$	Continuous variable for the total energy exchanged from fuel cell unit n to the cooling system during time step i	[J]
$n\_T_{fuelcell,n,i}$	Binary variable that is 1 when the temperature of fuel cell unit n at time step i exceeds $T_{fuelcell\_ref}$	[−]
$\epsilon_{he1,i}$	Continuous variable of the effectiveness of heat exchanger 1 for time step i	[−]
$\epsilon_{he2,i}$	Continuous variable of the effectiveness of heat exchanger 2 for time step i	[−]
$he1_{in\_on,i}$	Continuous variable of the temperature difference of the flows entering heat exchanger 1 for time step i	[°C]
$he2_{in\_on,i}$	Continuous variable of the temperature difference of the flows entering heat exchanger 2 for time step i	[°C]

The mathematical formulation then follows as:

$$\begin{aligned}\min \quad & \sum_{i\in I}\sum_{n\in N}(10 * n\_T_{fuelcell,n,i}(T_{fuelcell,n} - T_{fuelcell\_ref}) \\ & + (1 - n\_T_{fuelcell,n,i})(T_{fuelcell\_ref} - T_{fuelcell,n}))+ \\ & \sum_{i\in I}(n_{PU01,i}P_{PU01} + n_{PU02,i}P_{PU02} + 4flow_{total,i}) \qquad \forall i \in I\ , \forall n \in N \end{aligned} \tag{3.67}$$

Subject to:

$$T_{fuelcell\_ref} \geq T_{fuelcell,n,i} - n\_T_{fuelcell,n,i} * 200 \qquad \forall i \in I\ , \forall n \in N \tag{3.68}$$

$$T_{fuelcell\_ref} \leq T_{fuelcell,n,i} + (1 - n\_T_{fuelcell,n,i}) * 200 \qquad \forall i \in I\ , \forall n \in N \tag{3.69}$$

$$flow_{he1,i} \leq flow_{total,i} * n_{PU01,i} \qquad \forall i \in I \tag{3.70}$$

$$flow_{he2,i} \leq flow_{total,i} * n_{PU02,i} \qquad \forall i \in I \tag{3.71}$$

$$n_{both\_he,i} = n_{PU01,i} * n_{PU02,i} \qquad \forall i \in I \tag{3.72}$$

$$n_{both\_he,i} = 1 \implies flow_{he1,i} = 2flow_{he2,i} \qquad \forall i \in I \tag{3.73}$$

$$flow_{total,i} = flow_{he1,i} + flow_{he2,i} + flow_{bp,i} \qquad \forall i \in I \tag{3.74}$$

$$flow_{total,i} * n_{valve,i} = flow_{he1,i} + flow_{he2,i} \qquad \forall i \in I \tag{3.75}$$

$$\varepsilon_{he1,i} = PWL(flow_{he1,i}) \qquad \forall i \in I \tag{3.76}$$

$$\varepsilon_{he2,i} = PWL(flow_{he2,i}) \qquad \forall i \in I \tag{3.77}$$

$$he1_{in\_on,1} = (\frac{T_{fc\_start} + T_{fc,1}}{2} - T_C) * n_{PU01,1} \tag{3.78}$$

$$he2_{in\_on,1} = (\frac{T_{fc\_start} + T_{fc,1}}{2} - T_C) * n_{PU02,1} \tag{3.79}$$

$$T_{he1,1} = -\varepsilon_{he1,1} * he1_{in\_on,1} + \frac{T_{fc\_start} + T_{fc,1}}{2} \tag{3.80}$$

$$T_{he2,1} = -\varepsilon_{he2,1} * he2_{in\_on,1} + \frac{T_{fc\_start} + T_{fc,1}}{2} \tag{3.81}$$

$$he1_{in\_on,i} = (\frac{T_{fc,i} + T_{fc,i-1}}{2} - T_C) * n_{PU01,i} \qquad i \in I \setminus \{1\} \tag{3.82}$$

$$he2_{in\_on,i} = (\frac{T_{fc,i} + T_{fc,i-1}}{2} - T_C) * n_{PU02,i} \qquad i \in I \setminus \{1\} \tag{3.83}$$

$$T_{he1,i} = -\varepsilon_{he1,i} * he1_{in\_on,i} + \frac{T_{fc,i} + T_{fc,i-1}}{2} \qquad i \in I \setminus \{1\} \tag{3.84}$$

$$T_{he2,i} = -\varepsilon_{he2,i} * he2_{in\_on,i} + \frac{T_{fc,i} + T_{fc,i-1}}{2} \qquad i \in I \setminus \{1\} \tag{3.85}$$

$$\begin{aligned} & T_{total,i} * flow_{total,i} * c_{p,EG} = T_{fc,i} * flow_{total,i} * c_{p,EG} \\ & - \sum_{n\in N}(Q_{fuelcell,n,i}/Ts) \qquad \forall i \in I\ , \forall n \in N \end{aligned} \tag{3.86}$$

$$T_{total,i} * flow_{total,i} = T_{he1,i} * flow_{he1,i} + T_{he2,i} * flow_{he2,i} + T_{fc,i} * flow_{bp,i} \qquad \forall i \in I \tag{3.87}$$

$$heat_{fc} * Ts - Q_{fuelcell,n,i} = (T_{fuelcell,n,i} - T_{fuelcell\_start}) * m_{fc} * c_{p,fc} \qquad \forall i \in I\ , \forall n \in N \tag{3.88}$$

$$heat_{fc} * Ts - Q_{fuelcell,n,i} = (T_{fuelcell,n,i} - T_{fuelcell,n,(i-1)}) * m_{fc} * c_{p,fc} \qquad \forall i \in I\ , \forall n \in N \tag{3.89}$$

$$Q_{fuelcell,n,1} \leq \frac{1}{6} flow_{total,1} * c_{p,EG} * (65 - (T_{total,1} - T_{total\_start})/2) * Ts \qquad \forall n \in N \tag{3.90}$$

$$\begin{aligned} & Q_{fuelcell,n,i} \leq \frac{1}{6} flow_{total,i} * c_{p,EG} * (65 - (T_{total,i} - T_{total,(i-1)})/2) * Ts \\ & \forall i \in I \setminus \{1\}, \forall n \in N \end{aligned} \tag{3.91}$$

Objective function 3.67 minimises the sum of three different components. The first set of sums is the deviation of the fuel cell temperature from the reference fuel cell temperature. If the fuel cell temperature is below the reference temperature, then the first term in the sum is equal to 0 as $n\_T_{fuelcell,n,i}$ will be

equal to 0, and the second term in the sum will have a value greater than 0. If the temperature of the fuel cell unit is higher than the reference temperature, the first term will have a value greater than 0, and the second term a value of 0 as $n\_T_{fuelcell,n,i}$ will be equal to 1. The temperature overshoot has been given an additional weighting of 10 to discourage the optimiser from giving a result where there is an overshoot in fuel cell temperature paired with a reduction in pump power usage. The second component of the objective function is the minimisation of the power consumption of the river water pumps PU01 and PU02. The final component minimises the total flow as this directly correlates with the power consumption of the coolant circulation pumps PU05 and PU06. The total flow has been given an additional weight of 4 to encourage the optimiser to keep the flow low, as the power of the circulation pumps outweighs the power usage of the river water pumps.

Constraints 3.68 and 3.69 set the value of $n\_T_{fuelcell,n,i}$ to 1 for fuel cell unit n during time step i if the temperature of the fuel cell unit exceeds the reference temperature and to 0 if the fuel cell temperature is lower than the reference temperature. Constraints 3.70 - 3.75 regulate the flow of the cooling system. Constraints 3.70 and 3.71 ensure that there is no coolant flow through a heat exchanger if the corresponding river water pump is inactive. Constraints 3.72 and 3.73 determine that if both heat exchangers are active, the flow through the larger heat exchanger HE1 is twice that of the smaller heat exchanger HE2. Constraint 3.74 is the flow balance over the three-way valve. Constraint 3.75 determines the amount of flow through the heat exchangers based on $n_{valve,i}$.

Constraint 3.76 is a piecewise linear constraint where, with the use of a piecewise linear function, a value of $\varepsilon_{he1,i}$ can be derived from a value of $flow_{he1,i}$. Constraint 3.77 is a piecewise linear constraint where, with the use of a piecewise linear function, a value of $\varepsilon_{he2,i}$ can be derived from a value of $flow_{he2,i}$. Constraints 3.78 and 3.79 calculate the temperature difference at the inlet of the respective heat exchanger multiplied by the binary variable for the state of the river water pumps to ensure that the value is equal to 0 if the pumps are off for the first time step of the optimisation. Constraints 3.80 and 3.81 calculate the temperature of the coolant leaving the heat exchangers for the first time step of the optimisation. Constraints 3.82 and 3.83 calculate the temperature difference at the inlet of the respective heat exchanger multiplied by the binary variable for the state of the river water pumps to ensure that the value is equal to 0 if the pumps are off for all but the first time step of the optimisation. Constraints 3.84 and 3.85 calculate the temperature of the coolant leaving the heat exchangers for all but the first time step of the optimisation.

Constraint 3.86 corresponds to the heat flow balance over the fuel cell units. Constraint 3.87 is the heat flow balance of the combined flows of the heat exchanger section of the cooling system and the bypass. Constraints 3.88 and 3.89 are the heat flow balance within the fuel cell units for the first time step and all other time steps, respectively. Constraints 3.90 and 3.91 ensure that there is enough cooling capacity flowing through the fuel cell units for the first time step and all other time steps, respectively.

The total flow has a lower bound of 12 kg/s and an upper bound of 24.15 kg/s. This is to ensure that there is a decent level of flow at all times so the system can respond in an adequate time frame. If the flow is very low, it can take up to a minute before the result of the changes made to the cooling system reaches the fuel cell units. The upper bound ensures that the coolant flow optimiser has a viable solution. The other flows have a lower bound of 0 to ensure no backflow in the system. The flow through HE1 has an upper bound of 16 kg/s and the flow through HE2 of 8 kg/s to ensure the viable solution with the coolant flow optimiser. $Q_{fuelcell,n,i}$ has an upper bound set to 120% of the heat generated by the fuel cell unit, $heat_{fc}$.

3.2.2. 2 and 4 active fuel cell units variants

The difference between the 6 fuel cell units variant and the 4 or 2 fuel cell units variant comes down to a numerical change in constraints 3.90 and 3.91 and some changes to the lower bounds and upper bounds. The $\frac{1}{6}$ term in constraints 3.90 and 3.91 gets changed to $\frac{1}{4}$ for the 4 fuel cell units variant and to $\frac{1}{2}$ for the 2 fuel cell units variant. The lower bound for the total flow is 8 kg/s for the 4 fuel cell units variant and 4 kg/s for the 2 fuel cell units variant. The upper bound for the total flow is 16.1 kg/s for the 4 fuel cell units variant and 8.05 kg/s for the 2 fuel cell units variant.

3.2.3. Current-state optimiser coolant flow mathematical model

The coolant flow optimiser is an adaptation of the steady-state optimiser from section 3.1. The heat-flow related constraints 3.48 - 3.56 and the bounds on the total flow have been removed. The changes with regards to constraints 3.34, 3.35 and 3.36 as mentioned in sections 3.1.2 and 3.1.3 are also applied for the 4 fuel cell units and the 2 fuel cell units variants of the coolant flow optimiser.

To incorporate the solution from the heat flow optimiser, the following constraints were added:

$$flow_{he1} = flow_{he1\_start} \tag{3.92}$$
$$flow_{he2} = flow_{he2\_start} \tag{3.93}$$
$$flow_{bp} \geq flow_{bp\_start} \tag{3.94}$$

Constraints 3.92, 3.93 and 3.94 ensure that the flow through the heat exchangers is equal to the flow through the heat exchangers during the first time step of the heat flow optimiser and that the flow through the bypass is equal or greater than during the first time step of the heat flow optimiser. $flow_{he1\_start}$, $flow_{he2\_start}$ and $flow_{bp\_start}$ are the flow values through the heat exchangers and bypass as determined in the first step of the heat flow optimiser.

3.3. Differences between the optimisation models and the Simscape model

Most constraints used in the optimisation models are a one-to-one copy of the equations behind the Simscape blocks as laid out in section 2.1. There are, however, two areas where the optimisation model has opted for a simplification. The first simplification is the pressure drop calculations, where both the steady-state optimiser and the current-state optimiser use K-values for their calculations. The second simplification is that the current-state optimiser does not take the liquid volume of the system into account.

The K-values are determined at a specific temperature and flow. For this research, the K-values for each section were determined at their nominal flow and a coolant temperature of 40 °C. The influence of the flow rate and the kinematic viscosity for section 3 of the cooling system can be seen in figure 3.1. The lower bounds on flow were, in part, implemented to prevent this simplification from becoming a significant problem, as when one lowers the flow rate, one also has to lower the temperature of that flow to keep the same cooling capacity. Both these actions increase pressure loss.

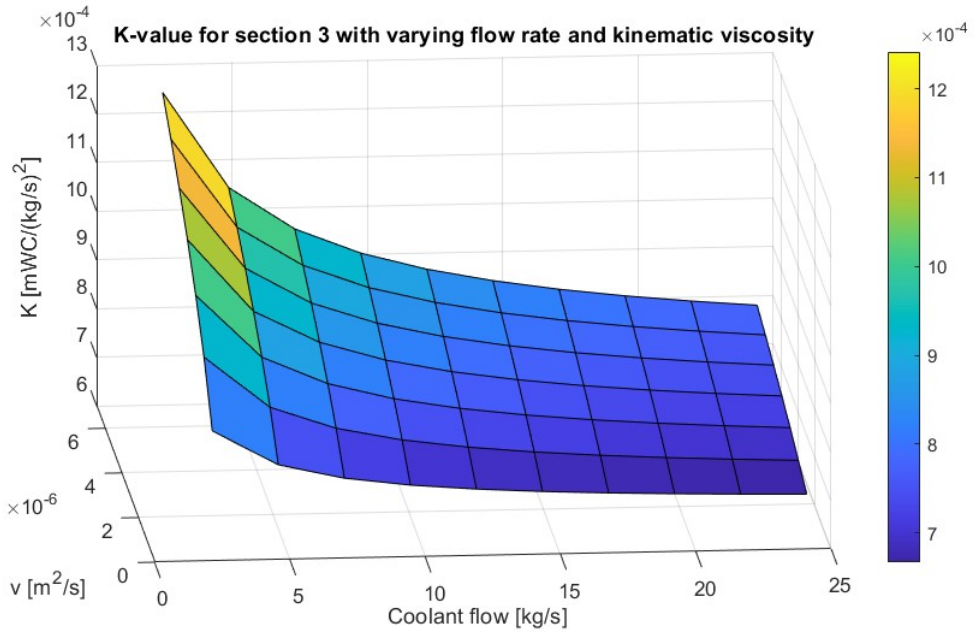

Figure 3.1: K-value for section 3 with varying flow rate and kinematic viscosity

When comparing the total flow of the steady-state solution from the optimiser and the total flow of the Simscape model in figure 3.2, it can seen that for most scenarios, the optimiser model overestimates the flow that is being generated. This is expected as with fewer fuel cell units active, the total flow is lower, thus increasing the relative pressure drop compared to the K-values, which have been determined using flow rates assuming 6 active fuel cell units.

In the Simscape model, the coolant can be categorised into three different categories. The first is the coolant that, at the time of a change in cooling system configuration, is being transported from the heat exchangers to the fuel cell units. This coolant can be considered the ”old” coolant as it was cooled according to the cooling system configuration of the previous time step. The second coolant category is the coolant that is being transported from the fuel cell units to the heat exchangers at the time of a change in cooling system configuration. This is coolant that was previously cooled and heated according to the cooling system configuration of the previous time step. The final category is the ”fresh” coolant, which is coolant of the previous two categories that has undergone a full circulation of the cooling system.

Accurately implementing these categories of coolant is possible as the flow and cooling system volume are known. However, after trying it out, it brought with it an increase in solving time for the optimisation problem that was deemed too much. With the current rendition, the current-state optimiser takes up to 5 seconds to find an optimal solution when given difficult starting values and three time steps. With the more accurate coolant calculations, there were scenarios where, after a minute, the optimiser had yet to find the optimal solution with two time steps.

The simplification of the coolant calculations can be seen in constraints 3.78 - 3.85 where the value for T_{fc} is the average of the starting temperature and the final temperature for that time step. Constraints 3.90 and 3.91 apply this same principle for T_{total}.

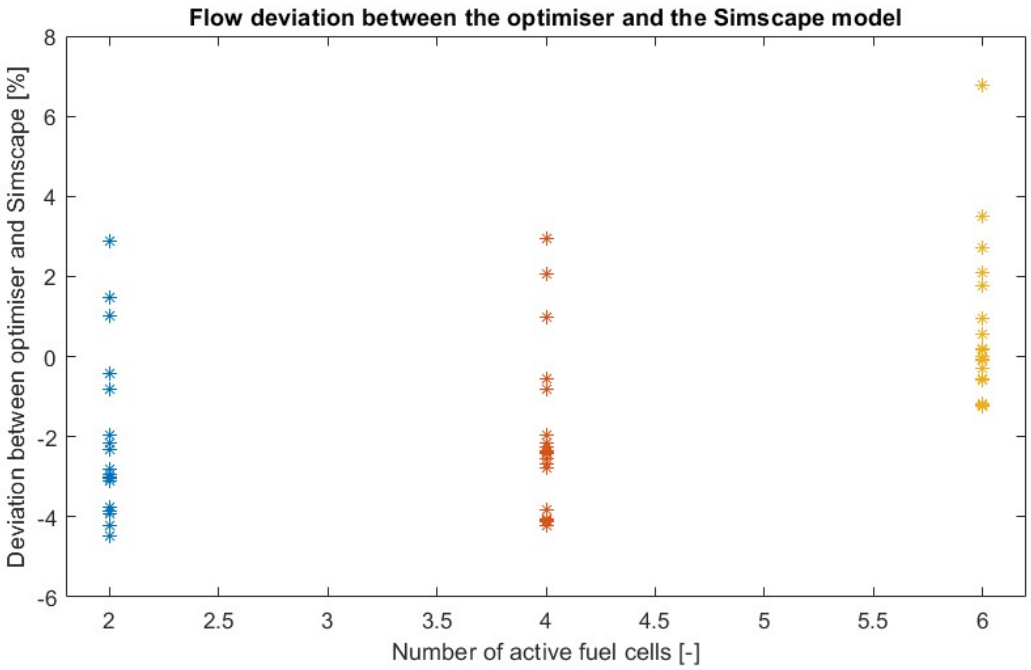

Figure 3.2: Flow deviation between the optimiser and the Simscape model for multiple scenarios

4

Control methods and simulations

This chapter will detail the different control methods used to control the cooling system in section 4.1. The chapter closes with section 4.2, which goes over the three types of simulations run to test the control methods.

4.1. Control methods

This section explains the seven control methods tested in this research. It starts with the more rudimentary methods of ”standard rule” and ”temperature difference,” which control based on one and two temperature measurements, respectively. Following this are ”load-based flow” and ”load-based pump”, which feature a basic algorithm to control based on one temperature measurement. The final three methods, ”lookup”, ”steady-state optimised”, and ”current-state optimised”, are based on the results of an optimiser or directly feature an optimisation model.

4.1.1. Standard rule

This method has been dubbed ”standard rule” as it is an evolution of the initially proposed rule set for this cooling system. The objective of this method is to control the cooling system based on the temperature of the coolant entering the fuel cell units. The temperature measurement is done in section 3 of the cooling system. The two river water pumps, the coolant circulation pump PU05, and the three-way valve are controlled by this control method with an interval of 60 seconds. Coolant circulation pump PU06 is always turned on with this rule set. A secondary rule set was added for river water temperatures at or below 15 °C as it seemed impossible to have one rule set capable of managing the temperature of the fuel cell units without massive overcooling in most scenarios. This additional rule set has the same base rules, but configures the cooling system differently such that the flow to the heat exchangers is reduced by 25%. Both rule sets maintain nominal flow through the fuel cell units in all scenarios. The flow through the heat exchangers does not exceed the nominal flow of that heat exchanger. For example, if there are 6 active fuel cell units and the measured temperature is 30 °C, the flow through HE1 shall be approximately 16 kg/s and the flow through the bypass approximately 8 kg/s.

The standard rule set is as follows:

$$
\begin{aligned}
T_{total} < 15°C &\implies no\ active\ heat\ exchangers \\
15°C \leq T_{total} \leq 25°C &\implies small\ heat\ exchanger\ active \\
25°C \leq T_{total} \leq 33°C &\implies large\ heat\ exchanger\ active \\
33°C \leq T_{total} &\implies both\ heat\ exchangers\ active
\end{aligned}
$$

4.1.2. Temperature difference

The control method, ”temperature difference”, is based on equation 2.20. If the flow through the fuel cell units is kept constant, then C_H is constant if one disregards the change in specific heat with a change in fluid temperature. With constant flow, one can directly correlate the heat load of the fuel cell

units with the temperature difference of the coolant over the fuel cell units. An additional temperature sensor is added before the three-way valve to achieve this. With this sensor and the one in sector 3, the temperature difference can be calculated. In the cooling system, there are three breakpoints, namely, the heat transfer of the heat exchangers. These breakpoints are at 700 kW, 1400 kW, and 2100 kW. The temperature difference brackets can be calculated from these breakpoints with the three nominal flows for 2, 4, and 6 active fuel cell units. A scenario with 2 active fuel cell units results in only 2 rules. In every case except when the fuel cell units are overheating, HE2 is active. This is because HE2 covers the first 700 kW bracket, the maximum nominal heat load of 2 fuel cell units.

To improve this method, a new assumption about the cooling system is explored. Pumps PU01 and PU02 are now assumed to be variable-speed pumps. Now, additional brackets can be added to lower the pump power used when the measured temperature difference is at the lower end of the initial brackets. The newly added breakpoints are at 350 kW, where pump PU02 runs at half speed, and 1050 kW, where pump PU01 runs at 75% speed.

The temperature brackets for 2 fuel cell units are:

$$\begin{aligned} \Delta T \leq 12°C &\implies n_{PU01} = 0,\ n_{PU02} = 0.5 \\ 12°C < \Delta T \leq 24°C &\implies n_{PU01} = 0,\ n_{PU02} = 1 \\ 24°C < \Delta T &\implies n_{PU01} = 1,\ n_{PU02} = 0 \end{aligned}$$

The temperature brackets for 4 fuel cell units are:

$$\begin{aligned} \Delta T \leq 6°C &\implies n_{PU01} = 0,\ n_{PU02} = 0.5 \\ 6°C < \Delta T \leq 12.4°C &\implies n_{PU01} = 0,\ n_{PU02} = 1 \\ 12.4°C < \Delta T \leq 18°C &\implies n_{PU01} = 0.75,\ n_{PU02} = 0 \\ 18°C < \Delta T \leq 24.8°C &\implies n_{PU01} = 1,\ n_{PU02} = 0 \\ 24.8°C < \Delta T &\implies n_{PU01} = 1,\ n_{PU02} = 1 \end{aligned}$$

The temperature brackets for 6 fuel cell units are:

$$\begin{aligned} \Delta T \leq 4°C &\implies n_{PU01} = 0,\ n_{PU02} = 0.5 \\ 4°C < \Delta T \leq 8.25°C &\implies n_{PU01} = 0,\ n_{PU02} = 1 \\ 8.25°C < \Delta T \leq 12°C &\implies n_{PU01} = 0.75,\ n_{PU02} = 0 \\ 12°C < \Delta T \leq 16.5°C &\implies n_{PU01} = 1,\ n_{PU02} = 0 \\ 16.5°C < \Delta T &\implies n_{PU01} = 1,\ n_{PU02} = 1 \end{aligned}$$

4.1.3. Load-based flow

This control method is based on the fact that the heat exchangers have been selected in a way that the small heat exchanger HE2 is capable of cooling 2 active fuel cell units, the large heat exchanger HE1 is capable of cooling 4 active fuel cell units, and together they are capable of cooling 6 active fuel cell units. So, rather than turning river water pumps on and off depending on the coolant's temperature, they are turned on or off depending on the amount of active fuel cell units.

This method alters the coolant flow to reduce the cooling system's power usage. The previous two methods used either the temperature of the coolant entering the fuel cell units or the temperature difference of the coolant over the fuel cell units. Neither of these measurements works, as knowing the flow is necessary to determine the state of the temperature of the fuel cell units definitively. A measurement that gives an inclination of the state of fuel cell units is the coolant temperature exiting the units. The nominal temperature for the fuel cell units is 65 °C. If the coolant exiting the fuel cell units is higher than 65 °C, then the temperature of the fuel cell units must also be higher than 65 °C as the fuel cell units can only heat coolant to its temperature. In this scenario, the cooling capacity of the cooling system needs to be increased; thus, the flow will be increased. If the temperature of the coolant exiting the fuel cell units is significantly lower than 65 °C, then there is an abundance of cooling capacity present in the cooling system, and thus, the flow can be lowered.

For this method to work, the control system has to know the state it is in. In the previous two methods, there was a clear if condition ”x” then system state ”y”; this method functions as if condition ”x” then system state ”y+1” or ”y-1” like operating a gearbox by telling it to go to the next gear. The gearbox needs to know which gear it is in before it can determine which gear it is supposed to go to. To achieve this in the control method, the variables k_2, k_4, and k_6 are introduced. These variables range from 1 to 4 in increasing flow rate and represent the state of the cooling system for 2, 4, and 6 active fuel cell units. The value for k that is currently not in use is set to 4 to ensure that there is always enough cooling when either more fuel cell units are turned on or when they are turned off. $k = 1$ means that the flow will be 50% of the nominal flow for that amount of active fuel cell units. This flow is increased by 16.7% for each 1 increase in k up to 100% of the nominal flow.

The rule set for 2 active fuel cell units:

$$\begin{aligned} k_4 = k_6 &= 4 \\ n_{PU01} &= 0 \\ n_{PU02} &= 1 \end{aligned}$$

$$\begin{aligned} T_{fc} > 65°C &\implies k_2 = 4 \\ T_{fc} > 64°C \ \wedge \ k_2 < 4 &\implies k_2 = k_2 + 1 \\ T_{fc} < 60°C \ \wedge \ k_2 > 1 &\implies k_2 = k_2 - 1 \end{aligned}$$

The rule set for 4 active fuel cell units:

$$\begin{aligned} k_2 = k_6 &= 4 \\ n_{PU01} &= 1 \\ n_{PU02} &= 0 \end{aligned}$$

$$\begin{aligned} T_{fc} > 65°C &\implies k_4 = 4 \\ T_{fc} > 64°C \ \wedge \ k_4 < 4 &\implies k_4 = k_4 + 1 \\ T_{fc} < 60°C \ \wedge \ k_4 > 1 &\implies k_4 = k_4 - 1 \end{aligned}$$

The rule set for 6 active fuel cell units:

$$\begin{aligned} k_2 = k_4 &= 4 \\ n_{PU01} &= 1 \\ n_{PU02} &= 1 \end{aligned}$$

$$\begin{aligned} T_{fc} > 65°C &\implies k_6 = 4 \\ T_{fc} > 64°C \ \wedge \ k_6 < 4 &\implies k_6 = k_6 + 1 \\ T_{fc} < 60°C \ \wedge \ k_6 > 1 &\implies k_6 = k_6 - 1 \end{aligned}$$

4.1.4. Load-based pump

Load-based pump is a combination of load-based flow and temperature difference. Where in temperature difference, the river water pumps were controlled based on the temperature difference of the coolant over the fuel cell units, in load-based pump, it is done similarly to how load-based flow does it. The number of active fuel cell units determines whether pumps PU01 and PU02 are active. Here, just like with temperature difference, these pumps are considered variable-speed pumps, and their speed is controlled. The flow of the coolant is kept nominal, both through the fuel cell units and heat exchangers. The same variables k_2, k_4 and k_6 are introduced, but here they range from 1 - 5 corresponding to 25%, 50%, 67%, 83%, and 100% of the flow of the active river water pumps.

The rule set for 2 active fuel cell units:

$$\begin{aligned} k_4 = k_6 &= 5 \\ n_{PU05} &= 0 \\ n_{PU06} &= 1 \\ n_{valve} &= -1 \end{aligned}$$

$$\begin{aligned} T_{fc} > 64°C &\implies k_2 = 5 \\ T_{fc} > 62°C \ \wedge \ k_2 < 5 &\implies k_2 = k_2 + 1 \\ T_{fc} < 54°C \ \wedge \ k_2 > 5 &\implies k_2 = k_2 - 1 \end{aligned}$$

The rule set for 4 active fuel cell units:

$$\begin{aligned} k_2 = k_6 &= 5 \\ n_{PU05} &= 0.938 \\ n_{PU06} &= 0 \\ n_{valve} &= -1 \end{aligned}$$

$$\begin{aligned} T_{fc} > 64°C &\implies k_4 = 5 \\ T_{fc} > 62°C \ \wedge \ k_4 < 5 &\implies k_4 = k_4 + 1 \\ T_{fc} < 54°C \ \wedge \ k_4 > 5 &\implies k_4 = k_4 - 1 \end{aligned}$$

The rule set for 6 active fuel cell units:

$$\begin{aligned} k_2 = k_4 &= 5 \\ n_{PU05} &= 0.982 \\ n_{PU06} &= 1 \\ n_{valve} &= -1 \end{aligned}$$

$$\begin{aligned} T_{fc} > 64°C &\implies k_6 = 5 \\ T_{fc} > 62°C \ \wedge \ k_6 < 5 &\implies k_6 = k_6 + 1 \\ T_{fc} < 54°C \ \wedge \ k_6 > 5 &\implies k_6 = k_6 - 1 \end{aligned}$$

4.1.5. Lookup

Lookup is based on a dataset of 363 different scenarios for which the steady-state solution has been determined using the steady-state optimiser as explained in section 3.1. These scenarios cover a range of 11 different river water temperatures starting at 5 °C with steps to 2 °C until 25 °C, 11 different heat loads starting at 50 kW with steps of 30 kW until 350 kW and the three different active fuel cell unit configurations. This control method requires a measurement of the river water temperature, a value for the heat load of the fuel cell units, and the number of active fuel cell units. The values for the river water temperature and the heat load are rounded up to the closest bracket within the data set to ensure that the system never inherently has too little cooling.

4.1.6. Steady-state optimised

This method uses the steady-state optimiser as explained in section 3.1 To calculate the optimal cooling system configuration based on the current heat load of the fuel cell units and the temperature of the river water. The optimiser runs every 60 seconds; however, when a change in heat load is detected by way of increasing or decreasing the fuel cell power, the optimiser will activate. The idea behind this is to differentiate it further from the lookup method.

4.1.7. Current-state optimised

Current-state optimised uses a combination of the steady-state optimiser from section 3.1 and the current state optimiser from section 3.2. Like steady-state optimised, this method acts every 60 seconds or when a change in heat load is detected. First, the steady-state optimiser is run. This is to provide an initial guess for the heat flow portion of the current state optimiser, which reduces overall computation time, especially when the system is near the steady state operating condition. With the initial guess, the heat flow portion of the current state optimiser is run for three times steps of 60 seconds each. The additional time steps help in reducing temperature overshoots and undershoots. The values for the flow variables for the first time step are then used in the coolant flow portion of the current state optimiser to calculate the most efficient configuration of the coolant circulation pumps PU05 and PU06 and the position of the three-way valve.

4.2. Simulations

Simulations with three types of load configurations are run to test the effectiveness of the control methods. The selection for the river water temperatures is based on the data collected by three measurement sites along the Dutch part of the river Rhine over two years [35]. The measurements can be seen in figure 4.1 and primarily range between 5 - 25 °C. For this reason, five different river water temperatures were simulated, starting at 5 °C with steps of 5 °C until 25 °C. The range of the heat load of the fuel cell units is determined based on the electrical power provided by Ballard [10]. They provide a power range of 55 - 200 kW. Because a fuel cell unit achieves an efficiency higher than 50% at low loads, the minimum heat load is assumed to be 50 kW. The maximum heat load is 350 kW, as this is the heat load that the cooling system is designed to cope with. The simulations are run with four different heat loads ranging from 50 kW to 350 kW in 100 kW intervals. The simulations provide insight into the temperature control performance, the on/off cycles of the pumps, and the cooling system power consumption of the different control methods. Fuel cell temperature control is essential because both the fuel cell performance as well as durability are affected by operating temperature. The number of pump on/off cycles directly affects the wear of the pumps and should, for that reason, be minimised if possible [27]. Cooling system power consumption affects the operating expense of the system.

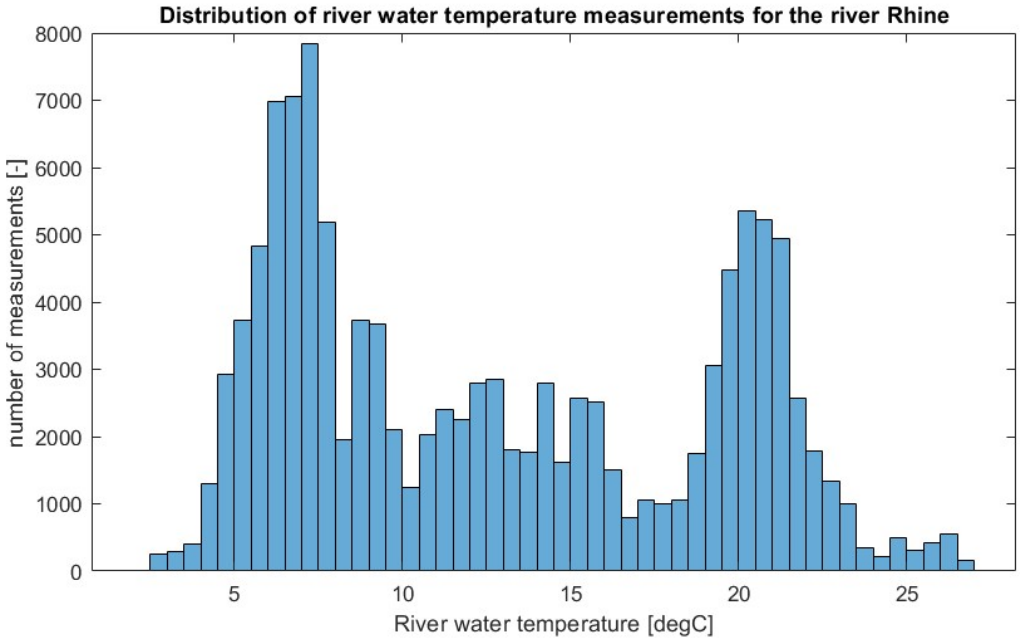

Figure 4.1: Distribution of river water temperature measurements for the river Rhine

4.2.1. Constant load

As the name suggests, the constant load simulations feature a constant heat load provided by the fuel cell units. This leads to three sets of 20 simulations as the combination of heat load and river

water temperature are simulated for 2, 4, and 6 active fuel cell units. The main aim of the constant load simulations is to assess the control methods' viability and tune them. If managing the fuel cell temperature under constant loads appears impossible, it will undoubtedly fail under changing loads.

4.2.2. Step load

The step load simulations consist of three sets of 5 simulations. The starting load of these simulations is 100 kW, which then increases to 300 kW 130 seconds into the simulation. After a total of 790 seconds of simulation time, the heat load is reduced to its original value for the remainder of the simulation. This is shown in figure 4.2. The times of 130 seconds and 790 seconds were chosen, as with a sample time of 60 seconds; these are inopportune timings where it takes another 50 seconds before the rule sets of the methods are used. Methods that perform well with this timing will also perform well with other more fortunate timings. For these simulations, the methods will be tested for temperature control of the fuel cell units. Both the maximum temperature overshoot and the time it takes for the temperature to settle back to 65 °C are important metrics.

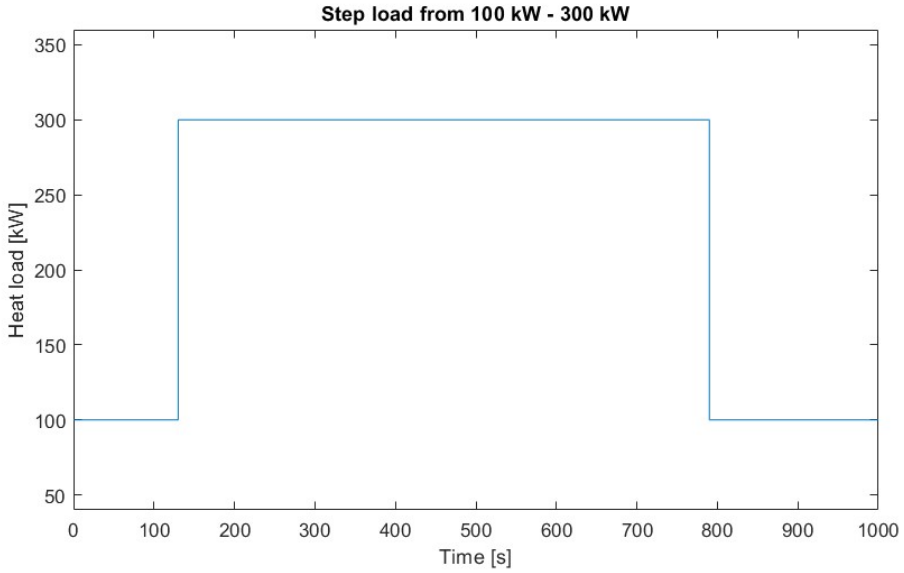

Figure 4.2: Step load from 100 kW to 300 kW

4.2.3. Scenario

The scenario simulations are simulations for each of the five river water temperatures with a duration of 2500 seconds, during which both the number of active fuel cell units and the heat load change. The heat load and fuel cell unit allocation can be seen in figure 4.3. The power consumption of the cooling system is the main focus of these simulations.

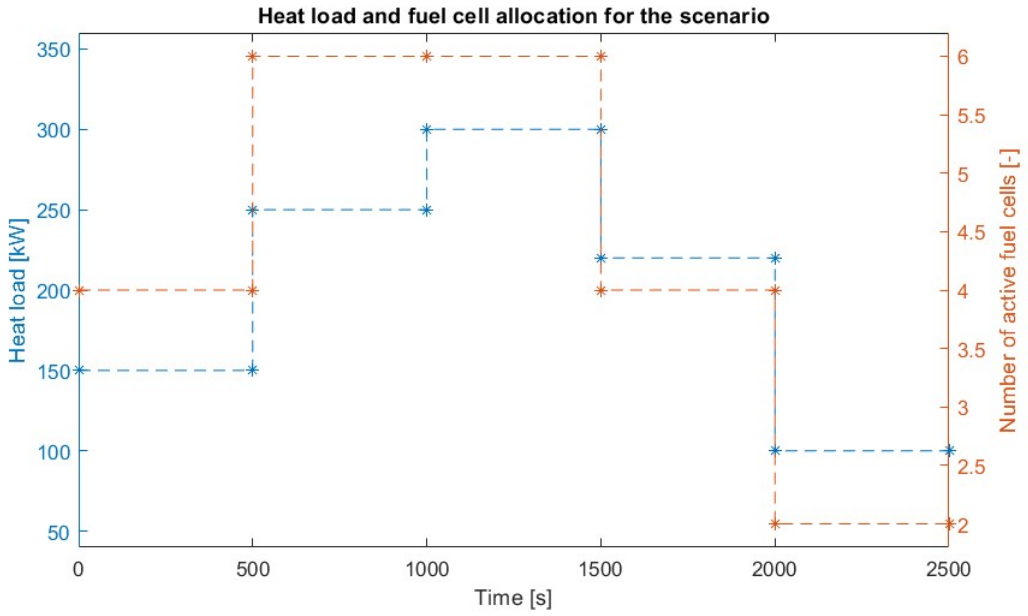

Figure 4.3: Heat load and fuel cell allocation for the scenario

5 Results

This chapter provides the results of applying the control methods detailed in section 4.1 on the cooling system from chapter 2. Section 5.1 shows the results for the constant load simulations, where the temperature management, pump on/off cycles, and the system power consumption of the methods are compared. This is followed by section 5.2, which compares the temperature management of the methods when they encounter an increase and a decrease in fuel cell heat load. This chapter closes with section 5.3, where the heat management and the power consumption are directly compared against one another during the scenario simulations.

5.1. Constant load

The methods are tested for their ability to keep the fuel cell temperature at 65 °C and ensure that it does not exceed 68 °C. Furthermore, the amount of on/off cycles of the pumps and the power consumption of the cooling system are compared. The first 333 seconds of the 1000-second simulations are not taken into account when assessing the performance of the methods for constant load to ensure that the data is not affected by start-up conditions.

Current-state optimised did not do the constant load simulations. The main reason is that due to the method using optimisation software, it had to be simulated on the slower hardware together with steady-state optimised. These simulations were skipped as they were deemed to be the least important because, in an ideal situation, the current-state optimiser under constant load would provide the same inputs to the cooling system as the steady-state optimiser.

5.1.1. Standard rule

Before addressing the overall simulation results of standard rule for constant load, it is essential to highlight a flaw in the rule set, which directly leads to the creation of the additional rule set for cold weather. The main problem with this rule set is that it can only look at one temperature measurement and is further unaware of the state the system is in. If the heat load of the fuel cell units is 350 kW, then with a nominal coolant flow through them, the coolant needs to have a temperature of approximately 40 °C or lower for the fuel cell unit to be sufficiently cooled. A scenario where the temperature of the coolant entering the fuel cell units is 50 °C can mean one of two things. Either the fuel cell unit requires more cooling, which is why the temperature is high, or the fuel cell unit has a lower heat load, meaning that a higher inlet temperature can still provide sufficient cooling to the fuel cell unit. Standard rule is incapable of differentiating between these two scenarios and, for that reason, will always err on the side of caution and thus increase the cooling capacity of the cooling system by, in this case, turning on both heat exchangers. This is fine if the fuel cell units had a high heat load and were overheating, but if the heat load was low this results in the cooling system massively overcooling for the next 60 seconds. The next time a temperature measurement is taken, the temperature of the coolant will be very low, which could lead to the rule set changing to a cooling configuration that does not provide enough cooling capacity for the current heat load, meaning that for the next 60 seconds, the coolant is heating up. This forms a cycle where the control method keeps switching between too much cooling capacity and too

little cooling capacity. This effect is amplified when the river water temperature is lower as the inherent cooling capacity of the system increases. Without reducing the inherent cooling capacity by reducing the flow through the heat exchangers, there were scenarios where the coolant reached temperatures under the 15 °C threshold, resulting in no active heat exchangers and the fuel cell unit overheating.

Figure 5.1 shows a constant load simulation for the standard rule set with 4 active fuel cell units, a heat load of 350 kW, and river water temperature of 5 °C. Here, the cooling capacity is not decreased, and it can be seen that the coolant inlet temperature called T_{in} dips below 15 °C, which results in a spike in coolant and fuel cell temperature. In comparison, in figure 5.2, there is a reduction in cooling capacity, and the temperature of the coolant does not go lower than 20 °C. After the initial start-up spike in fuel cell temperature, this method can keep the fuel cell temperature at a constant 65 °C.

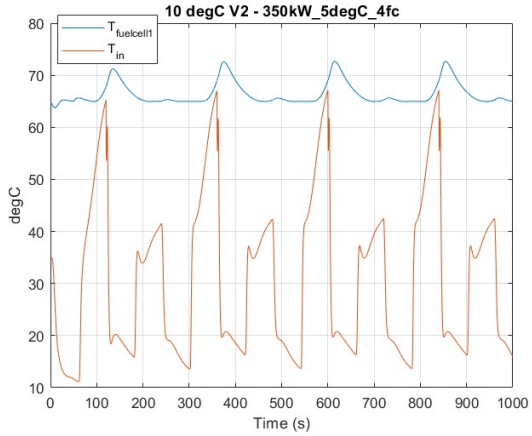

Figure 5.1: 4 fuel cell units, heat load of 350 kW and river water of 5 °C without cold weather rule

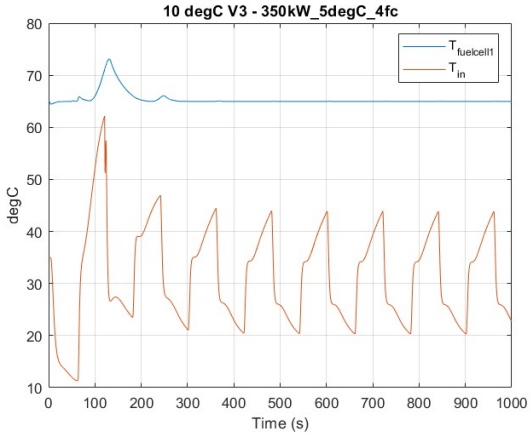

Figure 5.2: 4 fuel cell units, heat load of 350 kW and river water of 5 °C with cold weather rule

The standard rule set fails to maintain a fuel cell temperature of 65 °C in 3 out of the 60 simulations. It experiences a temperature overshoot of less than 1 °C during the 6 active fuel cell units and 350 kW heat load simulations with a river water temperature of 10 °C and 15 °C. A slightly larger temperature overshoot of 1.68 °C happens during the simulation with 4 active fuel cell units, 350 kW heat load, and 15 °C river water. The temperature of the fuel cell unit and the coolant entering the fuel cell unit for this simulation are shown in figure 5.3. This is a case of the system alternating between overcooling and undercooling.

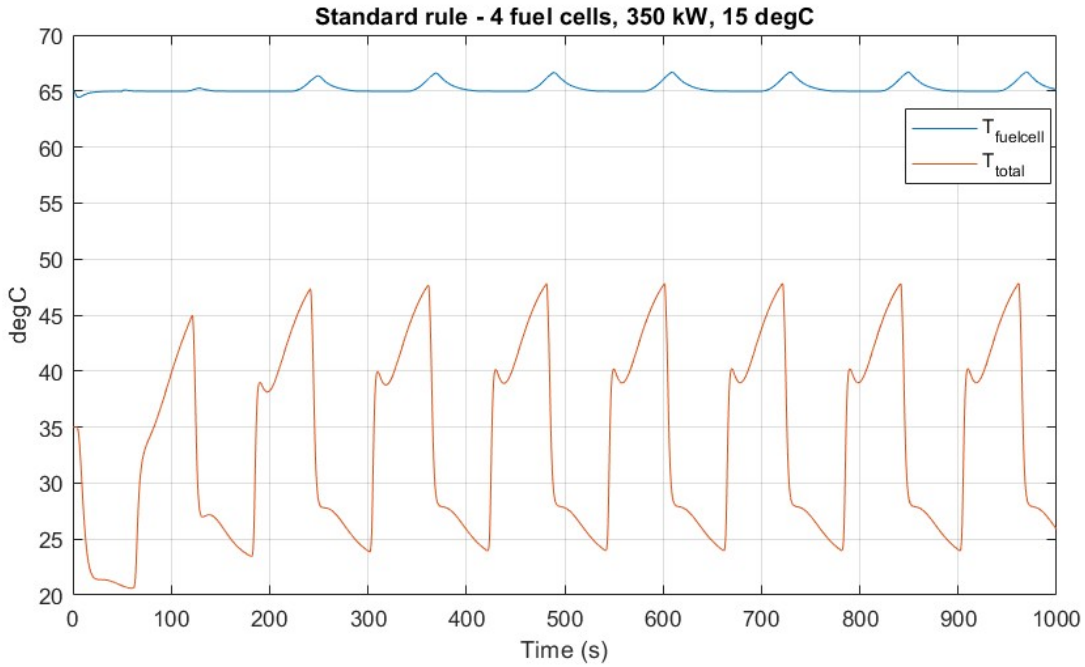

Figure 5.3: Standard rule constant load with 4 fuel cell units, 350 kW heat load and 15 °C river water

In regards to the pumps turning on and off, this method performs poorly. In 39 out of the 60 simulations, there were pumps consistently turning on and off. In most of these simulations, there were 5 instances of a pump performing a full on/off cycle, with the second most common being 11 instances of pumps performing a full on/off cycle. The highest number of on/off cycles is 16.

Table 5.1 shows the total power consumption of the cooling system when the river water temperature varies between 5 °C and 25 °C. For 4 and 6 active fuel cell units, the majority of the power consumption comes from the circulation pumps, with their share varying between 65% - 85%. When only 2 fuel cell units are active, this changes, and the share of power consumption of the circulation pumps varies between 46% - 75%. This discrepancy is mainly due to the power used by the river water pumps per kW heat load being higher when only 2 fuel cell units are active, meaning that this method is comparatively less efficient for 2 fuel cell units.

Table 5.1: Cooling system power consumption depending on river water temperature and heat load for standard rule in kW

	Heat load:	50 kW	150 kW	250 kW	350 kW
2 fuel cell units	5 degC	4.0102	5.3010	5.0020	5.7637
	10 degC	4.3181	4.9783	5.5894	5.8939
	15 degC	4.9167	4.9485	4.9718	5.9025
	20 degC	4.9258	5.5100	5.8833	5.9002
	25 degC	6.7229	6.7480	6.7680	6.7835
4 fuel cell units	5 degC	9.5555	9.6547	13.0302	13.4282
	10 degC	11.3570	12.3161	13.3961	13.2477
	15 degC	11.3145	12.2799	13.3413	13.3646
	20 degC	12.2055	13.2964	13.1846	14.2013
	25 degC	13.0801	13.1476	14.2009	14.2270
6 fuel cell units	5 degC	12.4468	13.9786	14.5782	15.4936
	10 degC	12.7439	14.4799	15.4265	15.4618
	15 degC	13.0016	14.3825	15.2952	15.3566
	20 degC	13.6324	14.9352	15.3088	16.3199
	25 degC	14.1390	15.2426	16.2705	16.3216

5.1.2. Temperature difference

The temperature difference rule set maintains a fuel cell temperature of 65 °C for all 60 simulations. This was to be expected as the temperature brackets were rounded down to ensure that enough cooling was available at all times. Interestingly enough, there are 4 simulations where pumps turn on or off. This is paired with a higher cooling system power consumption at lower river water temperatures because the specific heat capacity of 50% ethylene glycol is temperature dependent in the Simscape model as is plotted as discussed in section 2.1.5. At lower river water temperatures, the cooling system achieves a lower coolant temperature, which decreases the specific heat capacity of the 50% ethylene glycol, resulting in a higher temperature change over the fuel cell units. This is mainly noticed at lower river water temperatures and 350 kW heat load with 2 active fuel cell units as the difference between PU02 being active and PU01 being active is substantial with the low power consumption that 2 active fuel cell units require for coolant circulation.

The power consumption share of the circulation pumps is between 45.8% - 92.7% for 2 active fuel cell units, between 72.4% - 97.5% for 4 active fuel cell units, and between 65.7% - 97.8% for 6 active fuel cell units. The total power consumption of the cooling system when the river water temperature varies between 5 °C and 25 °C can be seen in table 5.2.

Table 5.2: Cooling system power consumption depending on river water temperature and heat load for temperature difference rule in kW

	Heat load:	50 kW	150 kW	250 kW	350 kW
2 fuel cell units	5 degC	3.3154	4.9650	4.9959	6.8050
	10 degC	3.2630	3.2862	5.0015	6.8127
	15 degC	3.2594	3.2937	5.0054	5.8464
	20 degC	3.2697	3.2977	5.0062	5.0185
	25 degC	3.2762	3.3008	5.0067	5.0154
4 fuel cell units	5 degC	9.7677	11.5490	11.2772	13.3726
	10 degC	9.7896	11.5531	11.1931	13.3715
	15 degC	9.8036	11.5515	11.1966	13.3679
	20 degC	9.8145	11.5482	11.1924	13.3569
	25 degC	9.8192	11.5380	11.1864	13.3438
6 fuel cell units	5 degC	11.1188	12.1023	16.2567	16.3766
	10 degC	10.8677	12.1423	16.2967	16.4017
	15 degC	10.8545	12.1721	16.3332	16.4238
	20 degC	10.8900	12.2008	16.3573	16.4325
	25 degC	10.9213	12.2237	16.3797	16.4346

5.1.3. Load-based flow

Load-based flow fails to keep the temperature of the fuel cell unit at a constant 65 °C in 7 out of 60 simulations. In 4 simulations, it keeps the overshoot below 1 °C. For 2 fuel cell units with 250 kW heat load and a river temperature of 25 °C, there is a recurring overshoot of 1.49 °C. For 4 fuel cell units with 350 kW heat load and a river temperature of 10 °C, there is a recurring overshoot of 1.56 °C. The most extreme recurring overshoot is for 2 active fuel cell units with a heat load of 350 kW and a river water temperature of 10 °C, where the overshoot is 2.38 °C. The temperature of the fuel cell units, the temperature of the coolant exiting the fuel cell units, and the mass flow through the fuel cell units can be seen in figure 5.4. This overshoot is a result of not tuning the rule set strictly enough. While it does keep the fuel cell temperature below 68 °C, the combination of overheating and constant changes in pump speed are not desired. For instance, a more strictly tuned rule set would lower the temperature at which the flow is reduced. From the figure, it can be seen that the temperature goes towards an equilibrium first at approximately 53 °C and then the time step afterwards at approximately 58 °C. Thus, a rule set with a lower bound of 57 °C would have resulted in a fuel cell unit with a constant temperature and no pump changing speed.

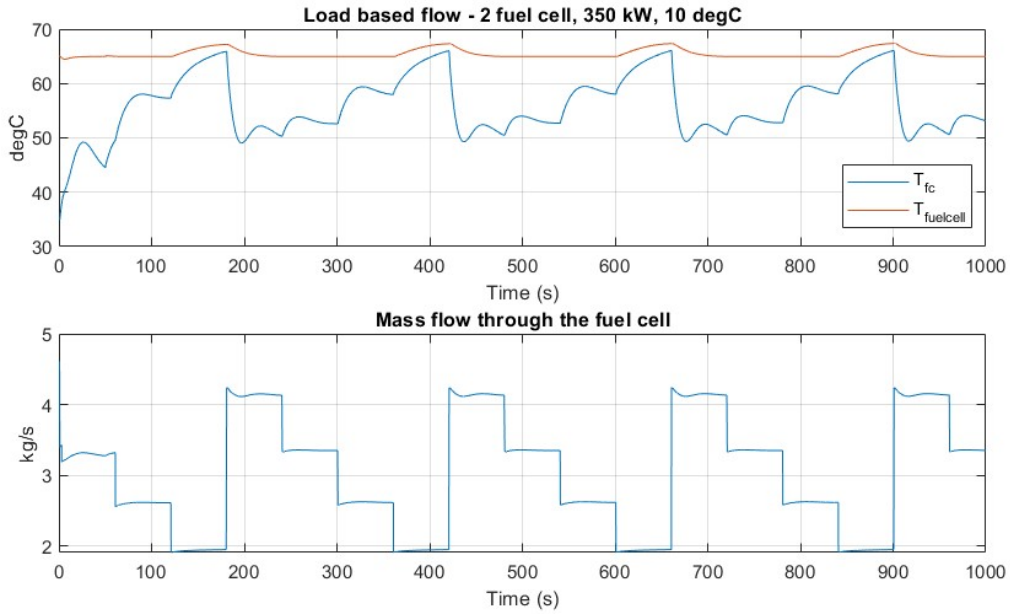

Figure 5.4: Load-based flow constant load for 2 fuel cell units with a heat load of 350 kW and river water temperature of 10 °C. The top figure shows the fuel cell and coolant temperature. The bottom figure shows the coolant mass flow through the fuel cell unit

The 7 instances where there is a temperature overshoot are also the only 7 instances with a change in pump speed. That means that all other 53 simulations found an equilibrium with a certain flow speed and outlet temperature between 60 °C and 64 °C. When there is frequent change in pump speed, this is paired with a comparatively higher cooling system power consumption. Taking the simulation from figure 5.4, it was determined that with the second lowest mass flow, an equilibrium could have been reached were the rule set less strict. This means that the system was generating unnecessarily high flows for half the time. From equation 2.14, it can be seen how pump power scales to the third power when compared with flow. This means that half the time, the system is consuming a lot more power, and the power saved by generating too little flow for a quarter of the time is not nearly enough to make up for this. So, while a less strict rule set has the downside that it may find the suboptimal equilibrium, it does prevent cases like this, which are more wasteful when it comes to energy consumption. To put this into numbers, the power consumed with 2 active fuel cell units with a 350 kW heat load and 10 °C river water temperature is 2.59 kW. The same simulation except for a river water temperature of 15 °C consumes 2.20 kW.

The power consumption share of the circulation pumps is between 23.16% - 61.63% for 2 active fuel cell units, between 17.24% - 63.23% for 4 active fuel cell units, and between 16.13% - 64.88% for 6 active fuel cell units. The total power consumption of the cooling system when the river water temperature varies between 5 °C and 25 °C can be seen in table 5.3. The simulations where there was a temperature overshoot can be seen from the data showing a spike in power consumption when the river temperature rises.

Table 5.3: Cooling system power consumption depending on river water temperature and heat load for load-based flow in kW

	Heat load:	50 kW	150 kW	250 kW	350 kW
2 fuel cell units	5 degC	2.5110	2.5213	2.5126	2.8983
	10 degC	2.5248	2.5116	2.5126	3.8835
	15 degC	2.5266	2.5063	2.5114	3.2951
	20 degC	2.5170	2.5051	2.5097	4.6987
	25 degC	2.5068	2.5037	3.8698	5.0154
4 fuel cell units	5 degC	4.4566	4.4792	4.4608	4.4702
	10 degC	4.4842	4.4600	4.4621	6.8740
	15 degC	4.4877	4.4498	4.4612	5.5189
	20 degC	4.4718	4.4488	4.4589	7.3103
	25 degC	4.4526	4.4472	6.8548	10.0051
6 fuel cell units	5 degC	6.6981	6.7364	6.7030	6.7217
	10 degC	6.7468	6.7021	6.7070	10.5248
	15 degC	6.7541	6.6854	6.7078	8.2500
	20 degC	6.7263	6.6866	6.7061	10.7831
	25 degC	6.6926	6.6862	7.4485	15.9523

5.1.4. Load-based pump

Of the 60 simulations, only 5 fail to maintain a fuel cell temperature of 65 °C. Of these, 2 simulations have an overshoot of 0.21 °C or lower, which is negligible. Of the remaining three simulations, there is only one with an overshoot over 1 °C. In this simulation, shown in figure 5.5, the maximum overshoot is 1.32 °C. The conditions in this simulation are 6 active fuel cell units, a heat load of 350 kW, and a river temperature of 5 °C. What happens is that when the coolant exiting the fuel cell units reaches a temperature of 64 °C or higher, the cooling system cools the coolant to such a degree that the time it takes for the coolant to reach the temperature bracket where k does not change is long enough for k to be lowered to the point where the cooling system does not provide enough cooling, starting the cycle again. This is why it happens at 5 °C but doesn't happen at higher river water temperatures, as the cooling capacity of the cooling system is lower at those higher temperatures.

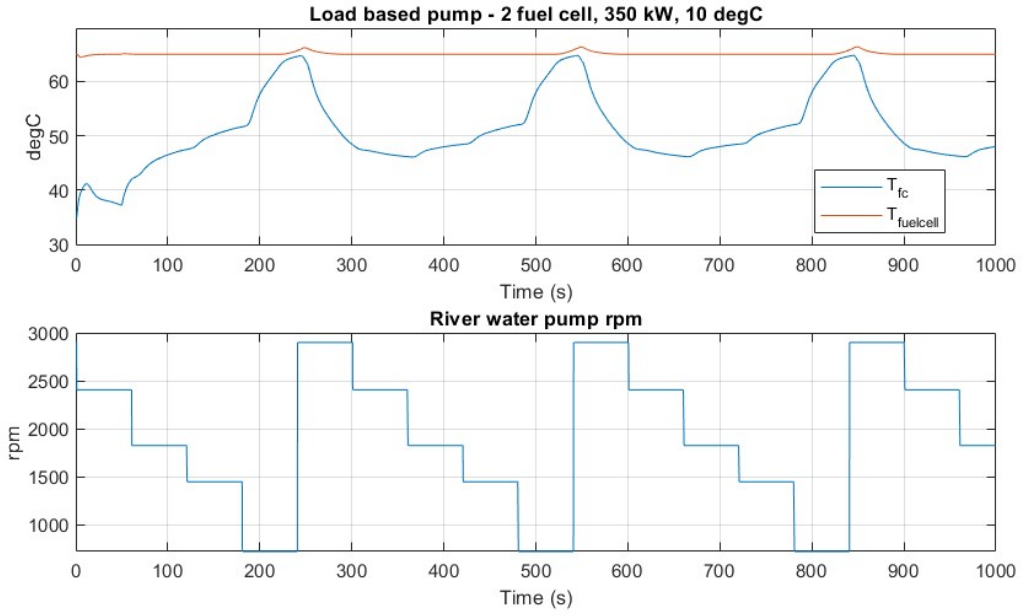

Figure 5.5: Load-based pump constant load for 6 fuel cell units with a heat load of 350 kW and river water temperature of 5 °C. The top figure shows the fuel cell and coolant temperature. The bottom figure shows the river water pump rpm

10 simulations involve a regular change in pump speed. Other than the 5 simulations with a temperature

overshoot, these simulations feature a situation in which the pump speed keeps alternating between two values. In these simulations, the pumps change their pump speed between 5 - 8 times over the course of 667 seconds.

The power consumption share of the circulation pumps is between 61.63% - 99.03% for 2 active fuel cell units, between 63.23% - 99.09% for 4 active fuel cell units, and between 64.88% - 99.16% for 6 active fuel cell units. Table 5.4 shows the power consumption of the cooling system in the 60 constant load simulations. The same phenomena as witnessed with load-based flow can be seen here, where there is a power consumption spike for simulations with a temperature overshoot.

Table 5.4: Cooling system power consumption depending on river water temperature and heat load for load-based pump in kW

	Heat load:	50 kW	150 kW	250 kW	350 kW
2 fuel cell units	5 degC	3.0578	3.0920	3.1110	3.4923
	10 degC	3.0543	3.0967	3.1620	3.3334
	15 degC	3.0652	3.0988	3.2257	3.6720
	20 degC	3.0719	3.1005	4.0242	4.1937
	25 degC	3.0790	3.1001	3.3220	5.0154
4 fuel cell units	5 degC	6.2430	6.3045	6.3629	7.8056
	10 degC	6.2008	6.3205	6.4714	6.7878
	15 degC	6.2322	6.3295	7.1126	7.4348
	20 degC	6.2537	6.3375	6.7638	8.4332
	25 degC	6.2758	6.3396	7.4099	10.0051
6 fuel cell units	5 degC	10.2074	10.3227	10.4038	12.5338
	10 degC	10.1668	10.3455	10.6243	11.0524
	15 degC	10.2138	10.3568	12.0269	11.7541
	20 degC	10.2462	10.3663	11.0155	13.5580
	25 degC	10.2784	10.3680	11.7157	15.9523

5.1.5. Lookup

There are only 2 simulations with a temperature overshoot. While the overshoots are relatively low at 0.12 °C and 1.16 °C, this is only because the simulation ended. During these simulations, there is a slow rise in coolant temperature throughout the simulation, which results in it reaching a break point where there is not enough cooling capacity, and the fuel cell temperature increases above 65 °C along with the coolant. The simulations with a temperature overshoot were for 2 fuel cell units with a heat load of 350 kW and 5 °C and 10 °C river water. The reason for this overshoot is the inaccuracy of the optimisation model at low flow rates and temperatures as described in section 3.3. Figure 5.6 shows the temperatures of the fuel cell units, coolant entering the fuel cell units and coolant exiting the fuel cell, and the mass flow through the fuel cell units and heat exchanger. The steady rise in temperature of the coolant over time can be seen. The coolant flow through the heat exchanger is equal to 0.35 kg/s. The steady-state optimiser calculates a mass flow through the heat exchanger of 0.50 kg/s. The flow resistance increases as a result of the higher kinematic viscosity, and the lower flow rate results in a 30% reduction in flow rate through the heat exchanger, but this also results in a 30% reduction in cooling capacity as for both these flow rates, the effectiveness of the heat exchanger is equal to 1, meaning that the flow would have cooled down to the temperature of the river water.

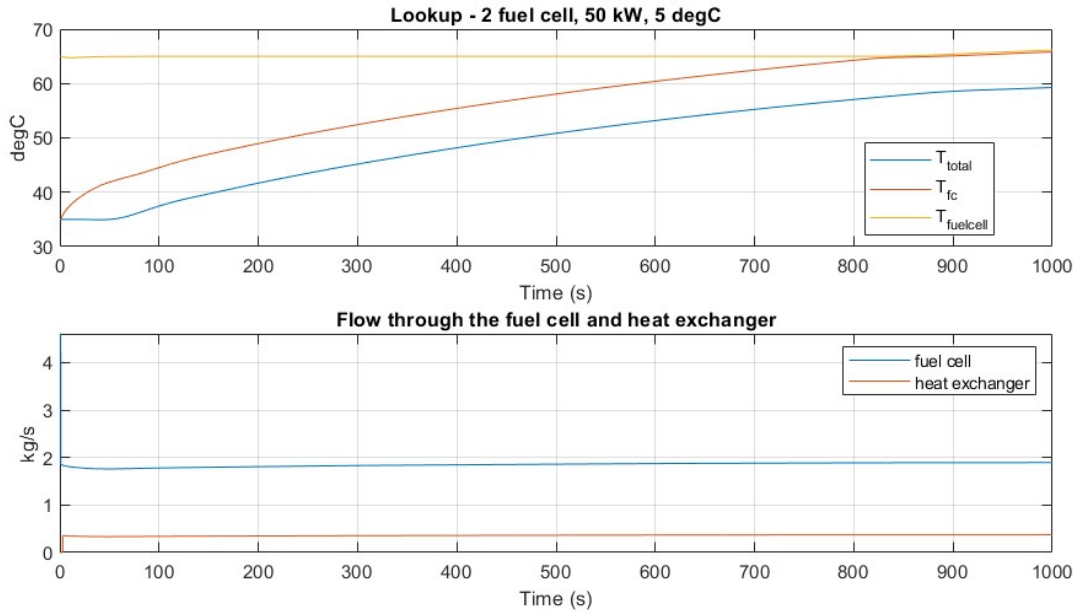

Figure 5.6: Lookup constant load for 2 fuel cell units with a heat load of 50 kW and river water temperature of 5 °C. The top figure shows the fuel cell temperature and coolant temperatures. The bottom figure shows the coolant mass flow through the fuel cell unit and heat exchanger

As lookup is a method that relies on external factors to determine the cooling system's configuration, there are no simulations that feature a change in pump speed. The power consumption share of the circulation pumps is between 19.46% - 40.40% for 2 active fuel cell units, between 16.30% - 41.12% for 4 active fuel cell units, and between 16.17% - 65.91% for 6 active fuel cell units. The power consumption for each of the 60 simulations can be seen in table 5.5.

Table 5.5: Cooling system power consumption depending on river water temperature and heat load for lookup in kW

	Heat load:	50 kW	150 kW	250 kW	350 kW
2 fuel cell units	5 degC	2.3954	2.4174	2.4505	2.5091
	10 degC	2.3954	2.4221	2.4650	2.8003
	15 degC	2.3948	2.4258	2.4784	3.2348
	20 degC	2.3939	2.4339	2.5343	4.6892
	25 degC	2.3929	2.4427	2.8952	5.1051
4 fuel cell units	5 degC	2.5614	2.6726	3.1960	4.4639
	10 degC	2.5630	2.7164	4.4054	4.8768
	15 degC	2.5639	2.7654	4.4222	5.4787
	20 degC	2.5659	2.9156	4.5085	7.2287
	25 degC	2.5679	3.2681	5.0049	8.0663
6 fuel cell units	5 degC	2.8765	3.3447	4.8141	6.6592
	10 degC	2.8801	4.7028	4.8941	7.0639
	15 degC	2.8835	4.7171	5.0422	7.7215
	20 degC	2.8901	4.7517	6.6900	10.1064
	25 degC	2.8969	4.7924	7.1215	16.4337

5.1.6. Steady-state optimised

Steady-state optimised suffers from the same problems lookup had, but more severe. There are 7 simulations with a temperature overshoot, with the highest being 2.03 °C. This simulation is shown in figure 5.7 and just as with lookup, this is a case of too little flow through the heat exchanger as a result of low flow rate and high kinematic viscosity, which results in too little cooling.

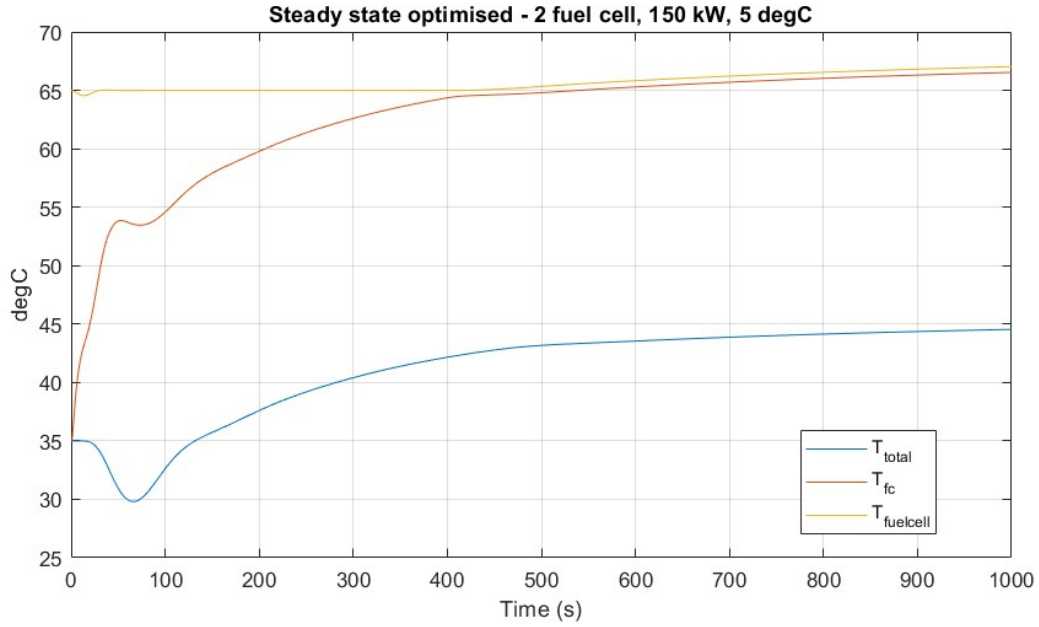

Figure 5.7: Steady-state optimised constant load for 2 fuel cell units with a heat load of 150 kW and river water temperature of 5 °C

As steady-state optimised is a method that relies on external factors to determine the configuration of the cooling system, there were no simulations that feature a change in pump speed. The power consumption share of the circulation pumps is between 19.46% - 56.78% for 2 active fuel cell units, between 16.11% - 49.27% for 4 active fuel cell units, and between 18.52% - 65.92% for 6 active fuel cell units. The power consumption for each of the 60 simulations can be seen in table 5.6. This method, as well as lookup, has a significant increase in power consumption when the river water temperature increases from 20 °C to 25 °C with 6 active fuel cell units and a heat load of 350 kW. The reason for this is that in the other simulations, the fuel cell units do not require near-maximum coolant flow, but this simulation does. Compared to the simulation with 20 °C, the power consumption of PU05 doubles, and PU06 is turned on.

Table 5.6: Cooling system power consumption depending on river water temperature and heat load for steady-state optimised in kW

	Heat load:	50 kW	150 kW	250 kW	350 kW
2 fuel cell units	5 degC	2.3946	2.4123	2.4455	2.5084
	10 degC	2.3947	2.4152	2.4558	2.7245
	15 degC	2.3941	2.4185	2.4701	3.2341
	20 degC	2.3931	2.4228	2.4923	4.4550
	25 degC	2.3923	2.4300	2.7292	5.1045
4 fuel cell units	5 degC	2.5607	2.6406	3.0331	4.4618
	10 degC	2.5620	2.6626	4.3937	4.7743
	15 degC	2.5632	2.6959	4.4113	5.4819
	20 degC	2.5646	2.7547	4.4401	7.2548
	25 degC	2.5673	2.8791	4.7801	8.0685
6 fuel cell units	5 degC	2.8758	3.1387	4.7934	6.6670
	10 degC	2.8789	3.2667	4.8445	6.9405
	15 degC	2.8829	3.5523	4.9370	7.7244
	20 degC	2.8882	4.7114	5.8534	9.4961
	25 degC	2.8964	4.7406	6.8742	16.4316

5.2. Step load

The step load simulations, as described in 4.2.2, aim to see how the control methods cope with a change in heat load. To achieve this, 130 seconds into the simulation, the heat load of the fuel cell units increased from 100 kW to 300 kW. 790 seconds into the simulation, the heat load decreased back to 100 kW. These simulations were run for river water temperatures ranging between 5 - 25 °C and 2, 4 and 6 active fuel cell units.

5.2.1. Standard rule

The fuel cell temperature for all 15 simulations with standard rule is displayed in figure 5.8. For some simulations, there is a fuel cell temperature spike around 60 seconds into the simulation. This coincides with a sudden spike in the temperature of the internal fuel cell coolant, yet the reason for this spike is not known as, at the time, ample cooling capacity was available from the main cooling system. The temperature spike is minor enough that it can be assumed that it had minimal influence on the overall simulation. Standard rule handles changes in heat load well. There is a small spike in fuel cell temperature at the time of the heat load increase, but this is due to the delay in coolant transport within the internal fuel cell cooling system. It takes a while for the new colder coolant to arrive within the fuel cell unit. A recurring temperature overshoot can be seen with 6 active fuel cell units and a river water temperature of 5 °C.

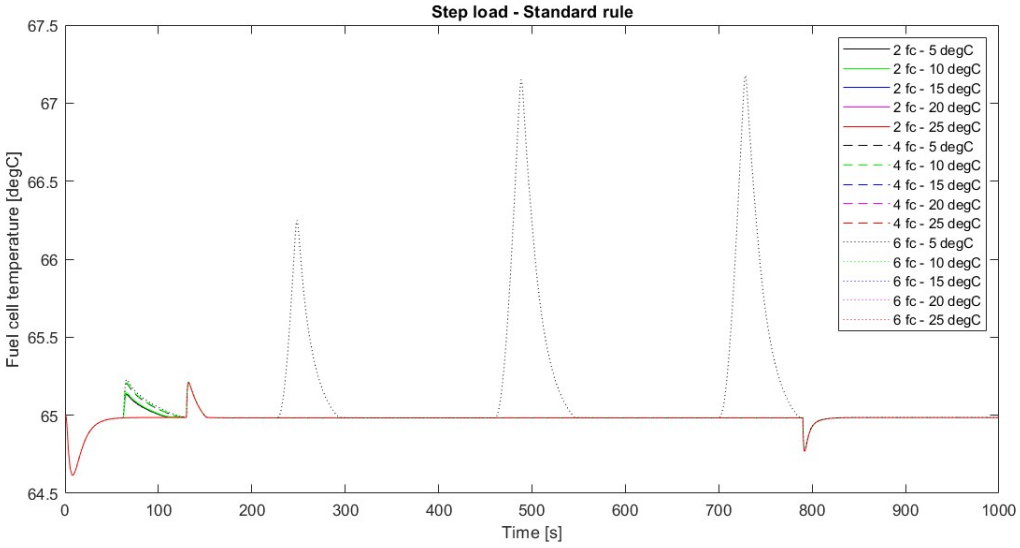

Figure 5.8: Fuel cell temperature for the step load simulations controlled with standard rule

5.2.2. Temperature difference

There is a significant variance in the response to an increase in heat load for temperature difference. The temperature brackets result in situations where the cooling system has a large amount of spare cooling capacity at the time of the heat load increase and other situations where there is barely any spare cooling capacity. This can be seen in figure 5.9, where there are simulations with basically no temperature spike and others with a temperature spike reaching a temperature above 72 °C. These simulations have exposed a weakness in how this method is set up. The method requires constant mass flow through the cooling system. The way this method was set up did not properly take into account the effect of changing the cooling system configuration on the system flow. This resulted in a variance in flow depending on which heat exchangers were active. Furthermore, this method is also affected by the change in kinematic viscosity with a change in temperature, contributing to a change in coolant flow rate. During the simulation with 6 fuel cell units and a river water temperature of 25 °C, a dip in temperature can be seen during the spike. This is where the cooling system changes configuration. Still, as the flow is higher than nominal due to the reason just discussed, the temperature difference over the fuel cell units is lower than it would be with a nominal flow. The cooling system is changed to a

configuration that does not provide enough cooling. There are two options to solve this problem. Either the temperature brackets are made more strict to account for possible higher flow, or the circulation pumps are separately controlled to ensure nominal flow at all times.

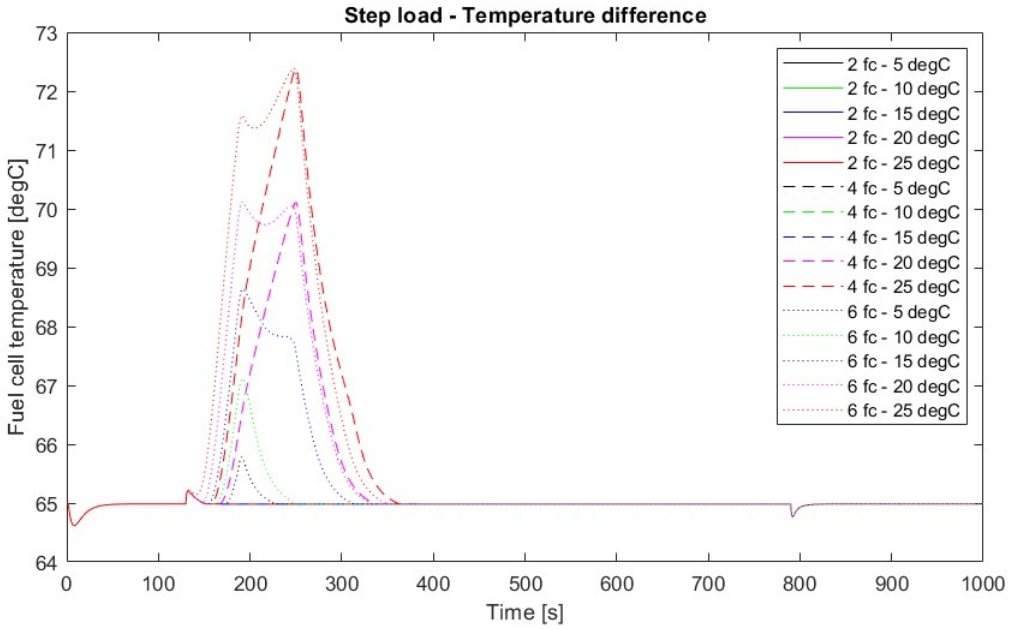

Figure 5.9: Fuel cell temperature for the step load simulations controlled with temperature difference

5.2.3. Load-based flow

Load-based flow and load-based pump suffer from the effects of startup because they start at high cooling while the start requires low cooling, meaning that at the time of the step in heat load, the coolant temperature is low. Figure 5.10 shows the fuel cell temperatures for load-based flow. Three different scenarios happen when the heat load increases. The first scenario is that a significant spike in fuel cell temperature occurs, which is then dealt with by increasing the coolant flow in the subsequent time step. An example of this is 2 active fuel cell units with 25 °C river water. The second scenario is a smaller increase in temperature where, at 180 seconds into the simulation, when the system checks the outlet temperature, the coolant is still below 64 °C due to the coolant having a low temperature due to the start-up. This results in prolonged heating, as seen with 4 active fuel cell units and river water temperature of 20 °C. The final scenario is when the system has enough cooling capacity, resulting in a minor temperature spike. A simulation worth highlighting is the simulation with 2 active fuel cell units and 20 °C river water. This simulation has a second temperature spike after the initial temperature spike. Once again, due to the low coolant temperature as a result of the start-up, the initial spike is relatively low. After this initial spike, the system is on its way to settling into equilibrium, but the temperature measurement at 240 seconds is slightly below 60 °C, resulting in the second larger temperature spike as there is no spare cooling capacity this time. After the second spike, the system finds an equilibrium with no subsequent temperature spikes.

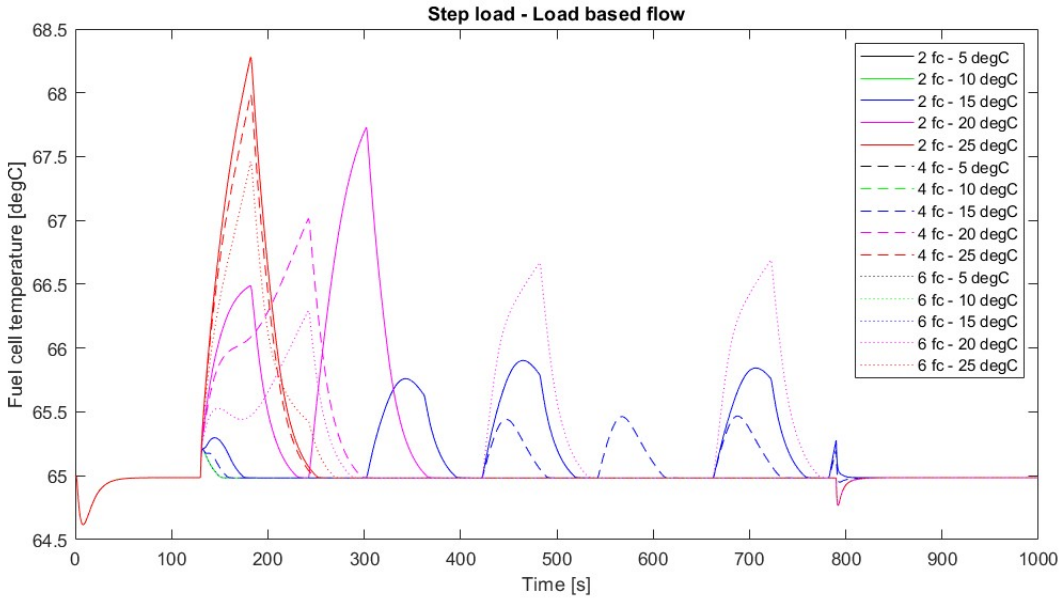

Figure 5.10: Fuel cell temperature for the step load simulations controlled with load-based flow

5.2.4. Load-based pump

The effects of start-up are even more clearly seen with load-based pump in figure 5.11. All the temperature spikes are delayed due to the additional cooling capacity due to the start-up. When the spike happens depends on the heat exchanged by the heat exchangers and the heat load of the fuel cell units. The largest initial spikes are for 20 °C river water. This is due to timing, as one would reasonably expect 25 °C river water to experience a higher temperature spike. However, for 25 °C river water, the outlet temperature reaches a temperature higher than 62 °C before 240 seconds into the simulations, resulting in an increase in cooling capacity from that point onwards, negating the temperature spike.

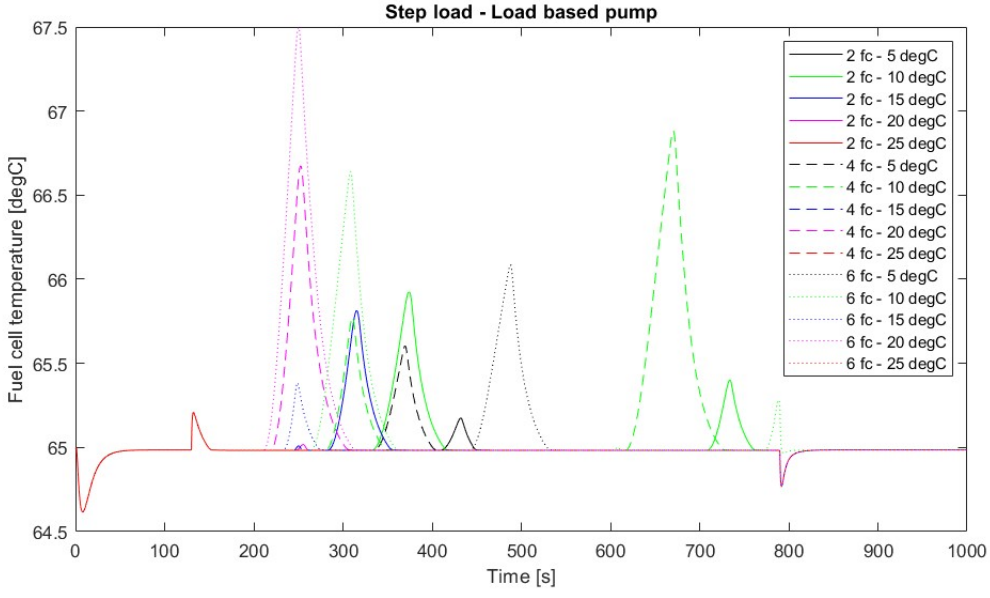

Figure 5.11: Fuel cell temperature for the step load simulations controlled with load-based pump

5.2.5. Lookup

Lookup experiences the largest temperature overshoot, as seen in figure 5.12. However, this is expected as this method has little spare cooling capacity, meaning that for 50 seconds, the fuel cell units are generating 200 kW more heat than the cooling system can cope with. Furthermore, the spikes are as wide as they are because even when the cooling capacity is increased, it is only increased to cope with the heat load generated by the fuel cell units and not to transfer the additional heat energy stored as fuel cell temperature. Because there is some spare cooling capacity, the fuel cell temperature reaches 65 °C after a while.

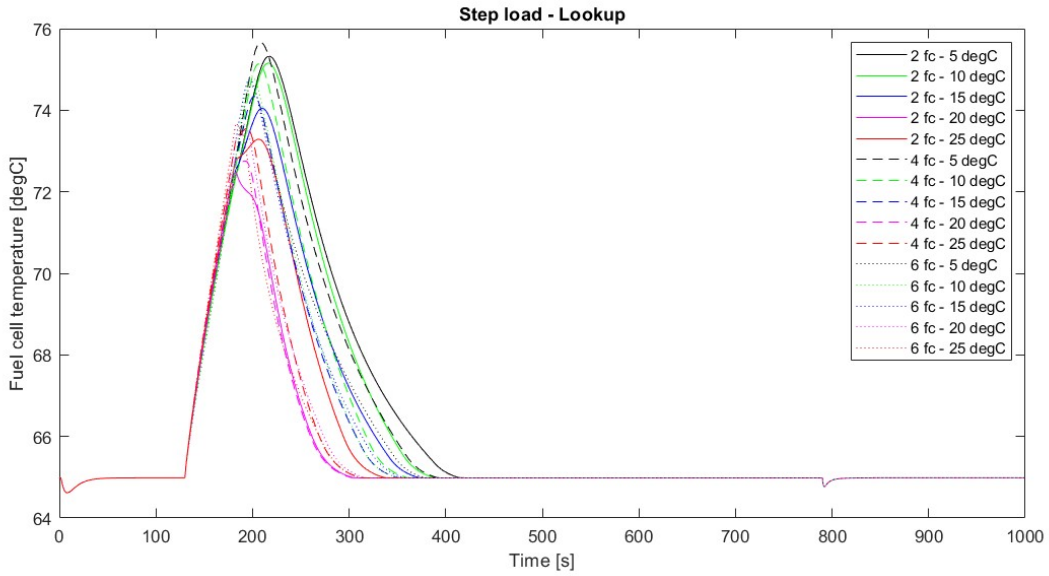

Figure 5.12: Fuel cell temperature for the step load simulations controlled with lookup

5.2.6. Steady-state optimised

The main difference between steady-state optimised and lookup is that lookup has slightly more spare cooling capacity, while steady-state optimised can react to a change in heat load. Both these differences can be seen when comparing figure 5.12 with figure 5.13. Due to being able to react, steady-state optimised has significantly lower maximum fuel cell temperatures and manages, in most cases, to bring the fuel cell temperature back to 65 °C faster than lookup. In the cases where it takes longer to reach 65 °C, like with active 2 fuel cell units and 5 °C river water, the reason is the general lack of cooling capacity discussed in section 5.1.6.

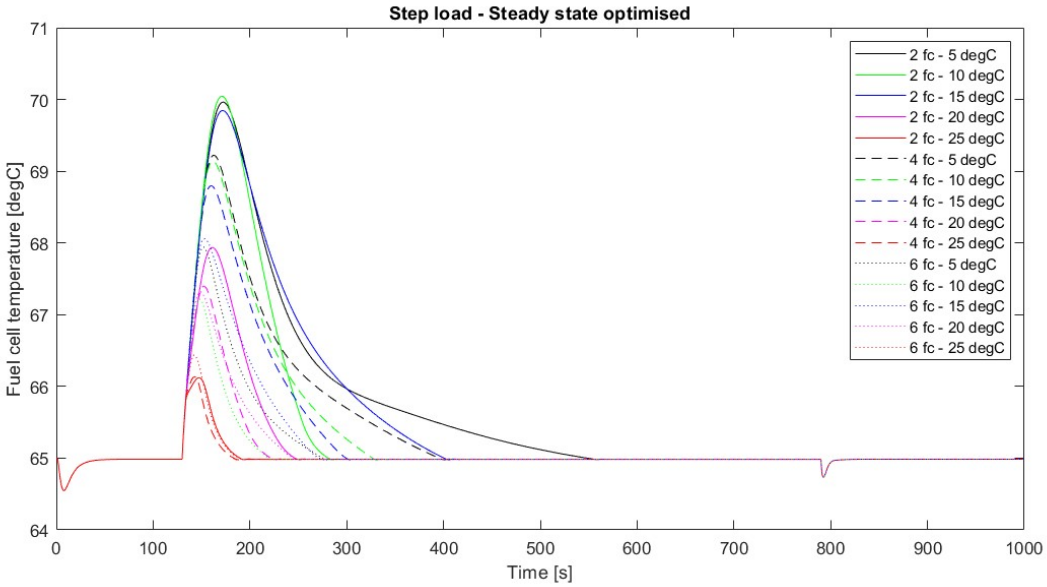

Figure 5.13: Fuel cell temperature for the step load simulations controlled with steady-state optimised

5.2.7. Current-state optimised

Figure 5.14 shows the fuel cell temperature for step load controlled by the current-state optimiser. The steady-state error seen with current-state optimised is the result of two factors. Constraints 3.90 and 3.91 ensure that there is enough cooling capacity in the coolant flow through the heat exchanger. However, there is no additional temperature margin here compared to steady-state optimised. This means that if the actual flow is less than the flow determined by the optimiser due to the reason discussed in section 3.3, the fuel cell units will have a constant temperature overshoot. Here, the temperature overshoot is not constant and slowly rises over time. This is due to how the coolant flow inside the fuel cell units is modelled. A Simscape constant mass flow block is used to provide the coolant flow, but this generates 332 W of additional heat load, which slowly raises the internal fuel cell coolant temperature and, consequently, the fuel cell temperature. Adding a temperature margin to the coolant exiting the fuel cell units would remove the steady-state error at the cost of a slight power consumption increase. Comparing the temperature control performance of current-state optimised versus steady-state optimised, it can be seen that current-state optimised has lower peak temperatures and reaches 65 °C significantly faster than steady-state optimised.

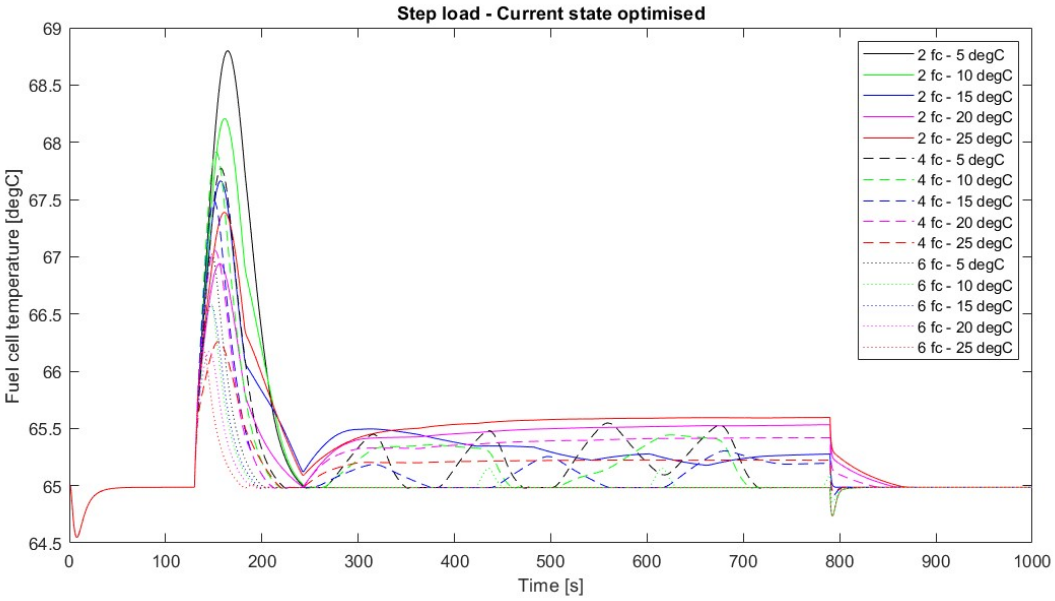

Figure 5.14: Fuel cell temperature for the step load simulations controlled with current-state optimised

5.3. Scenario

The scenario simulations are intended as shortened real-life scenarios as discussed in section 4.2.3. With the constant load and step load simulations, the general performance of the control methods has been documented, while for the scenario simulations, the performance of the methods is directly compared to one another. The two performance categories being examined are the fuel cell temperature control ability and the power consumption of the cooling system.

Figure 5.15 shows the fuel cell temperature for all 7 control methods with a river water temperature of 5 °C. The underperformance of steady-state optimised and especially lookup is evident compared to the other methods. Both standard rule and load-based pump experience recurring temperature spikes at the highest load. Temperature difference has a good performance, which is to be expected as the method does not take river water temperature into account and, therefore, has a lot of spare cooling capacity at low river water temperatures. The minimum flow rate for load-based flow is capped at half the nominal flow rate. With a river water temperature this low, it provides substantial spare cooling capacity, so there are no temperature spikes. Current-state optimised also performs well.

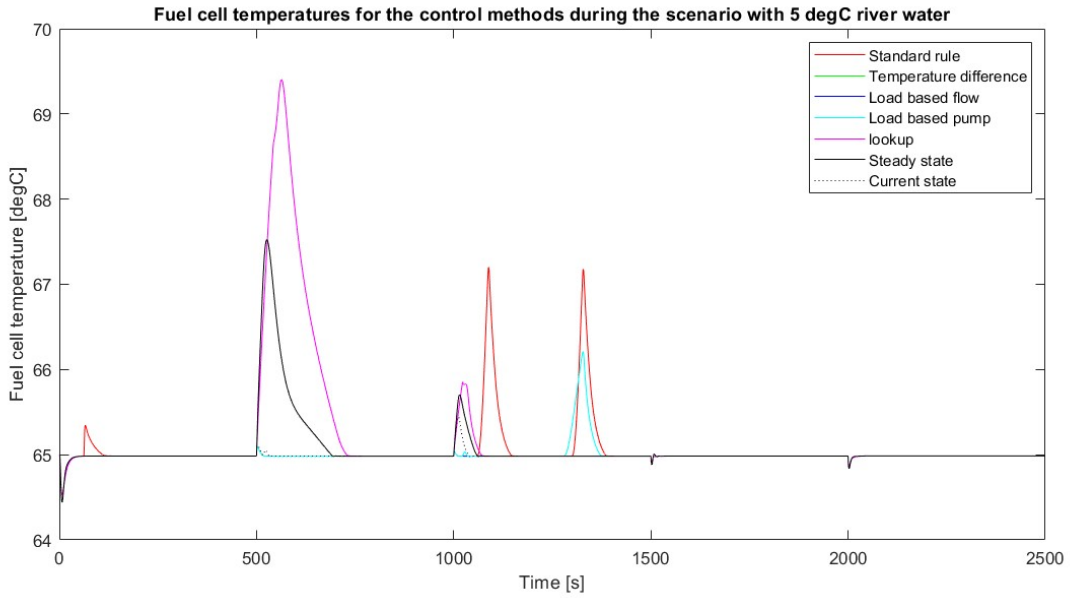

Figure 5.15: Fuel cell temperatures with different control methods for scenario with 5 °C river water

The fuel cell temperature for river water of 10 °C can be seen in figure 5.16. Most notable here is that with the step in load 1000 seconds into the simulation, steady-state optimised performs better than current-state optimised. In this instance steady-state optimised already has relatively cool coolant entering the fuel cell units and decides to increase the coolant flow, which happens fast throughout the system, minimising the temperature spike. Current-state optimised ops for increasing the cooling capacity by turning on an additional heat exchanger. This is the less optimal solution and stems from current-state optimised having separated the coolant flow calculations from the heat flow calculations. While steady-state optimised being the better option during a change in heat load seems to be the exception, this further supports the notice that the way current-state optimised is currently programmed is flawed. This is furthered supported by the current-state optimised being unable to maintain a fuel cell temperature of 65 °C at the highest load.

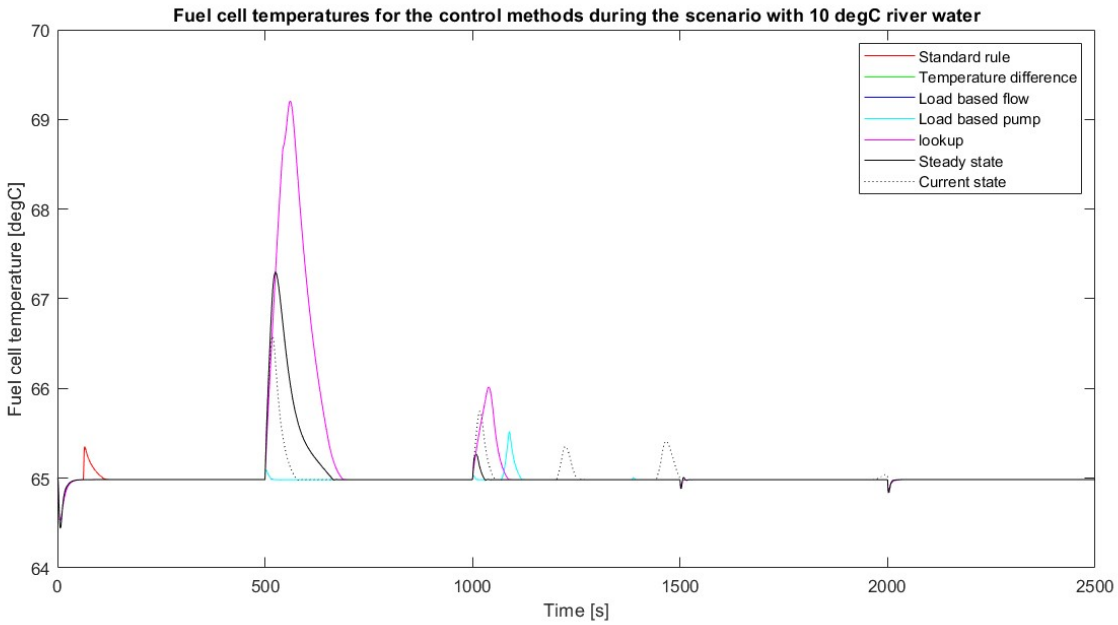

Figure 5.16: Fuel cell temperatures with different control methods for scenario with 10 °C river water

The fuel cell temperatures for 15 °C river water are entirely as one would expect them to be. Current-state optimised performs better than steady-state optimised, lookup being the worst performer regarding heat load increases and standard rule, temperature difference, load-based flow, and load-based pump showing minimal temperature spikes.

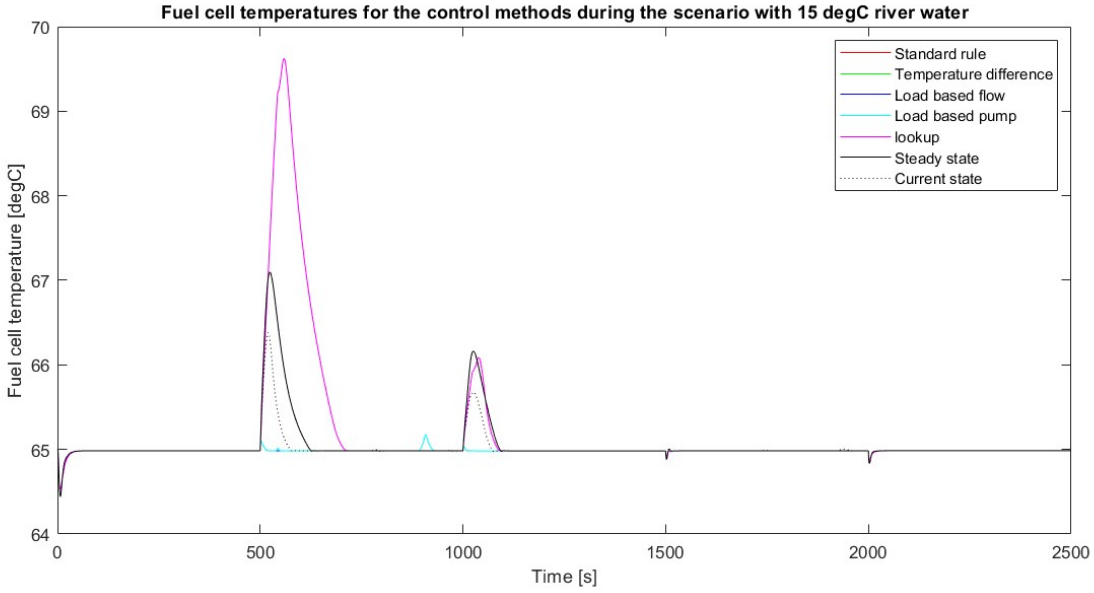

Figure 5.17: Fuel cell temperatures with different control methods for scenario with 15 °C river water

When the river water temperature reaches 20 °C, temperature overshoots for temperature difference can be seen in figure 5.18. Furthermore, load-based flow experiences significant recurring temperature spikes during the highest load. Current-state optimised also fails to maintain fuel cell temperature between 1500 and 2000 seconds.

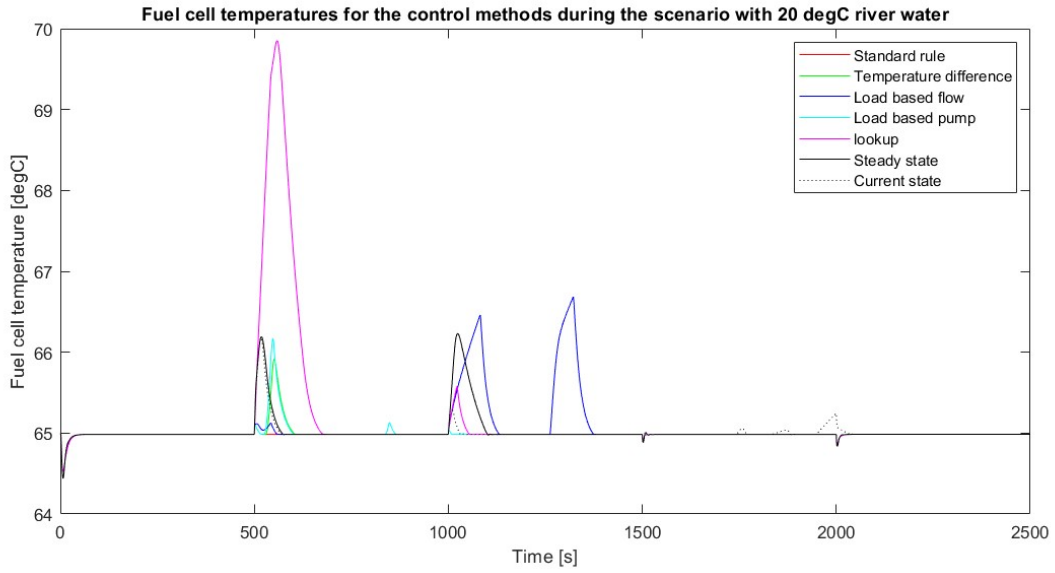

Figure 5.18: Fuel cell temperatures with different control methods for scenario with 20 °C river water

Figure 5.19, showing the temperature of the fuel cell units for 25 °C river water, shows the effect of temperature difference not having the spare cooling capacity due to cold river water. It incurs a significant temperature overshoot 500 seconds into the simulation, where it was minimal for 20 °C river water and non-existent for colder river water. Load-based pump also experiences a significant temperature overshoot at this time, although the duration is shorter. Load-based flow has recurring temperature overshoots between 500 - 1000 seconds resulting in a large overshoot at 1000 seconds. Current-state optimised once again fails to maintain fuel cell temperature between 1500 - 2000 seconds, and the start of a steady state error can be seen at the end of the simulation.

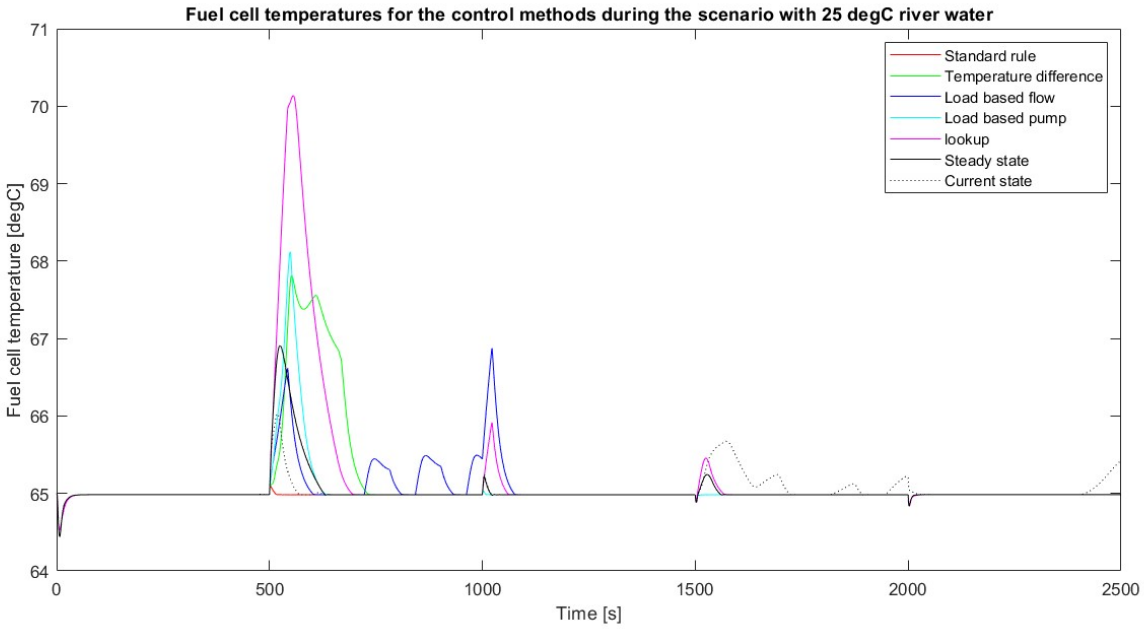

Figure 5.19: Fuel cell temperatures with different control methods for scenario with 25 °C river water

Regarding cooling system power consumption, there are 3 distinct levels of performance, which can

be seen in figure 5.20 that shows the total energy used by the cooling system during the scenario simulations for each control method. The first bracket of performance is standard rule and temperature difference. Both these methods are massively held back by maintaining a nominal coolant flow at all times. Temperature difference has a constant energy consumption across the range of different river water temperatures as it does not take the impact of river water temperature on the cooling system into account. This means that the method is especially wasteful at lower river temperatures. A more advanced version of the method where the temperature brackets depend on river water temperature would see improvements in power consumption. It would be reasonable to assume that the method would then sit comfortably between the performance of standard rule and load-based pump. The second bracket is load-based pump. Like standard rule and temperature difference, load-based pump maintains nominal coolant flow. However, by being able to reduce the river water pump speed, it can save a significant amount of energy. The final bracket contains load-based flow, lookup, steady-state optimised, and current-state optimised. All four of these methods can reduce the coolant flow, and this clearly shows in the power consumption. Load-based flow has the highest power consumption out of these four methods, which is expected as it is the only method not based on an optimiser. During low heat load, load-based flow will have the same river water pump allocation as during higher heat flow if the same amount of fuel cell units are active, which is inefficient. This, combined with the coolant flow almost always being more than optimal due to how the method works, results in higher energy consumption. Out of the three optimiser methods, lookup performs the worst as expected. Since the method has the inherent tendency to overcool slightly, it inherently consumes more energy. Interestingly, steady-state optimised is more energy efficient than current-state optimised for 10 °C and 20 °C river water. The scenario with 10 °C river water was where it was deemed possible that the current-state optimiser was less optimal than the steady-state optimiser, which may have contributed to steady-state optimiser being more energy efficient. What should also be considered is that steady-state optimised optimises just for the power consumption of the cooling system, while current-state optimised also takes the fuel cell temperature into account when solving the optimisation problem. This means that it will sacrifice energy efficiency for better control of fuel cell temperature.

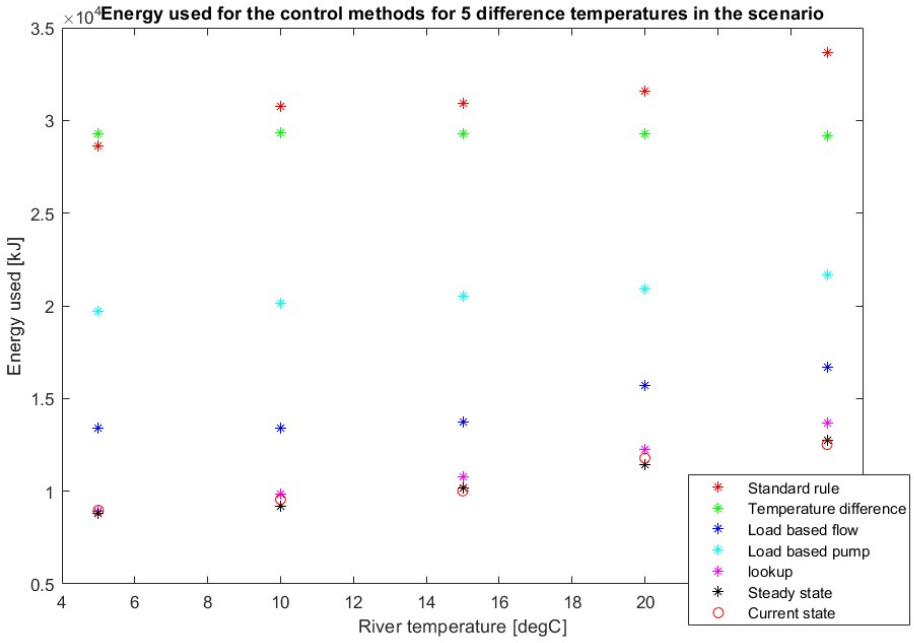

Figure 5.20: Total cooling system energy used during the scenario simulation per control method and river water temperature

6

Discussion and recommendations

In this chapter, the results are summarised and discussed in section 6.1. Following this, in section 6.2, recommendations are made for possible follow-up research.

6.1. Discussion

This section provides a discussion of the results from chapter 5. It starts with a summarisation of the research performed. Following this, in subsections 6.1.1, 6.1.2, and 6.1.3 the results for constant load simulations, step load simulations, and the scenario simulations are discussed. Afterwards, in subsection 6.1.4, the different control methods are discussed, and in subsection 6.1.5 limitations of this research are discussed.

The goal of this research was to test and compare the performance of different rule-based and optimisation-based control methods for controlling a cooling system consisting of multiple pumps, heat exchangers, and heat sources. To achieve this, a Simulink model was made to test these methods using three different simulation types. The constant load simulation aimed to figure out the constant performance of the control method as a ship tends to spend a long time at a specific power output. A second type of simulation, step load, was performed to see how the control methods were able to cope with an increase and a decrease in heat load. Finally, the third simulation type was a longer simulation, which aimed to be a condensed real-life power cycle, where in steps, the total power generation first increases and later decreases. What set this apart from step load was that here the number of active fuel cells changed over time.

6.1.1. Constant load discussion

The control methods can be categorised into two different groups. The first group consists of standard rule, load-based flow, and load-based pump, and these rule sets all rely on a single temperature measurement to control the cooling system. The second group consists of temperature difference, lookup, and steady-state optimised, which all rely on outside conditions to control the cooling system. Technically temperature difference does not, as it relies on two temperature measurements, but this is a worse substitute for having an accurate heat load measurement.

Standard rule is the worst control method. While it is capable of decent temperature management, the power consumption is a lot higher. The maximum power consumption of the circulation pumps is significantly higher than that of the river water pumps, and standard rule has a nominal coolant flow rate at all times, meaning high circulation pump power consumption at all times. Load-based pump also has nominal coolant flow rate, but it can more efficiently use the river water pumps. Another aspect that makes standard rule bad compared to other methods is the amount of on/off cycles. Not only does standard rule experience on/off cycles in significantly more simulations than the other methods, but the average number of on/off cycles is also high.

From a temperature control perspective, load-based flow and load-based pump had comparable performance. Load load-based pump was more strictly tuned compared to load-based flow which helped

with temperature control. Neither method experienced on/off cycles as, at all times, a level of flow was maintained. Load-based pump did experience more changes in pump speed as more simulations had changes in pump speed, and with 6 active fuel cell units, there are 2 pumps that change the speed at the same time. With regards to power consumption, load-based flow is the clear better option. Being able to reduce the more power-consuming part of the cooling system is the obvious better choice for reducing power consumption. Another upside of reducing coolant flow rather than river water flow is that with a reduction in coolant flow, the heat exchanger effectiveness increases. So while cooling effectiveness over the fuel cell units is lost due to a loss of flow, part of that loss is reclaimed by the heat exchanger as the temperature of the coolant entering the fuel cell units is lower than with the higher flow. This all combines to make load-based flow the best option out of the first group for constant load.

The second group consists of three methods that are different variations of the same principle. Of these, temperature difference is the clear worst option for constant load. While the method has no temperature overshoots nor pump on/off cycles, the power consumption is too high compared to other methods. The requirement of maintaining nominal flow for the heat load calculation results in a high cooling system power consumption. Lookup and steady-state optimised do experience temperature overshoots, but this is due to nonlinearities that are unaccounted for in the optimisation model, and thus, these methods can be further refined to mitigate this issue. For this reason, these temperature overshoots are not inherently due to the control method, but more due to lacking execution of these methods. Neither method experiences pump on/off cycles and steady-state optimised has a slight advantage with regards to power consumption.

The best-performing control method for constant load is steady-state optimised. The temperature regulation is good except for a few exceptions where the method suffers from nonlinearities. The method has no pump on/off cycles resulting in less wear on the pumps compared to other methods. Steady-state optimised also has the lowest power consumption out of all the methods, especially at low river water temperatures combined with low loads. In these circumstances, methods like load-based flow and load-based pump have higher power consumption due to them being unable to reduce the number of active heat exchangers and reduce the coolant flow respectively.

6.1.2. Step load discussion

From the results of the step load simulations in section 5.2 what became clear is that methods that consumed more power were able to better cope with an increase in heat load. This is due to these methods keeping the coolant at lower temperatures as they provide additional cooling which can deal with the increase in heat load. The better the constant load energy consumption, the worse the step load temperature management. Standard rule performs well in nearly every simulation and temperature difference performs poorly, unless there was already spare cooling capacity. Both load-based flow and load-based pump require the temperature measurement of the cooling exiting the fuel cell, and whether this coolant reaches the threshold just before the measurement or just after has big implications for the temperature overshoot. An unfortunate measurement can lead to 60 seconds of further fuel cell heating up. Lookup performs the worst in these simulations as was expected. Steady-state optimised has the added benefit that when the heat load increases, it recalculates the new cooling system configuration, but lookup is stuck in the old configuration for 50 seconds before it can change the cooling system configuration. This leads to significantly higher peak temperatures. When the cooling configuration did change, the spare cooling capacity was limited leading to a relatively slow descent in fuel cell temperature. Current-state optimised does provide more cooling to get the fuel cell temperature under control faster. However, due to the choice of not building in inherent spare cooling, there are multiple simulations where current-state optimised experiences a steady-state error, a deviation from the desired temperature that persists over time.

6.1.3. Scenario discussion

The final simulations were the scenario simulations from section 5.3. These simulations showed similar temperature performance as the constant load and step load simulations. The finding of the power consumption from constant load was also echoed in these simulations, meaning that relatively frequent changes in heat load had minimal effect on the relative performance of the control methods regarding the cooling system power consumption.

The worst performing control methods were standard rule and temperature difference. While standard rule had good temperature management in all simulations, the power consumption is too high compared to other methods. Temperature difference had good temperature management at low river water temperatures, but this came at the cost of cooling system power consumption, which at those low temperatures was the highest out of any method tested. At high river water temperatures, temperature difference lower power consumption than standard rule, but it experiences significant temperature overshoots.

Load-based pump and load-based flow had similar temperature management performance. With load-based flow being less strictly tuned compared to load-based pump it was expected that it would have more recurring temperature overshoots, which can be seen. What is worth noting is the benefit that load-based flow has compared to load-based pump when it comes to the maximum temperature overshoot during the first heat load increase of the 25 °C simulation. Here, the spike of load-based flow is significantly lower than load-based pump. This can be explained by load-based flow having a lower coolant temperature entering the fuel cell units. When the cooling needs to be increased, this increase in cooling capacity is felt pretty much instantly by the fuel cell unit. Compare this with load-based flow where it takes a bit of time before the new colder coolant arrives at the fuel cell units, leading to a higher spike in temperature. This, combined with the superior performance in cooling system power consumption, makes load-based flow the better control method of these two.

Even better still are the optimisation-based control methods. While lookup suffers from being unable to react to a change in heat load, steady-state optimised and especially current-state optimised perform well at higher river water temperatures. While these methods have a temperature overshoot at all river water temperatures, this is due to them being able to take the river water temperature into account, lowering the power consumption of the cooling system. It can be seen in figure 5.20 that the difference in energy used between load-based flow and the optimisation-based methods is larger at lower temperatures. Lookup has the highest energy consumption out of the three optimisation-based methods, which is expected as it is designed to offer more cooling than theoretically required. Steady-state optimised, on average, slightly outperformed current-state optimised when it came to power consumption; the trade-off is that current-state optimised has, in most cases, better temperature performance.

6.1.4. Discussion of different control methods

When comparing the performance of the control methods, optimisation-based control has significantly lower power consumption than the other methods, with load-based flow coming the closest in power consumption. Lookup and, to a lesser extent, steady-state optimised have bad temperature management when an increase in heat load occurs. Current-based optimised also performs worse than the rule-based control methods, with the exception being certain simulations of temperature difference. When it comes to pump on/off cycles, the optimised based methods outperform the rule-based methods as in steady state, the optimised-based methods do not require constant cooling system configuration changes. At the same time, there are multiple simulations in constant load where standard rule, load-based flow, and load-based pump experience these recurring changes.

Standard rule is the baseline rule-based control. One temperature measurement dictates the configuration. It is no surprise that this is the worst-performing control method. It is also no surprise that none of the other rule-based methods outperformed the optimisation-based methods as, theoretically, the optimisation-based methods can not be outperformed as it would require significant mistakes within the optimiser. The question is, how much does one want to add rules to the rule set or add an algorithm until the method becomes good enough or too complex where having an optimiser may be worth the effort? The optimiser has a significant drawback, being the need for a mathematical model of the system and the fuel cell heat load as input data. If these are available, an optimisation-based control method would seem like the obvious choice. Whether that be through a lookup table to avoid having to do the optimisation on board the ship or the best performance would be a current-state optimiser. By adding spare cooling capacity within the optimiser model, the problems that it encountered in this research will be negated and it has a large enough gap to load-based flow in power consumption performance that it would still perform better. If no such model is available, then going for an onboard algorithm like load-based flow would be a viable alternative. If that is considered too advanced, the next best option would be a combination of standard rule and temperature difference. Adding a rule that would

activate additional cooling when the coolant leaving the fuel cell exceeds a certain temperature would cause the temperature overshoot that temperature difference experiences to be mostly negated while maintaining the upside of no pump on/off cycles during constant load. To increase efficiency at low river water temperatures a winter rule set can be introduced.

Even though optimisation-based methods show superior performance, they would require a backup control system as, due to their reliance on models, there is a reasonable chance that the models are inaccurate. This can be due to various reasons, including fuel cell degradation, increased pipe flow resistance over time, or a component failing. Current-based optimised is especially susceptible to sensor measurement failure as this method requires additional temperature measurements of the coolant entering and leaving the fuel cell units. Additional redundancy can be introduced for the fuel cell heat load model. By measuring the coolant flow together with the coolant temperatures over the fuel cell units, the heat load of the fuel cell units can be calculated. Assuming the highest heat load out of the model based on fuel cell electric energy load and these measurements would reduce the risk of failure. The river water temperature measurement can be compared to historical river water temperature data. If the measured river water temperature is significantly lower than the historical river water temperature, the optimisation models will use the historical river water temperature as a precaution. This research shows the importance of accurate models for optimisation-based methods to function as simplifications with regard to resistance calculations and coolant thermal properties already result in steady-state errors in the temperature control. While it is safe to conclude that optimisation-based methods have the best performance, further research into the implementation of these methods is required.

6.1.5. Discussion on the research

This research clearly shows that a lot of energy can be saved with the cooling system of a ship. Findings from previous research that concluded that implementing variable-speed pumps within cooling leads to savings in power consumption are also echoed by this research. Methods that were able to reduce pump speed had lower power consumption compared to methods that were not able to reduce pump speed. While this is an obvious finding, this research provided an overview of the magnitude of the power savings. It should be noted, however, that the modelled cooling system on which the control methods were tested lacked validation data. While this means that the findings of this research can not be directly applied to the FPS Waal on which the modelled cooling system is based, this does not discredit the findings of this research. The thermal fluid properties used in the Simulink model are a realistic representation. Even if the valves are not modelled correctly, meaning that the pressure drop over the valves does not align with reality, the only repercussion this has on this research is that the value of the valve position of the three-way valve S is unrealistic. If the general pressure drop over the valve is too low, this model would have to compensate by closing the valve further than in reality to ensure the correct flow. The model tested in this research had realistic flows and pipe volumes, leading to realistic coolant transportation.

This research mentions fuel cell units; however, other than an estimation for the mass, specific heat capacity, and operating temperature, this research is separate from anything fuel cell related. When assessing the performance of control methods, as the aim of this research was, the accuracy of the fuel cell model is not relevant as long as one does not make conclusions about the fuel cell units, which this research does not do. This research examined the cooling system response to different environmental and heat load scenarios. While fuel cell temperature is mentioned as a metric that is looked at, the name is mainly due to the cooling system this research is based on rather than accurately representing an actual fuel cell unit.

The heat exchanger models used are simplified. They transfer heat based on the heat transfer in nominal conditions and an extrapolation of work points. The error caused by this is most likely small, and even then, it does not affect this research as the accuracy of the heat exchangers does not influence the performance of the control methods.

6.2. Recommendations

Two sets of recommendations stem from this research. The first set encompasses the recommendations that aim to improve the research performed here. The second set of recommendations is about

how the research performed here can be expanded upon.

The optimisation models have much room for improvement in this research. The problems that arose from linearised flow resistance and constant fluid properties have been extensively described. Approximations for flow resistance and fluid properties could be added for accuracy, although they would increase the computation time. The current way the optimisation model is set up is incapable of reducing the river water pump flow. Having both flows vary would change the piece-wise linear constraints 3.76 and 3.77 into 2-D piece-wise linear approximation. This limits the current optimisation models to fixed-speed pumps for the river water pumps.

The control methods used in this research were tuned to, during constant load, not exceed 68 °C. They were not tuned to minimise power consumption or further improve temperature management. While further tuning of these methods is unlikely to change the overall conclusions from this research, it would be interesting to know the limits of these methods and further strengthen the findings. The same goes for the simulations. While significant gaps in river water temperature are acceptable for testing the optimisation methods and temperature difference, for standard rule, load-based pump, and load-based flow, a slight variation in river water temperature could be the difference between constant temperature fluctuations and no temperature fluctuations. These methods should be tested with more river water temperatures. During this research, the cooling system components were assumed to be constant, except for the river water pumps, which were considered variable-speed pumps for temperature difference and load-based pump. This sort of research should be repeated on different layouts of cooling systems to see if the results are similar.

Different control methods should be tested. Load-based flow could be improved in performance by replacing the algorithm with a PID controller which attempts to keep the coolant leaving the fuel cell units at 65 °C.

The fuel cells were considered a heat source and a thermal mass in this research. A proper model for the coolant flow through the fuel cell unit and the fuel cell thermal balance would improve this research. This would enable real-life simulations where rather than a heat load, an electrical load can be used as input to the model, and with a more complete thermal balance equation over the fuel cell, the impact of cold outside air in winter can be an aspect that is looked at.

Expanding on this research would involve including the energy management system. An energy management system that can consider fuel cell temperature and use the battery to supplement additional energy allows the cooling system time to ramp up the cooling before the fuel cell heat load increases. This could be expanded upon even further with optimisation-based control to create a scenario where future loads are known and the result it could have on the cooling system management.

7

Conclusion

This research examined and compared the performance of rule-based and optimisation-based control methods when used on a cooling system with multiple pumps, heat exchangers, and fuel cell units. To achieve this, seven control methods were devised and tested on a model of a cooling system based on the FPS Waal in constant load, step load, and scenario simulations.

With a constant heat load, the optimisation-based methods perform better than rule-based methods when it comes to temperature management, pump on/off cycles, and cooling system power consumption. The optimisation-based methods suffer from nonlinearities in flow calculations and thermal fluid properties, which leads to simulations where the temperature is not sufficiently controlled. This can be prevented by improving the optimisation models. The best-performing rule-based control method is load-based flow. Still, this method suffers from pump on/off cycles, and at low heat load or low river water temperatures, the optimisation-based control methods have significantly lower cooling system power consumption.

The rule-based control methods did respond better to a change in heat load than the optimisation-based control methods. This is because these methods have too much cooling capacity at low heat loads, leading to spare cooling capacity when the heat load increases, forming a buffer. The optimisation-based control methods have minimal spare cooling capacity and are thus more susceptible to an increase in heat load. Especially lookup suffers from an increase in heat load as steady-state optimised and current-state optimised can instantly respond to a change in heat load. Current-state optimised suffers from nonlinearities, resulting in several steady-state errors.

During the scenario simulations, the methods are subjected to changes in heat load and the number of active fuel cell units. Optimisation-based control methods are again more susceptible to changes in heat load than rule-based control methods. However, they do have significantly lower cooling system power consumption. Steady-state optimised has a marginally lower power consumption compared to current-state optimised. Current-state optimised has better temperature management. The best-performing rule-based control method is load-based flow, which has the lowest cooling system power consumption and adequate temperature management. Lookup is the only control method that featured temperature spikes well above 68 °C.

Load-based flow's average power consumption over the scenario simulations is 39.2% higher than the average power consumption of steady-state optimised. Load-based pump, temperature difference, and standard rule perform significantly worse, with 96.4%, 179.5%, and 197.0%, respectively. Current-state optimised only has a 0.85% higher average power consumption and lookup a 5.85% higher average power consumption.

While the optimisation-based control methods significantly reduce energy consumption, they rely on an accurate cooling system and fuel cell heat load model. In this research, where the degradation of fuel cell units and cooling system components were ignored, the effects of model inaccuracies due to simplifications can be seen as steady-state errors in temperature control. In a practical scenario

where the state of the cooling system components changes over time, it can be expected that the models used for the optimisation-based control methods have more inaccuracies, resulting in worse temperature control. The modelling of optimisation models of a cooling system needs to be further explored before they can be implemented in practice.

Bibliography

[1] *About HyShip*. URL: https://hyship.eu/about/. (accessed: 2023-02-28).

[2] Wu Bi and T. Fuller. “Temperature Effects on PEM Fuel Cells Pt/C Catalyst Degradation”. In: *ECS Transactions* 11.1 (Sept. 2007), pp. 1235–1246. ISSN: 1938-5862. DOI: 10.1149/1.2781037.

[3] L. van Biert et al. “A review of fuel cell systems for maritime applications”. In: *Journal of Power Sources* 327 (Sept. 2016), pp. 345–364. DOI: 10.1016/j.jpowsour.2016.07.007.

[4] Sofia Boulmrharj et al. “Towards performance assessment of fuel cell integration into buildings”. In: *Energy Reports*. Vol. 6. Elsevier Ltd, Feb. 2020, pp. 288–293. DOI: 10.1016/j.egyr.2019.08.058.

[5] M. Cavo et al. “An advanced control method for fuel cells - Metal hydrides thermal management on the first Italian hydrogen propulsion ship”. In: *International Journal of Hydrogen Energy* (2022). ISSN: 03603199. DOI: 10.1016/j.ijhydene.2022.07.223.

[6] *Energy Density and Specific Energy of Battery*. URL: https://sinovoltaics.com/learning-center/storage/energy-density-and-specific-energy-of-battery/#:~:text=The%5C%20gravimetric%5C%20energy%5C%20density%5C%20or,W%5C%2Dhr%5C%2Fkg).. (accessed: 2023-02-28).

[7] *Energy Observer 2: a new zero-emission ship to meet the objectives of the International Maritime Organization*. URL: https://www.jeccomposites.com/news/energy-observer-2-a-new-zero-emission-ship-to-meet-the-objectives-of-the-international-maritime-organization/. (accessed: 2023-02-28).

[8] *FCS ALTSERWASSER*. URL: https://www.blue-growth.org/Blue_Growth_Technology_Innovation/Hydrogen_Ferries_Cruise_Ships_Cargo_Vessels_Fuel_Cells/FCS_Alsterwasser_Alster_Touristik_Hydrogen_FuelCell_Ships_Hamburg_Riverboat.htm. (accessed: 2023-02-28).

[9] *FPS Maas Retrofit Project*. URL: https://futureproofshipping.com/projects/the-maas/. (accessed: 2023-02-28).

[10] *Fuel Cell Power for Marine Applications*. URL: https://www.ballard.com/docs/default-source/spec-sheets/fcwavetm-specification-sheet.pdf?sfvrsn=6e44dd80_16. (accessed: 2024-02-02).

[11] Volker Gnielinski. “Neue Gleichungen für den Wärme- und den Stoffübergang in turbulent durchströmten Rohren und Kanälen”. In: *Forschung im Ingenieurwesen* 41.1 (Jan. 1975), pp. 8–16. ISSN: 0015-7899. DOI: 10.1007/BF02559682.

[12] *H2 Barge 1*. URL: https://about.nike.com/en/newsroom/releases/nike-launches-first-hydrogen-powered-inland-container-ship/The-%E2%80%9CH2-Barge-1%E2%80%9D. (accessed: 2024-04-14).

[13] S. E. Haaland. “Simple and Explicit Formulas for the Friction Factor in Turbulent Pipe Flow”. In: *Journal of Fluids Engineering* 105.1 (Mar. 1983), pp. 89–90. ISSN: 0098-2202. DOI: 10.1115/1.3240948.

[14] Jaeyoung Han, Jisoo Park, and Sangseok Yu. “Control strategy of cooling system for the optimization of parasitic power of automotive fuel cell system”. In: *International Journal of Hydrogen Energy* 40.39 (Oct. 2015), pp. 13549–13557. ISSN: 03603199. DOI: 10.1016/j.ijhydene.2015.08.067.

[15] Seyed Ehsan Hosseini and Brayden Butler. “An overview of development and challenges in hydrogen powered vehicles”. In: *International Journal of Green Energy* 17.1 (Nov. 2019), pp. 13–37. DOI: 10.1080/15435075.2019.1685999.

[16] Jun Hou, Jing Sun, and Heath Hofmann. “Control development and performance evaluation for battery/flywheel hybrid energy storage solutions to mitigate load fluctuations in all-electric ship propulsion systems”. In: *Applied Energy* 212 (Feb. 2018), pp. 919–930. ISSN: 03062619. DOI: 10.1016/j.apenergy.2017.12.098.

[17] *Hydrogen Overview*. URL: https://www.ge.com/content/dam/gepower-new/global/en_US/downloads/gas-new-site/future-of-energy/hydrogen-overview.pdf. (accessed: 2023-02-28).

[18] *Hydrogen Storage*. URL: https://www.energy.gov/eere/fuelcells/hydrogen-storage. (accessed: 2023-02-28).

[19] *International Convention for the Prevention of Pollution from Ships (MARPOL)*. URL: https://www.imo.org/en/about/Conventions/Pages/International-Convention-for-the-Prevention-of-Pollution-from-Ships-(MARPOL).aspx. (accessed: 2023-02-28).

[20] Gazi Kocak and Yalcin Durmusoglu. “Energy efficiency analysis of a ship’s central cooling system using variable speed pump”. In: *Journal of Marine Engineering and Technology* 17.1 (Jan. 2018), pp. 43–51. ISSN: 20568487. DOI: 10.1080/20464177.2017.1283192.

[21] *Leuchtturmprojekt: ELEKTRA*. URL: https://www.behala.de/elektra/. (accessed: 2023-02-28).

[22] Vincenzo Liso et al. “Thermal modeling and temperature control of a PEM fuel cell system for forklift applications”. In: *International Journal of Hydrogen Energy*. Vol. 39. 16. Elsevier Ltd, May 2014, pp. 8410–8420. DOI: 10.1016/j.ijhydene.2014.03.175.

[23] Anthony F. Mills and Carlos F.M. Coimbra. *Basic heat and mass transfer*. Prentice Hall, 2015, p. 1001. ISBN: 9780996305303.

[24] Efthimios G. Pariotis, Theodoros C. Zannis, and John S. Katsanis. “An integrated approach for the assessment of central cooling retrofit using variable speed drive pump in marine applications”. In: *Journal of Marine Science and Engineering* 7.8 (Aug. 2019). ISSN: 20771312. DOI: 10.3390/jmse7080253.

[25] *Paris Agreement*. URL: https://treaties.un.org/pages/ViewDetails.aspx?src=TREATY&mtdsg_no=XXVII-7-d&chapter=27&clang=_en (visited on 02/28/2023).

[26] *PEM fuel cell system*. URL: https://nl.mathworks.com/help/simscape/ug/pem-fuel-cell-system.html. (accessed: 2024-02-02).

[27] Nischal Pokharel et al. “Wear in centrifugal pumps with causes, effects and remedies: A Review”. In: *IOP Conference Series: Earth and Environmental Science*. Vol. 1037. 1. Institute of Physics, 2022. DOI: 10.1088/1755-1315/1037/1/012042.

[28] Elena Rozzi et al. “Green Synthetic Fuels: Renewable Routes for the Conversion of Non-Fossil Feedstocks into Gaseous Fuels and Their End Uses”. In: *Energies* 13.2 (Jan. 2020), p. 420. DOI: 10.3390/en13020420.

[29] Max Schwenzer et al. *Review on model predictive control: an engineering perspective*. Nov. 2021. DOI: 10.1007/s00170-021-07682-3.

[30] Colleen Spiegel. *PEM Fuel Cell Modeling and Simulation Using MATLAB ®*. Tech. rep.

[31] Chun Lien Su, Wei Lin Chung, and Kuen Tyng Yu. “An energy-savings evaluation method for variable-frequency-drive applications on ship central cooling systems”. In: *IEEE Transactions on Industry Applications* 50.2 (2014), pp. 1286–1294. ISSN: 00939994. DOI: 10.1109/TIA.2013.2271991.

[32] Xingwang Tang, Yujia Zhang, and Sichuan Xu. “Temperature sensitivity characteristics of PEM fuel cell and output performance improvement based on optimal active temperature control”. In: *International Journal of Heat and Mass Transfer* 206 (June 2023), p. 123966. ISSN: 00179310. DOI: 10.1016/j.ijheatmasstransfer.2023.123966.

[33] *United Nation Framework Convention on Climate Change*. URL: https://unfccc.int/files/essential_background/background_publications_htmlpdf/application/pdf/conveng.pdf (visited on 02/28/2023).

[34] Tuyen Van Vu et al. “Predictive Control for Energy Management in Ship Power Systems under High-Power Ramp Rate Loads”. In: *IEEE Transactions on Energy Conversion* 32.2 (June 2017), pp. 788–797. ISSN: 08858969. DOI: 10.1109/TEC.2017.2692058.

[35] *Waterinfo*. URL: https://waterinfo.rws.nl/#/publiek/watertemperatuur. (accessed: 2024-03-24).

A

Piecewise linear constraints

Figure A.1 shows the piecewise linear approximation used for constraints 3.48, 3.49, 3.76, and 3.77. Figure A.2 shows the piecewise linear approximation used for constraints 3.39 and 3.40.

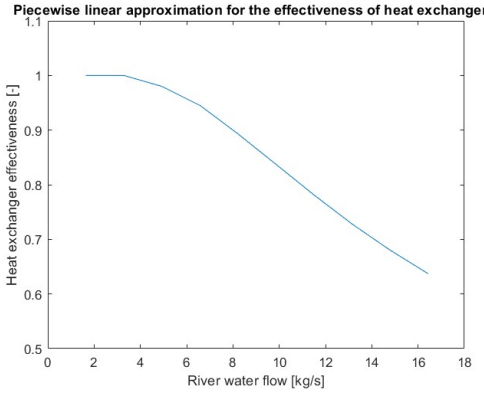

(a) Heat exchanger 1 effectiveness

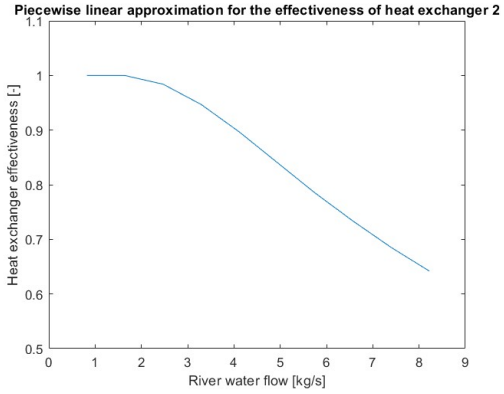

(b) Heat exchanger 2 effectiveness

Figure A.1: Piecewise linear approximations for heat exchanger effectiveness

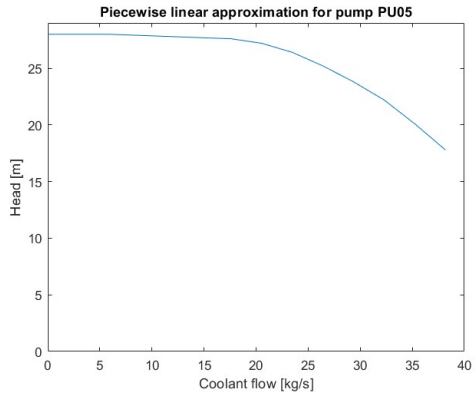

(a) PU05 linear approximation

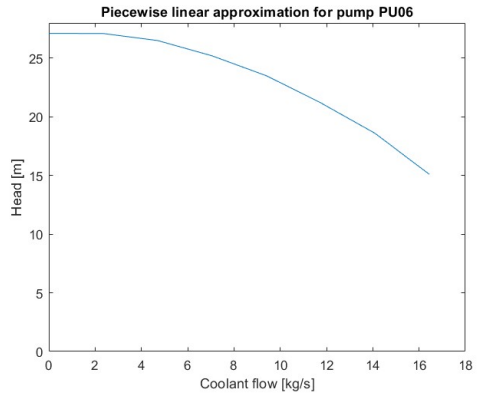

(b) PU06 linear approximation

Figure A.2: Piecewise linear approximations for pump head

B

Constant load simulations

Figure B.1 shows the legend for the constant load simulation figures. Colours are assigned to river water temperature and line style is assigned to fuel cell heat load. Figures B.2 - B.7 show the fuel cell temperature during the constant load simulations for standard rule, temperature difference, load-based flow, load-based pump, lookup, and steady-state optimised respectively.

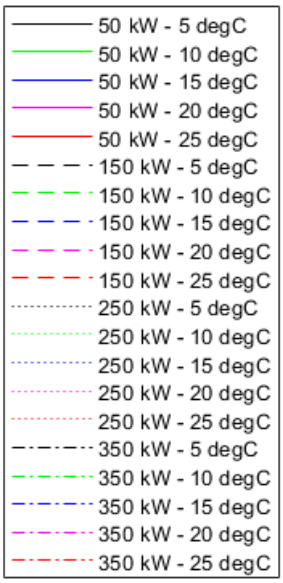

Figure B.1: Legend for figures B.2 - B.7

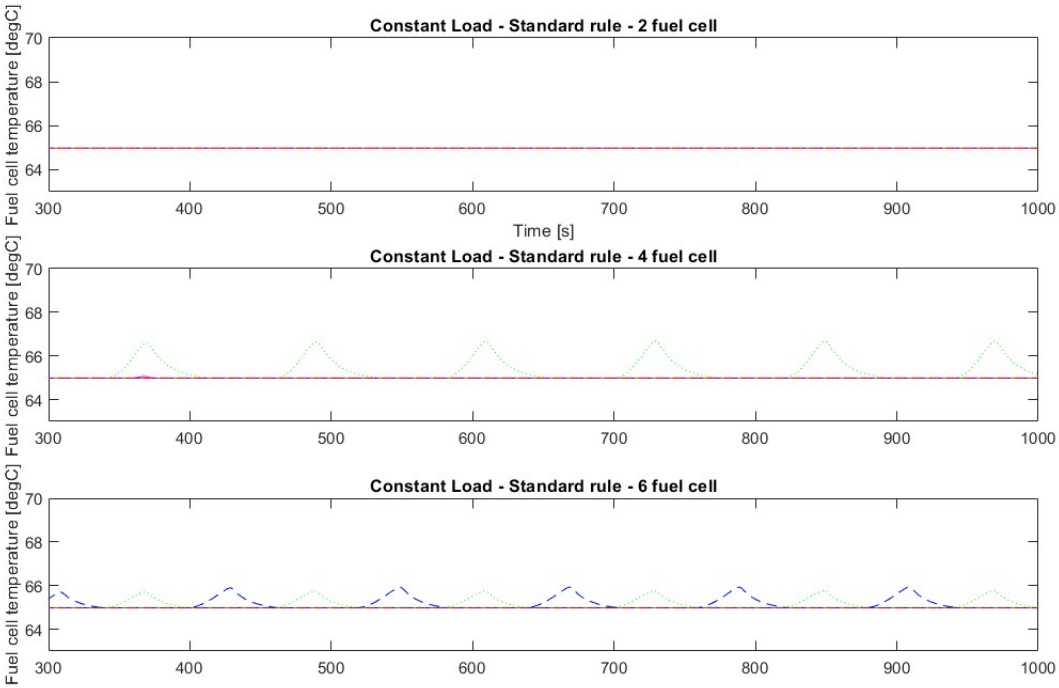

Figure B.2: Fuel cell temperature during constant load simulations with standard rule

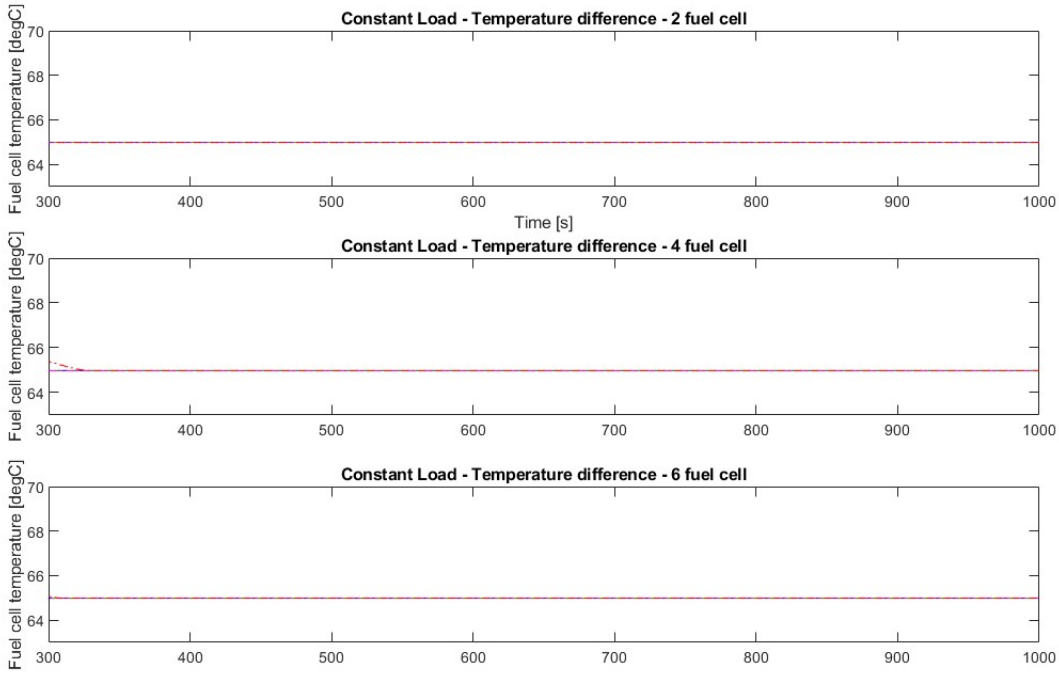

Figure B.3: Fuel cell temperature during constant load simulations with temperature difference

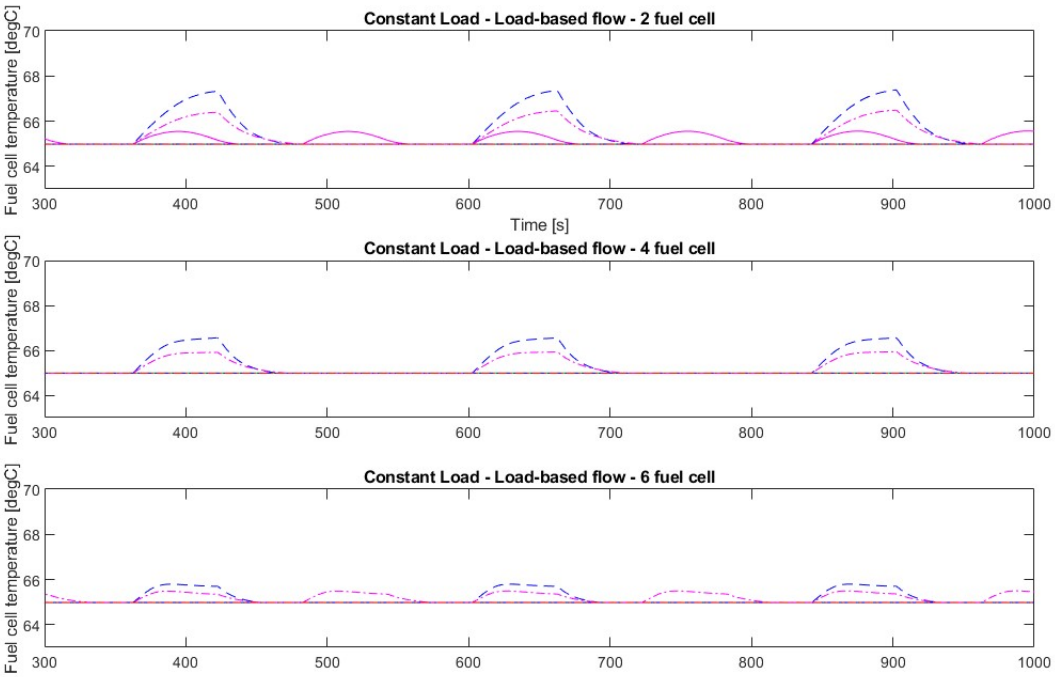

Figure B.4: Fuel cell temperature during constant load simulations with load-based flow

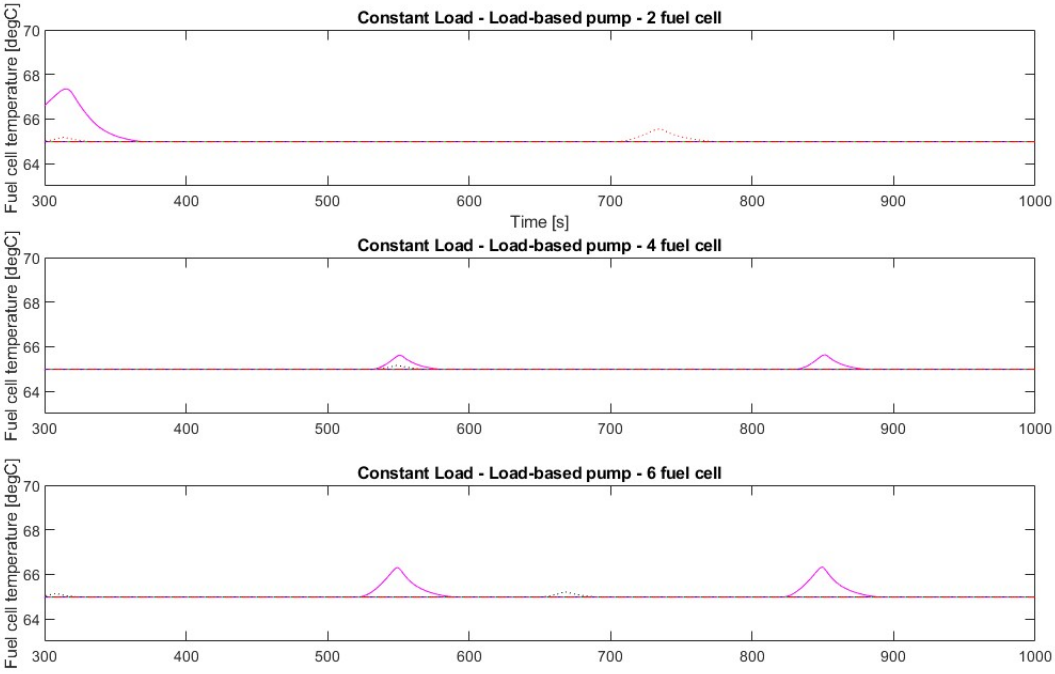

Figure B.5: Fuel cell temperature during constant load simulations with load-based pump

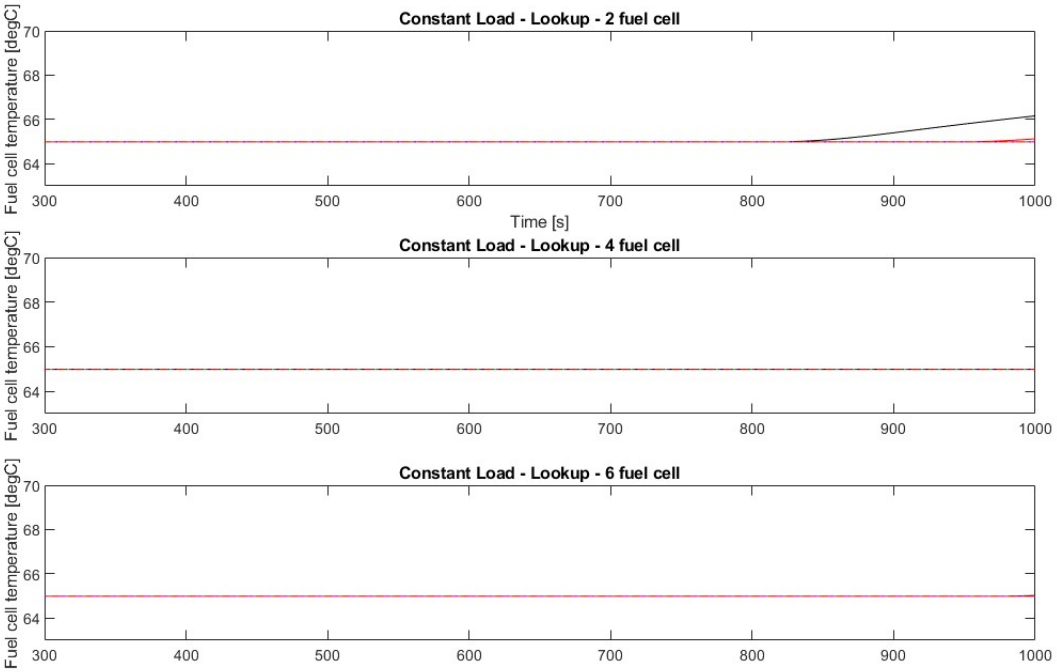

Figure B.6: Fuel cell temperature during constant load simulations with lookup

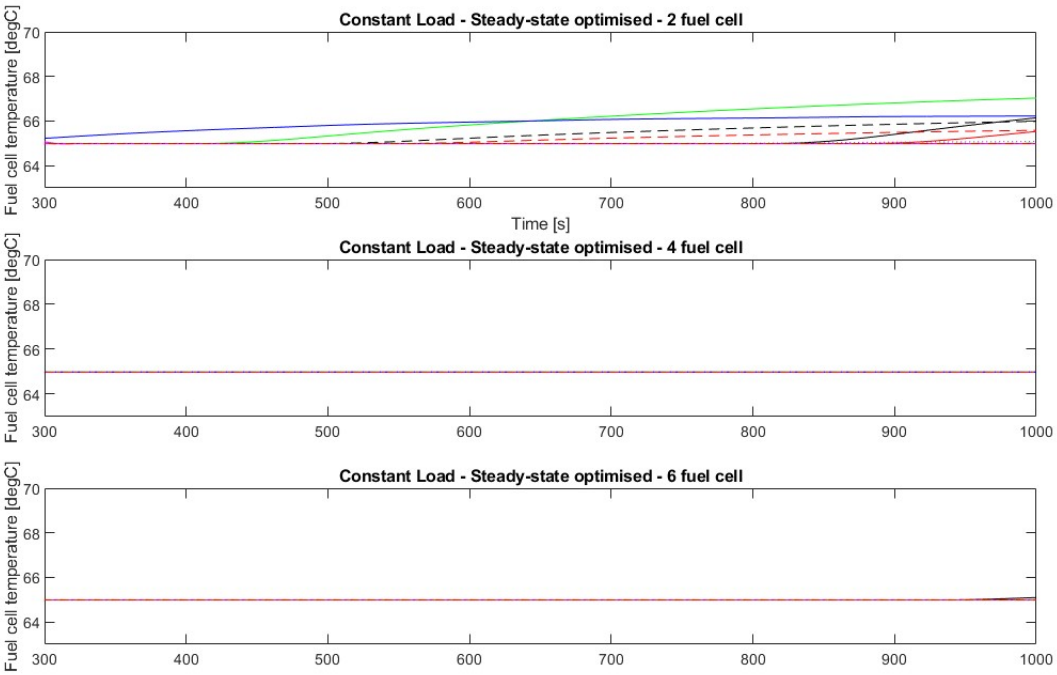

Figure B.7: Fuel cell temperature during constant load simulations with steady-state optimised